RL-TR-92-300
Final Technical Report
December 1992

VOLUME INTEGRAL EQUATIONS APPLIED TO CIRCULAR AND SQUARE CYLINDERS

University of Lowell Research Foundation

Rose W. Wang

APPROVED FOR PUBLIC RELEASE; DISTRIBUTION UNLIMITED.

Rome Laboratory
Air Force Materiel Command
Griffiss Air Force Base, New York

DISCLAIMER NOTICE

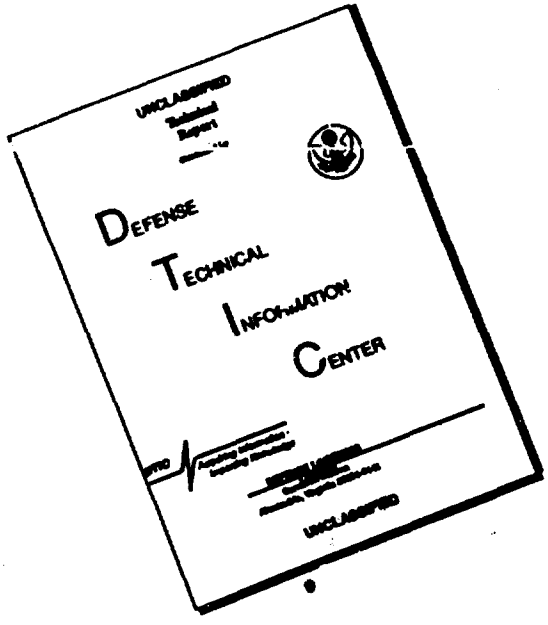

THIS DOCUMENT IS BEST QUALITY AVAILABLE. THE COPY FURNISHED TO DTIC CONTAINED A SIGNIFICANT NUMBER OF PAGES WHICH DO NOT REPRODUCE LEGIBLY.

This report has been reviewed by the Rome Laboratory Public Affairs Office (PA) and is releasable to the National Technical Information Service (NTIS). At NTIS it will be releasable to the general public, including foreign nations.

RL-TR-92-300 has been reviewed and is approved for publication.

APPROVED: Arthur D. Yaghjian

ARTHUR D. YACHJIAN
Project Engineer

FOR THE COMMANDER: John K. Schindler

JOHN K. SCHINDLER, Director
Electromagnetics & Reliability Directorate

If your address has changed or if you wish to be removed from the Rome Laboratory mailing list, or if the addressee is no longer employed by your organization, please notify RL(ERCT) Hanscom AFB MA 01731-5000. This will assist us in maintaining a current mailing list.

Do not return copies of this report unless contractual obligations or notices on a specific document require that it be returned.

REPORT DOCUMENTATION PAGE

Form Approved
OMB No. 0704-0188

1. AGENCY USE ONLY (Leave Blank)	2. REPORT DATE	3. REPORT TYPE AND DATES COVERED
	December 1992	Final

4. TITLE AND SUBTITLE
VOLUME INTEGRAL EQUATIONS APPLIED TO CIRCULAR AND SQUARE CYLINDERS

5. FUNDING NUMBERS
C - F30602-91-D-0001
Task 11
PE - 61102F
PR - 2305
TA - J4
WU - 09

6. AUTHOR(S)
Rose W. Wang

7. PERFORMING ORGANIZATION NAME(S) AND ADDRESS(ES)
University of Lowell Research Foundation
450 Aiken Street
Lowell MA 01854

8. PERFORMING ORGANIZATION REPORT NUMBER

9. SPONSORING/MONITORING AGENCY NAME(S) AND ADDRESS(ES)
Rome Laboratory (ERCT)
31 Grenier Street
Hanscom AFB MA 01731-3010

10. SPONSORING/MONITORING AGENCY REPORT NUMBER
RL-TR-92-300

11. SUPPLEMENTARY NOTES
Rome Laboratory Project Engineer: Arthur D. Yaghjian/ERCT (617) 377-3961

12a. DISTRIBUTION/AVAILABILITY STATEMENT
Approved for public release; distribution unlimited.

12b. DISTRIBUTION CODE

13. ABSTRACT (Maximum 200 words)

Three numerical integration methods are developed and used for evaluating the highly singular dyadic Green's function in the volume integral equations for scattering from dielectric cylinders. Numerical results indicate that for small permittivities or relatively small dielectric cylinders, the methods are quite efficient and give comparable accuracy. However, when both the relative permittivity and the size of the cylinder are increased, we experienced problems similar to those encountered by a number of previous researchers, namely, the results converge slowly for the TE polarization.

14. SUBJECT TERMS
Volume integral equations, Cylinders, Green's functions

15. NUMBER OF PAGES
104

16. PRICE CODE

17. SECURITY CLASSIFICATION OF REPORT	18. SECURITY CLASSIFICATION OF THIS PAGE	19. SECURITY CLASSIFICATION OF ABSTRACT	20. LIMITATION OF ABSTRACT
UNCLASSIFIED	UNCLASSIFIED	UNCLASSIFIED	U/L

TABLE OF CONTENTS

1. INTRODUCTION

The method of moments (MOM) applied to volume integral equations has been a common way of solving for the electromagnetic scattering from highly inhomogeneous bodies. Many researchers [1] have experienced difficulties in obtaining an accurate solution for bodies with a high relative permittivity. With a revised treatment for the singular dyadic Green's function [2] in the integrand of the volume integral equation, we hope to overcome these difficulties and obtain a benchmark solution for a three-dimensional multi-wavelength scatterer with edges and corners.

Richmond [3],[4], and Livesay and Chen [5] appear to be the first to use the volume integral equation for dielectric bodies. Their procedure is based on volume discretizations of the volume integral equation with pulse basis functions and point matching. However, for 3-D problems as well as for the 2-D problems of TE polarization, substantial inaccuracies are observed. Recently, Joachimowicz and Pichot [6] compared the different integral formulations for 2-D TE scattering problems and analysed the source of these errors. They introduced a new integral equation that included

surface integrals to take account of surface charges at discontinuities. Even though better performance was obtained, considerable errors can still be observed.

In this report we are trying to accomplish two goals: (1) to eliminate the source of errors and (2) to obtain a benchmark solution to permit comparisons with the theoretically exact series solution for 2-D scattering from dielectric cylinders; and if successful, to obtain a benchmark solution for the 3-D scattering from a dielectric cube. Initial progress towards these goals are described.

At first, we believed the inaccuracies of the solution of the past researchers were probably due to inaccuracies in computing the highly singular dyadic Green's function for the scattering from dielectric cylinder, and in particular, in their treatment of the self term. In both Richmond and Chen's papers [3]-[5], the kernel of the integral equation is calculated by replacing the square self cell by a circular disk having the same area or replacing the volume self cell by a sphere having the same volume. Thus, our first step was to perform the self cell integration as accurately as possible. For the case of scattering from a

dielectric square cylinder, our results indicated that there is less than 1% difference between Richmond using the equal area approximation and our more accurate revised approach. Thus, there appears no great advantage in using a more accurate self cell evaluation in computing the bistatic scattering from the dielectric square cylinders.

In the original pulse basis and point matching method, the electric field and the dielectric properties are assumed to be constant in each cell and the Green's function is evaluated at the center of each cell. In other words, there is one center point for each nonself cell calculation. In our second approach, we increased the number of integration points of the Green's function for each of these cells and checked for convergence. For TM polarization, our results converged rapidly, and there is less than 2% difference between computing each cell contribution of the Green's function with one center point and with 240 integration points. However, our results converged more slowly for the TE case, the difference between computing with one center point, 25 points and 100 points, as compared with 240 points, was 5%,2% and 1% respectively. Again

the increase in accuracy was not very large.

Our next approach involved performing the integration over both the self and nonself cells by changing the area integrals to line integrals. Making use of Gaussian Legendre quadrature integration techniques, we can significantly decrease the total number of integration points from the number we used for the area integration and achieve higher accuracy. Our results suggest that the line integration method proved to be most accurate method for evaluating the Green's function over each cell. The area integration method required more than 200 integration points to achieve the same accuracy as 80 integration points with the line integration method.

One of the criteria for the pulse basis functions to work is to have cells much smaller than a wavelength. Since there is no exact series solution for the square cylinder, the circular cylinder was used for determining the required cell size. The analytical series solution for scattering from the circular cylinder can be easily derived and coded numerically. We first check the validity of analytical formulation of the circular cylinder and accuracy by comparing it with the results which can

be found in many electromagnetic textbooks [7] and [8]. The internal $\overline{E}$ and $\overline{H}$ fields for both TM and TE cases were computed and inspected to detect any unusual rapid changes in the fields. With the help of our exact code for scattering from the circular cylinders, the results with different cell sizes in the integral equations can be compared. The numerical results indicate that a minimal cell size of $\lambda/10$ (where λ is the wavelength in the dielectric material) in the TM case, gives approximately 2% of error in the far-field scattering from a long circular cylinder of radius = 0.3 λ and permittivity equal to 3. Similar accuracy is observed in the TE case for low values of permittivity.

As mentioned above, three different approaches have been used to evaluate the Green's function over each cell - center point, area integration, and line integration, for the scattering from dielectric cylinders. There is practically no distinction between the three methods in computing scattering from the dielectric cylinders in the case of TM polarization. The results are in good agreement with the exact solution to less than 5% maximum error. However, this is not the case

for TE polarization, when the permittivity is large or when the size of the circular cylinder is large. Even though the cell size decreases, better agreement is needed between the numerical data and exact solution. The curves tend to converge very slowly to the exact curve.

One explanation of the deficiency may be due to the square cell representation of the circular cylinder. The jagged edges may produce an error. Tables 1 and 2 show the comparsion between different cells size for the scattering from a dielectric circular and square cylinder for $\epsilon r = 3$, radius = 0.3 λ ($k_o a = 1.88$), for TM and TE polarization respectively. Observed that, unlike the square cylinder case, the results for the circular cylinder oscillate about the exact solution as the cell size decreases or the number of cells per dielectric wavelength increases. However, the oscillations are quite small. This suggests that the jagged edges cause minor oscillations, and are not the main source of the error. We tried to verify this by computing the RCS versus $k_o a$ of the square and circular cylinders with large permittivity ($\epsilon r = 10$), where k_o is the free space wave number, and 'a' is

		Circular Cylinder $\epsilon_r = 3$, $k_o a = 1.88$		Square Cylinder $\epsilon_r = 3$, $k_o a = 1.88$	
N	λ/Δ *	RCS 0 (dB)	RCS 180 (dB)	RCS 0 (dB)	RCS 180 (dB)
5	10	0.39695	10.19377	-2.16554	11.36273
6	12	0.48410	9.94038	-2.21087	11.37733
7	13	0.29716	10.38816	-2.23595	11.38627
8	15	0.32672	10.34977	-2.25133	11.39211
9	17	0.41695	10.16945	-2.26145	11.39614
10	19	0.44676	10.07070	-2.26848	11.39903
11	21	0.43276	10.09018	-2.27357	11.40117
12	23	0.48777	9.97323	-2.27737	11.40280
13	25	0.38840	10.21299	-2.28030	11.40406
14	27	0.44939	10.10223	-2.28259	11.40507
15	29	0.41067	10.15351	-2.28443	11.40588
Exact Soln.		0.48667	10.02144		

Table 1. Comparison between Bistatic scattering of Circular and Square dielectric Cylinders, TM polarization using different size of square cells.

* λ dielectric wavelength
Δ size of square cell
N number of segments per radius.

		Circular Cylinder $\epsilon r = 3$, $k_o a = 1.88$		Square Cylinder $\epsilon r = 3$, $k_o a = 1.88$	
N	λ/Δ *	RCS 0 (dB)	RCS 180 (dB)	RCS 0 (dB)	RCS 180 (dB)
5	10	-11.24765	8.97380	-11.40775	10.93251
6	12	-11.03964	8.71287	-11.37207	10.92116
7	13	-12.36419	8.93033	-11.33195	10.91392
8	15	-13.65737	9.12377	-11.29794	10.90898
9	17	-12.52884	8.86450	-11.27067	10.90544
10	19	-12.61856	8.86981	-11.24895	10.90280
11	21	-13.06285	8.90101	-11.23151	10.90077
12	23	-12.26397	8.71944	-11.21733	10.89916
13	25	-13.66110	8.97206	-11.20564	10.89785
14	27	-12.82131	8.97206	-11.19589	10.89678
15	29	-13.62015	8.93140	-11.19541	10.89599
Exact Soln.		-13.60743	8.85784		

Table 2. Comparison between Bistatic scattering of Circular and Square dielectric Cylinders, TE polarization using different size of square cells.

* λ dielectric wavelength
Δ size of square cell
N number of segments per radius.

the radius of the circular cylinder or half-side length of the square cylinder. The curves for different cell sizes agree quite closely up to a cylinder size of $k_o a$ equal to about 1.5 for both the square and circular cylinder (see Fig. 70). Especially notice that the scattering curves of the dielectric square cylinder strongly separate as $k_o a$ increases beyond 3.0. This result again indicates that the jagged edge in the circular cylinder case is not the main source of the error.

Despite our improved computational accuracy, the method of moments with pulse basis functions and point matching for bistatic TE scattering from large cylinders with large permittivities did not give accurate results. Some authors have suggested that the volume integral equation solved with pulse basis functions produces a false surface charge density [1]. Using pulse basis functions to represent the unknown polarization introduces fictitious charge layers at every cell boundary. Nevertheless, some researchers have been successful in obtaining accurate results with more sophisicated techniques, such as linear basis functions with polygonal cells [9], polyhedral cells [10], rooftops basis functions with triangular cells [11], square cells

[12], and tetrahedral cells [13]. Still, a serious drawback of these methods is the large number of unknowns required per cell.

Since the existing volume integral equation solved with pulse basis functions does not deal adequately with surface charge density in the TE polarization case, we are presently revising the formulation of the volume integral equation to retain pulse basis functions and yet avoid the fictitious charge density problem.

2. EXACT SOLUTION FOR THE CIRCULAR DIELECTRIC CYLINDER

Our first task is to generate a general computer code for the exact solution of bistatic scattering from a lossless dielectric circular cylinder (Fig. 1) The results of this code are then compared to the exact solutions found in many electromagnetics scattering books and papers. We select Ruck's Radar Cross Section Handbook [7] and Barber's Light Scattering by Particles book [8] as our reference for their more comprehensive examples.

With our exact code developed, the internal fields can also be obtained. This is done to see if there is any abnormality or large variation in magnitude and phase in the internal fields that requires special attention or treatment.

The exact solution is then compared to the MOM solutions using the center point, area and line integral approaches for evaluating the Green's function over the self cells to evaluate the bistatic scattering from an infinite circular lossless dielectric cylinder. Finally, we will apply the MOM codes to infinitely long square lossless dielectric cylinders.

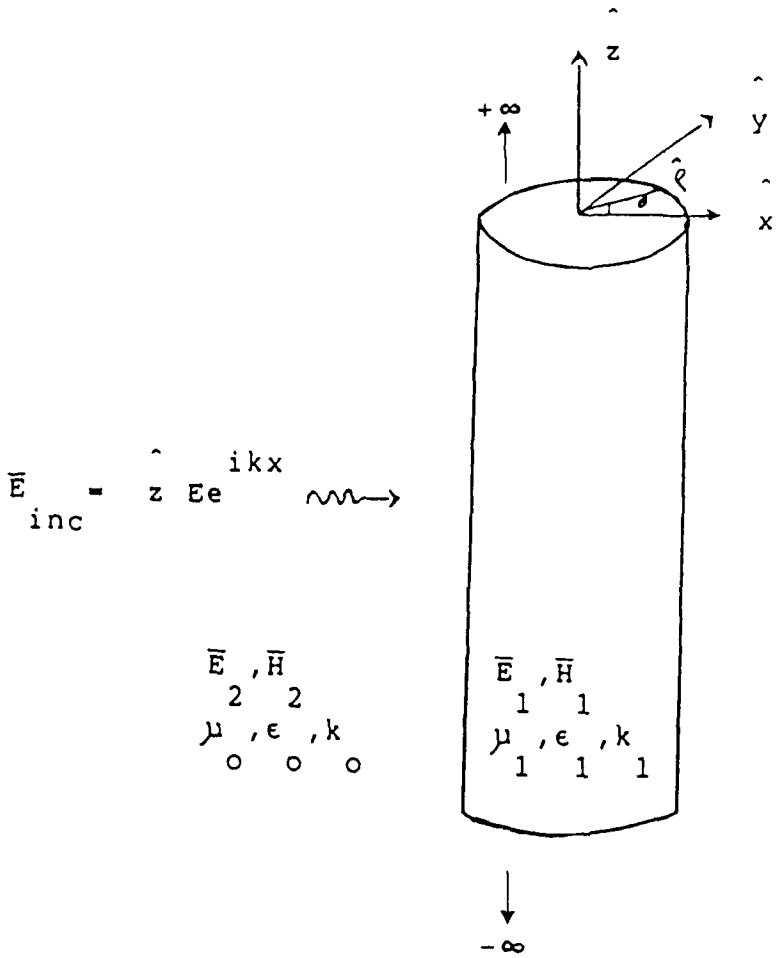

Fig. 1 Scattering from a dielectric cylinder

2.1 Brief Derivation of Exact Formula

2.1.1 TM Case

Let $\bar{E}^{inc} = \hat{z}\, e^{ikx}$ (1)

$$\bar{E}_1 = \hat{z}\, E_{1z} \qquad \rho \leq a \qquad (2)$$

$$\bar{E}_2 = \bar{E}_{scat} + \bar{E}_{inc} \qquad \rho \geq a \qquad (3)$$

From Maxwell's equation

$$\nabla \times \bar{E} = i\omega\mu\bar{H} \qquad (4)$$

$$H_\phi = \frac{i}{\omega\mu}\frac{\partial E_z}{\partial \rho} \qquad (5)$$

$$H_\rho = \frac{1}{i\rho\omega\mu}\frac{\partial E_z}{\partial \rho} \qquad (6)$$

Using boundary conditions for $\bar{E}_{tan}$ and $\bar{H}_{tan}$ at $\rho = a$

$$E_{1z} = E_{2z} \qquad (7)$$

$$H_{1\phi} = H_{2\phi} \qquad (8)$$

and letting

$$E_{1z} = \sum_{n=-\infty}^{\infty} a_n J_n(k_1\rho)\, e^{in\phi} \qquad \rho \le a \tag{9}$$

$$E_{2z} = \{\sum_{n=-\infty}^{\infty} t_n H_n^{(1)}(k_o\rho) + \sum_{n=-\infty}^{\infty} J_n(k_o\rho)\} e^{in\phi} \qquad \rho \ge a \tag{10}$$

$$H_{1\phi} = \frac{ik_1}{w\mu_1} \sum_{n=-\infty}^{\infty} a_n J_n'(k_1\rho)\, e^{in\phi} \qquad \rho \le a \tag{11}$$

$$H_{2\phi} = \frac{ik_o}{w\mu_o} \{\sum_{n=-\infty}^{\infty} t_n H_n^{(1)\prime}(k_o\rho) + \sum_{n=-\infty}^{\infty} J_n'(k_o\rho)\} e^{in\phi} \qquad \rho \ge a \tag{12}$$

we find

$$a_n = \frac{k_o\{J_n(k_o\rho)H_n^{(1)\prime}(k_o\rho) - H_n^{(1)}(k_o\rho)J_n'(k_o\rho)\}}{k_o J_n(k_o\rho)H_n^{(1)\prime}(k_1\rho) - k_1 H_n^{(1)}(k_o\rho)J_n'(k_1\rho)} \tag{13}$$

$$t_n = \frac{k_1 J_n(k_o\rho)J_n'(k_1\rho) - k_o J_n(k_1\rho)J_n'(k_o\rho)}{k_o J_n(k_o\rho)H_n^{(1)\prime}(k_1\rho) - k_1 H_n^{(1)}(k_o\rho)J_n'(k_1\rho)} . \tag{14}$$

2.1.2 TE Case

Let $\bar{H}^{inc} = \hat{z}\, e^{ikx}$ (1)

$$\bar{H}_1 = \hat{z}\, H_{1z} \qquad \rho \leq a \qquad (2)$$

$$\bar{H}_2 = \bar{H}_{scat} + \bar{H}_{inc} \qquad \rho \geq a \; . \qquad (3)$$

From Maxwell's equation

$$\nabla \times \bar{H} = -i\omega\epsilon\bar{E} \qquad (4)$$

$$E_\phi = \frac{1}{i\omega\epsilon}\frac{\partial H_z}{\partial \rho} \qquad (5)$$

$$E_\rho = \frac{i}{\omega\epsilon}\frac{\partial H_z}{\partial \rho} \; . \qquad (6)$$

Using boundary conditions for $\bar{E}_{tan}$ and $\bar{H}_{tan}$ at $\rho = a$

$$H_{1z} = H_{2z} \qquad (7)$$

$$E_{1\phi} = E_{2\phi} \qquad (8)$$

and letting

$$H_{1z} = \sum_{n=-\infty}^{\infty} b_n J_n(k_1\rho)\, e^{in\phi} \qquad \rho \le a \tag{9}$$

$$H_{2z} = \{\sum_{n=-\infty}^{\infty} s_n H_n^{(1)}(k_o\rho) + \sum_{n=-\infty}^{\infty} J_n(k_o\rho)\}e^{in\phi} \qquad \rho \ge a \tag{10}$$

$$E_{1\phi} = \frac{k_1}{i\omega\epsilon_1} \sum_{n=-\infty}^{\infty} b_n J_n'(k_1\rho)\, e^{in\phi} \qquad \rho \le a \tag{11}$$

$$E_{2\phi} = \frac{k_o}{i\omega\epsilon_o}\{\sum_{n=-\infty}^{\infty} s_n H_n^{(1)\prime}(k_o\rho) + \sum_{n=-\infty}^{\infty} J_n'(k_o\rho)\}e^{in\phi} \qquad \rho \ge a \tag{12}$$

we find

$$b_n = \frac{\frac{k_o}{\epsilon_o}\{J_n(k_o\rho)H_n^{(1)\prime}(k_o\rho) - H_n^{(1)}(k_o\rho)J_n'(k_o\rho)\}}{\frac{k_o}{\epsilon_o}J_n(k_1\rho)H_n^{(1)\prime}(k_o\rho) - \frac{k_1}{\epsilon_1}H_n^{(1)}(k_o\rho)J_n'(k_1\rho)} \tag{13}$$

$$s_n = \frac{\frac{k_1}{\epsilon_1}J_n(k_1\rho)J_n'(k_o\rho) - \frac{k_o}{\epsilon_o}J_n(k_o\rho)J_n'(k_1\rho)}{\frac{k_o}{\epsilon_o}J_n(k_1\rho)H_n^{(1)\prime}(k_o\rho) - \frac{k_1}{\epsilon_1}H_n^{(1)}(k_o\rho)J_n'(k_1\rho)}\,. \tag{14}$$

3. RESULTS FROM THE EXACT CODE

The results for the far field scattering obtained from the exact solution in Section 2.1 of the dielectric lossless circular cylinder are compared to the exact solutions from Ruck's Radar cross section Handbook [7], (Figs. 2-3) and Barber's Computational Methods [8] (Figs. 4-10).

Figs. 2-3 show the normalized scattering cross section of a circular cylinder with $\epsilon r = 2.56$, $\mu r = 1.0$ with varying $k_o a$ for vertical polarization (TM) and perpendicular polarization (TE) respectively. Figs. 2a and 3a are the exact solutions from Ruck's book. Figs. 2b and 3b are from our simulation. The good agreement confirms our numerical code for the exact solution.

Figs. 4-5 show the angular scattered intensity for a circular cylinder with size parameter of 50 and an index of refraction of 1.5 for TM and TE polarization. The plotting increment is 0.2 degree. The solutions from Barber's book are shown in Figs. 4a and 5a respectively. Agreement with Barber's solution is good.

Figs. 6-7 show the internal intensity along the

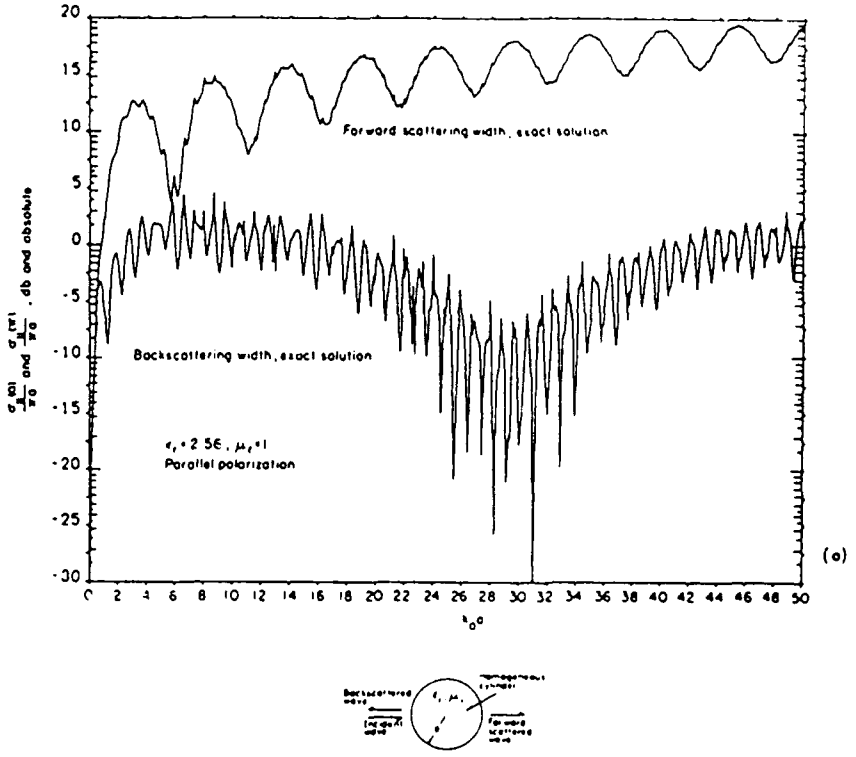

Normalized scattering widths for a long circular cylinder, er = 2.56, ur = 1, TM.

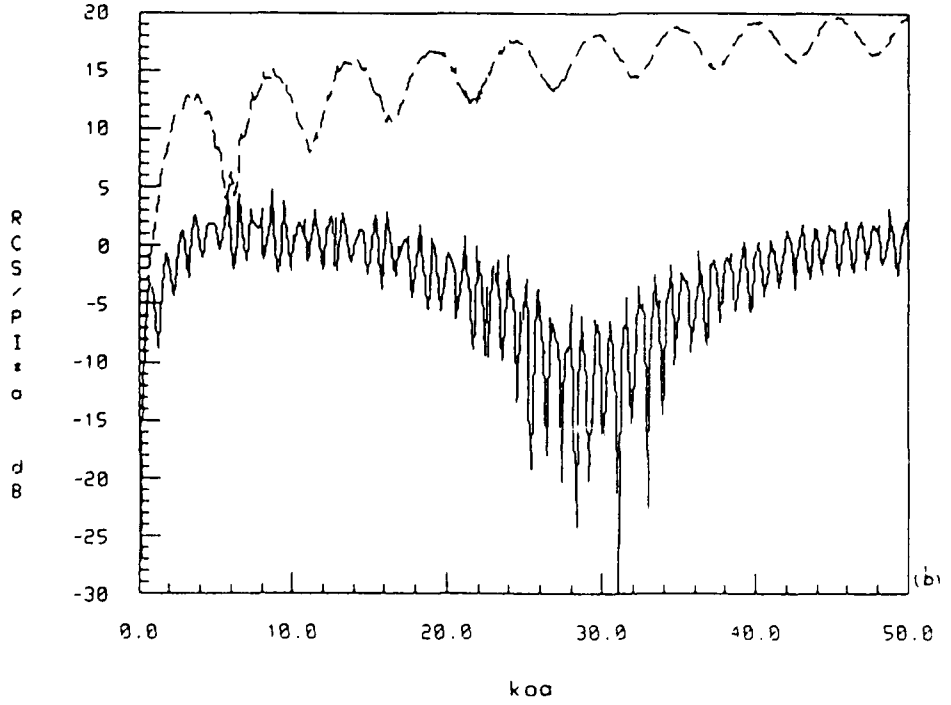

Fig. 2

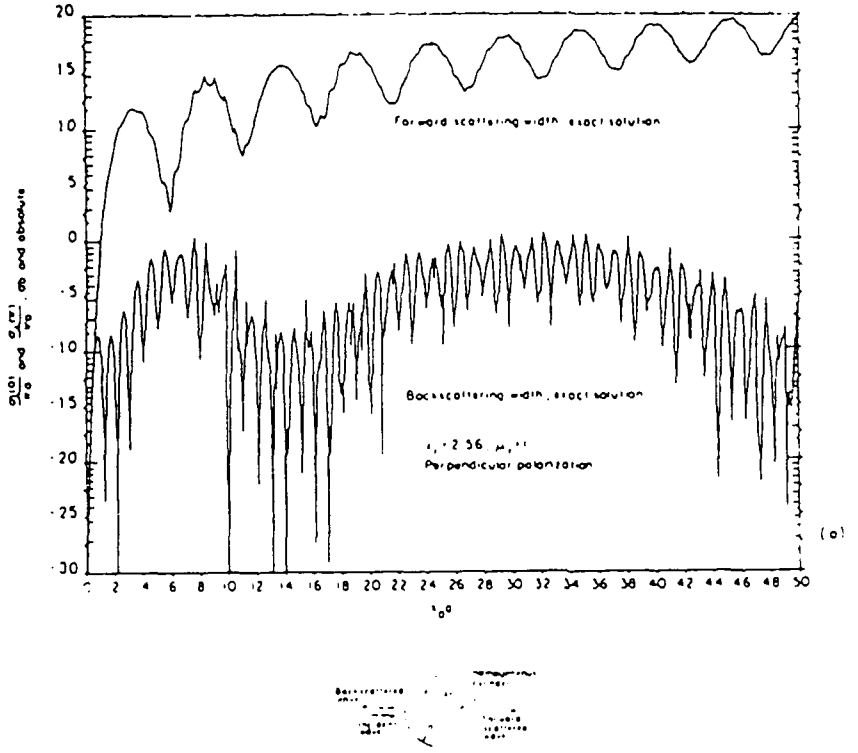

Normalized scattering widths for a long circular cylinder, $\epsilon_r = 2.56$, $\mu_r = 1$, TE.

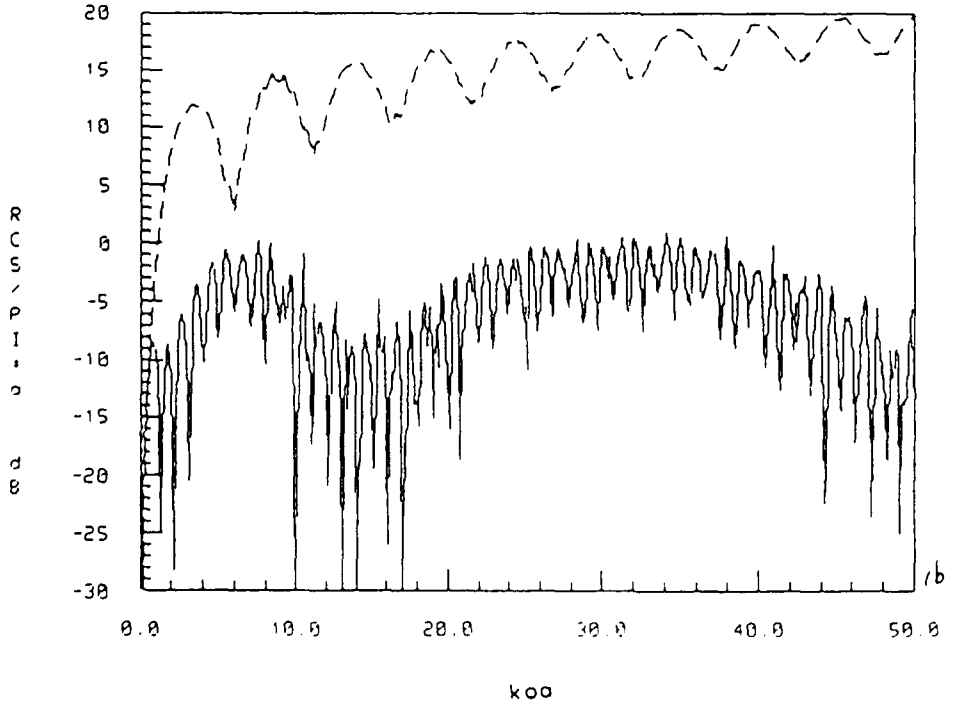

Fig. 3

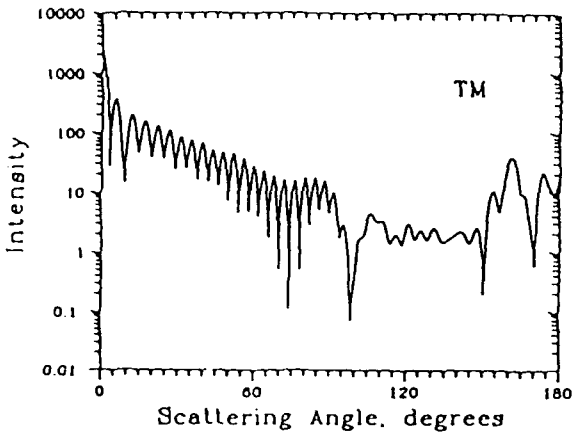

Fig 2 4 Angular scattered intensity for a circular cylinder with a size parameter of 50 and an index of refraction of 1 5 for TM polarization The plotting increment is 0.2° Sample numerical results are 2254, 6 482, and 18 14 at 0, 90, and 180°, respectively

a)

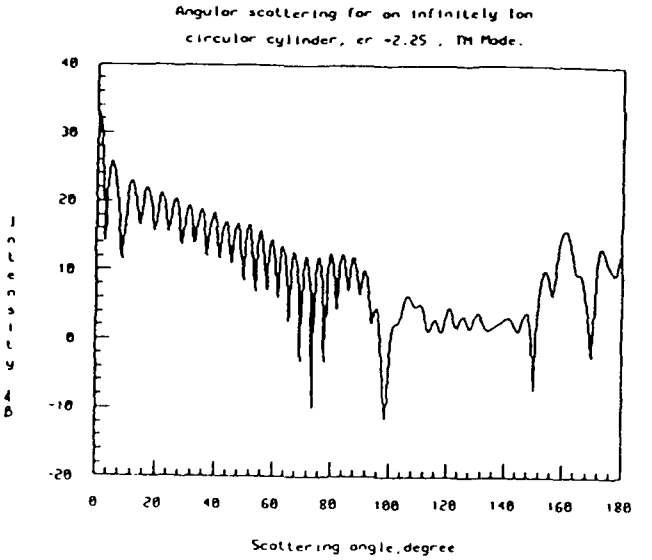

b)

Fig. 4

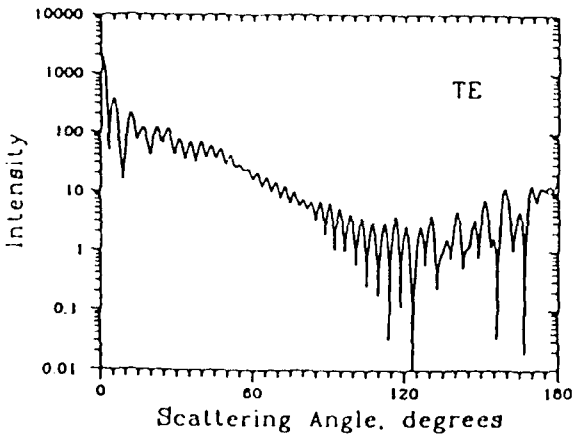

Fig 2 5 Angular scattered intensity for a circular cylinder with a size parameter of 50 and an index of refraction of 1 5 for TE polarization The plotting increment is 0 2° Sample numerical results are 2263, 6 809, and 19 37 at 0, 90, and 180°, respectively

a)

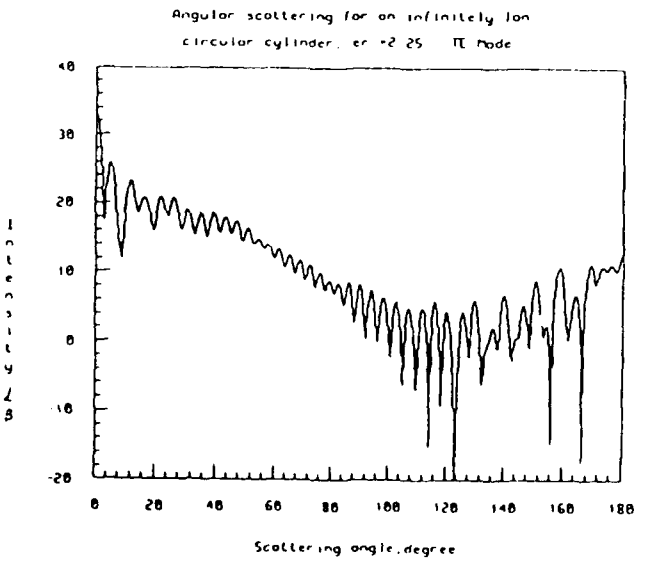

b)

Fig. 5

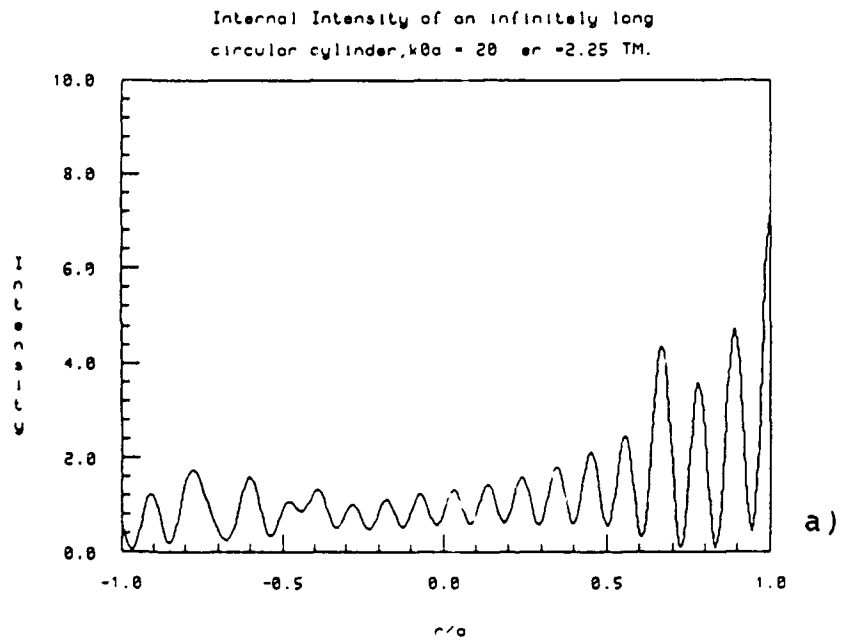

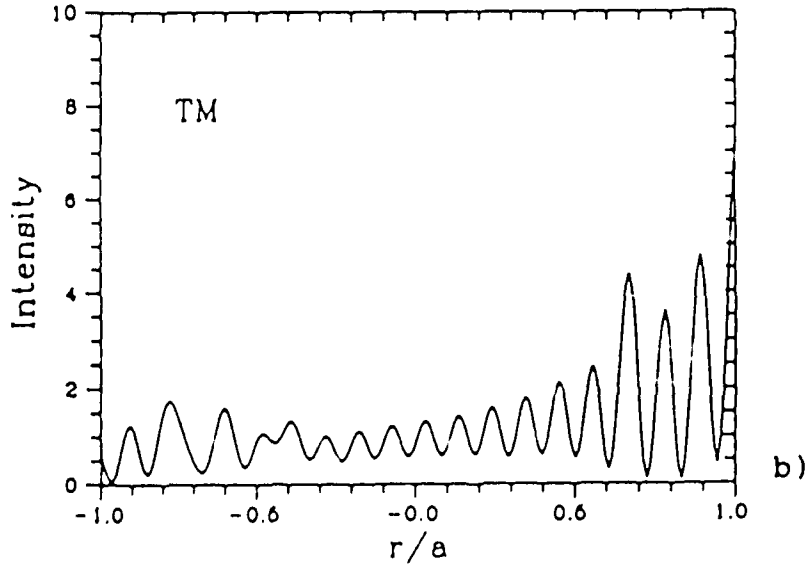

Fig. 2.28 The internal intensity along the x axis as a function of r/a for a circular cylinder with a size parameter of 20 and an index of refraction of 1.5 for TM polarisation. The incident wave propagates from left to right. The calculation used 400 points. Sample numerical results are 0.6810 and 7.569 at $r/a = -1$ and $+1$, respectively.

Fig. 6

x-axis as a function of r/a for a circular cylinder with a size parameter of 20 and an index of refraction 1.5 for TM and TE polarization. The incident wave propagates from left to right. The calculation used 400 points. The exact computed solutions (Figs. 6a-7a) are in excellent agreement with the reference solutions (Figs. 6b-7b).

Figs. 8-10 show the scattering intensity at 0, 90 and 180 degrees as a function of size parameter for a circular cylinder with an index refraction of 1.5 for TM polarization. The calculations used 1001 points. Figs. 8a-10a are the computed solutions. The agreement with the reference solutions (Fig. 8b-10b) are excellent.

We can thus conclude that our exact solution code for the scattering from a long circular cylinder is working reliably.

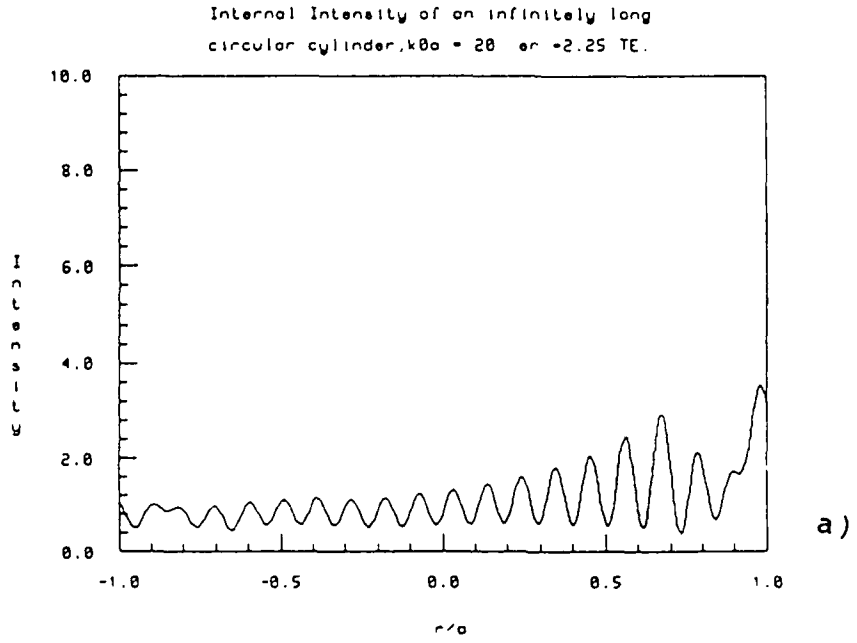

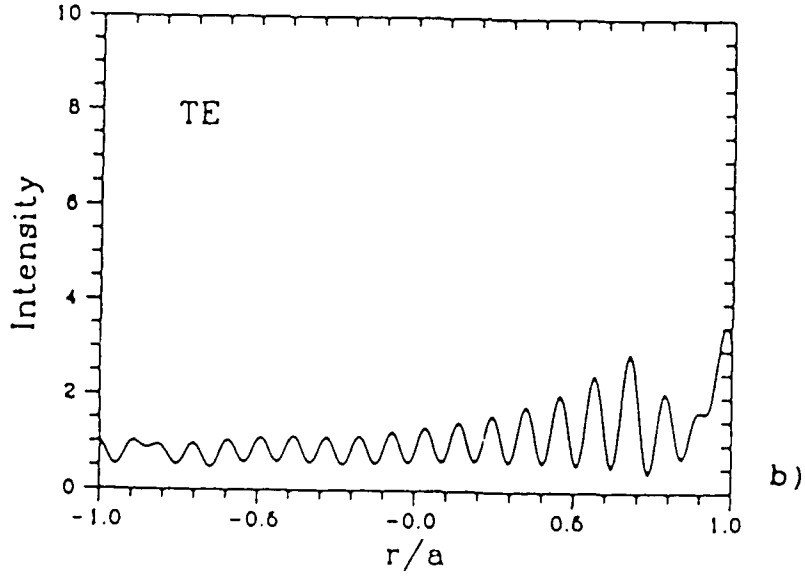

Fig. 2.30 The internal intensity along the x axis as a function of r/a for a circular cylinder with a size parameter of 20 and an index of refraction of 1.5 for TE polarization. The incident wave propagates from left to right. The calculation used 400 points. Sample numerical results are 1.055 and 3.131 at r/a = −1 and +1, respectively

Fig. 7

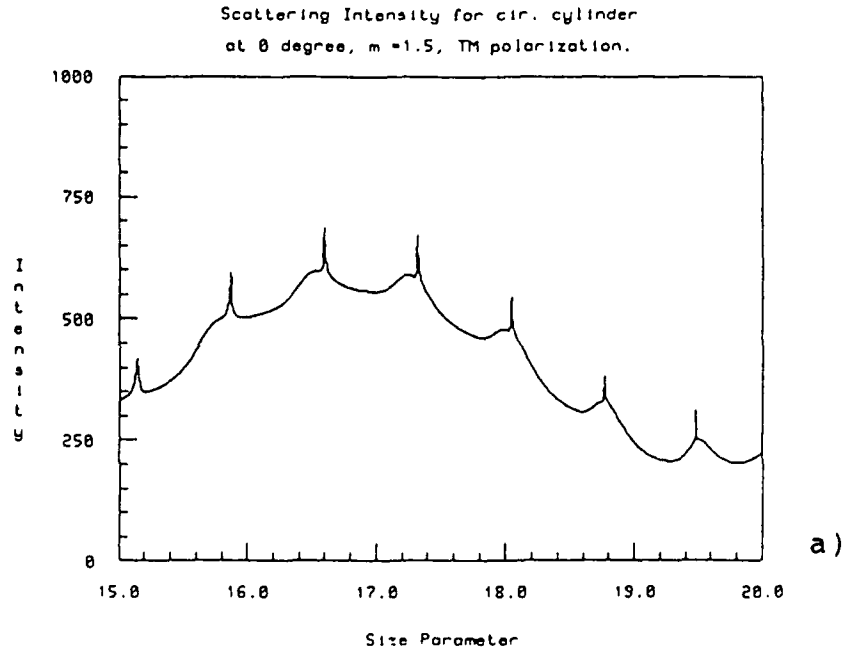

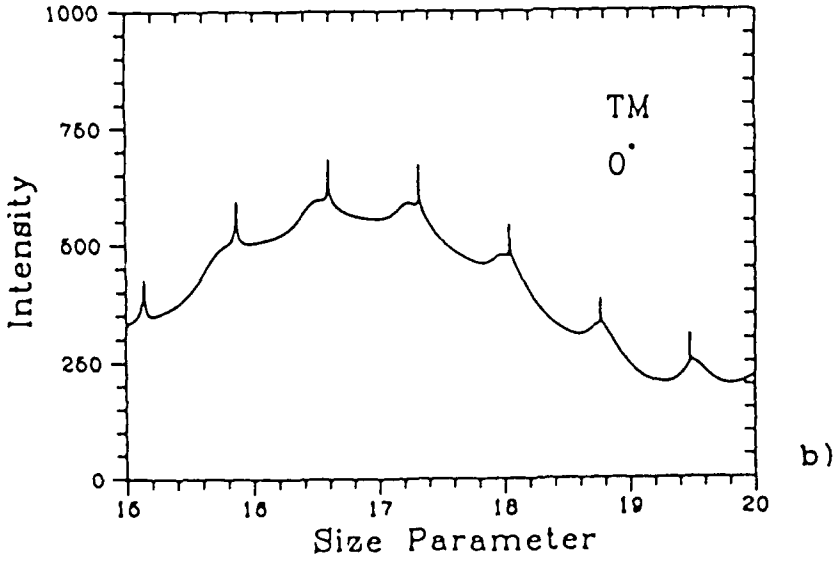

Fig. 2.12 Scattered intensity at 0° as a function of size parameter for a circular cylinder with an index of refraction of 1.5 for TM polarization. The calculation used 1001 points. Sample numerical results are 328.1, 512.5, and 222.3 at size parameters of 15, 17.5, and 20, respectively.

Fig. 8

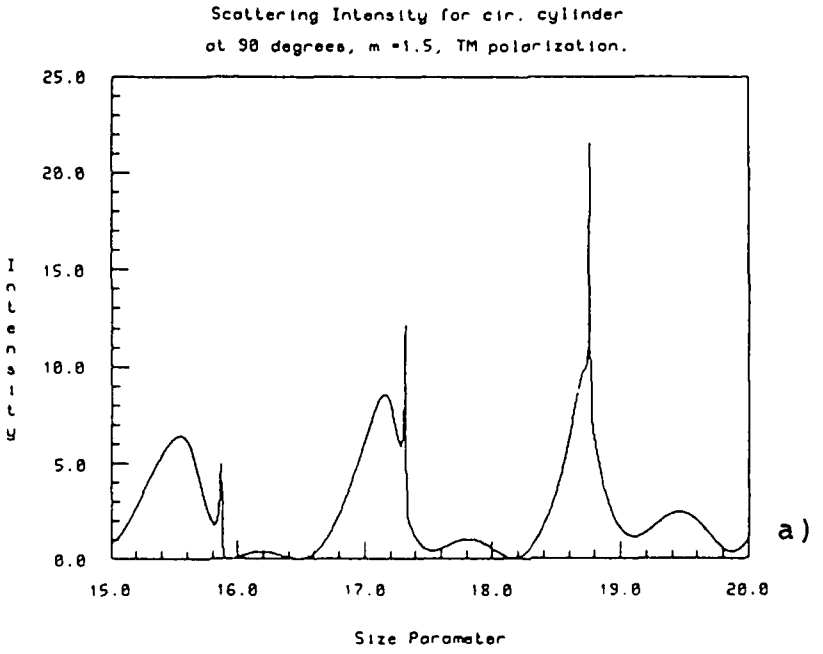

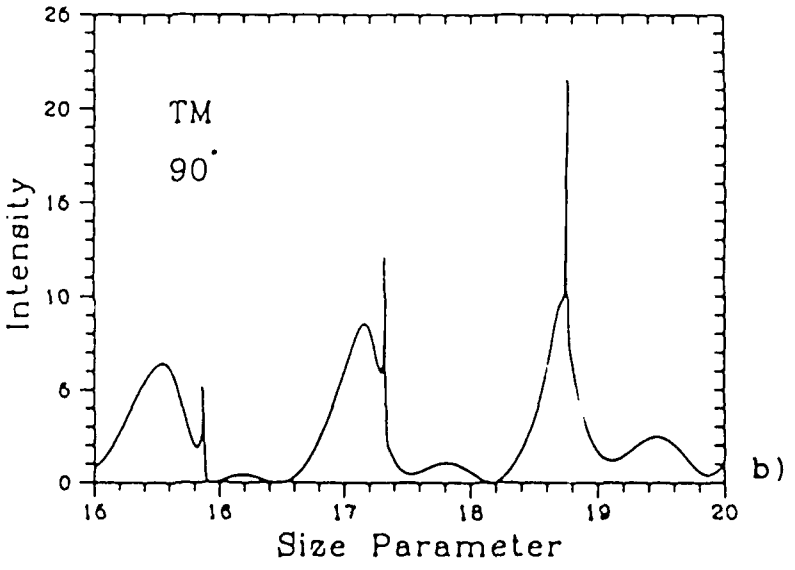

Fig. 2.13 Scattered intensity at 90° as a function of size parameter for a circular cylinder with an index of refraction of 1.5 for TM polarization. The calculation used 1001 points. Sample numerical results are 0.7907, 0.4846, and 1.073 at size parameters of 15, 17.5, and 20, respectively.

Fig. 9

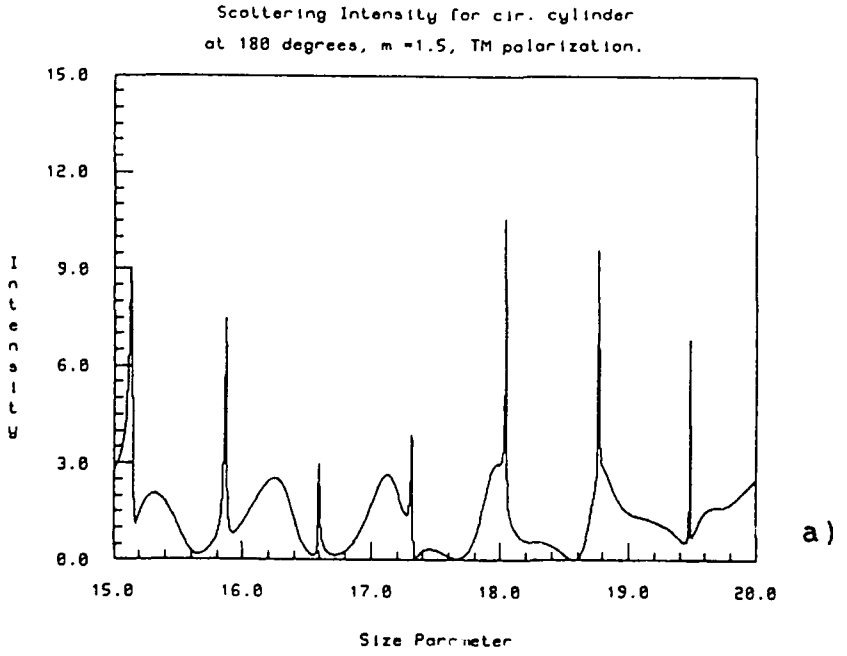

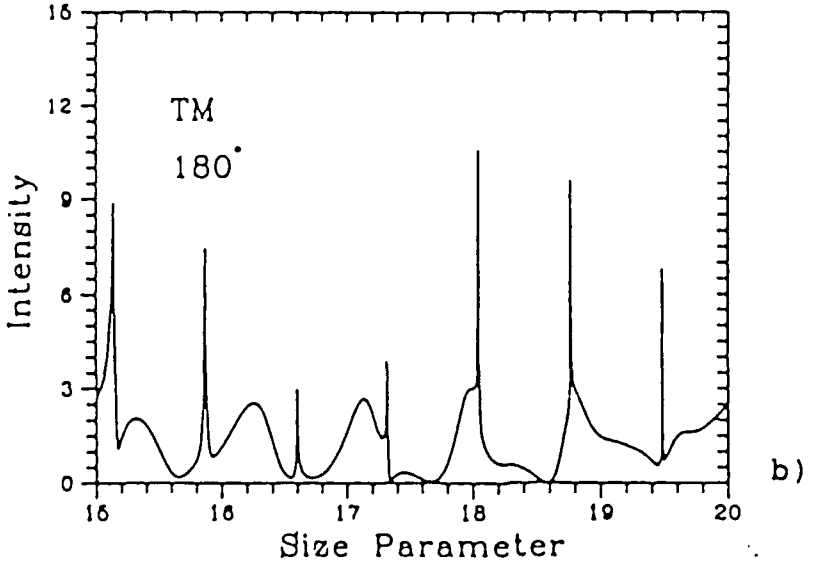

Fig. 2.14 Scattered intensity at 180° as a function of size parameter for a circular cylinder with an index of refraction of 1.5 for TM polarisation. The calculation used 1001 points. Sample numerical results are 2.725, 0.3091, and 2.519 at size parameters of 15, 17.5, and 20, respectively.

Fig. 10

4. INTERNAL FIELDS

The Internal fields of the dielectric circular cylinder can be computed using the equations of Section 2.1 for both the TM and TE cases.

The magnitudes of the E fields across the diameter with various relative permittivities of an infinitely long circular dielectric cylinder are shown in Figs. (11-15)a and the phases in Figs.(11-15)b. The H fields cases (TE polarization) are shown in Figs. 16-20.

Fig. 11 shows the normalized internal E field (TM case) versus distance (r/λ) across the diameter of the cylinder with size parameter $k_o a = 5$ and relative permittivity of 2.56. The calculation used 400 points in r/λ. The normalized internal field is defined as $|E|/|Emax|$ or $|H|/|Hmax|$.

Figs. 12-15 show the normalized internal E field versus distance (r/λ) across the cylinder ($k_o a = 5$) with relative permittivities = 4,10,20 and 50, respectively. Similarly, the H fields from TE polarization are shown in Figs. 16-20.

Figs. 21-30 show the normalized internal field

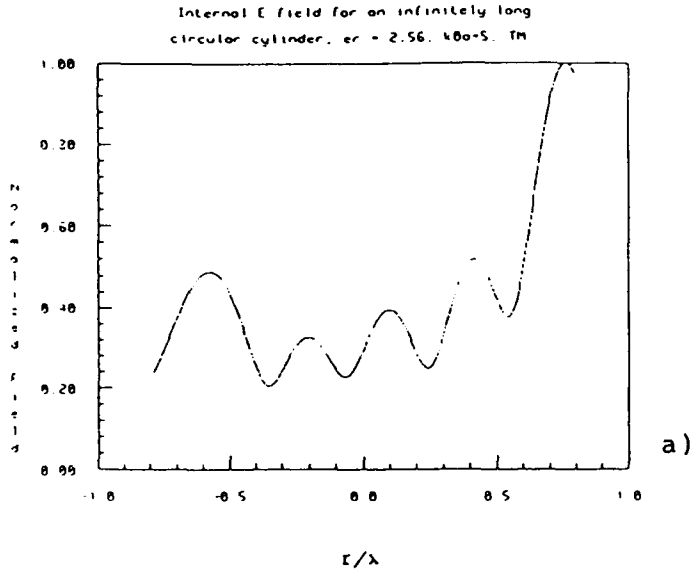

a)

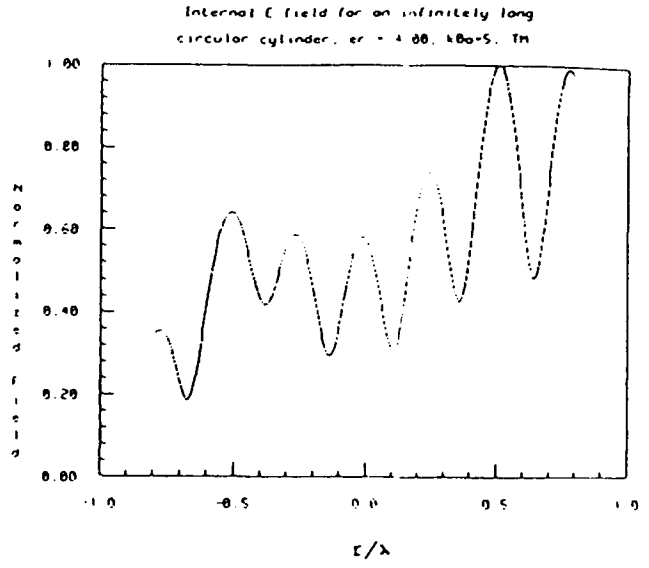

a)

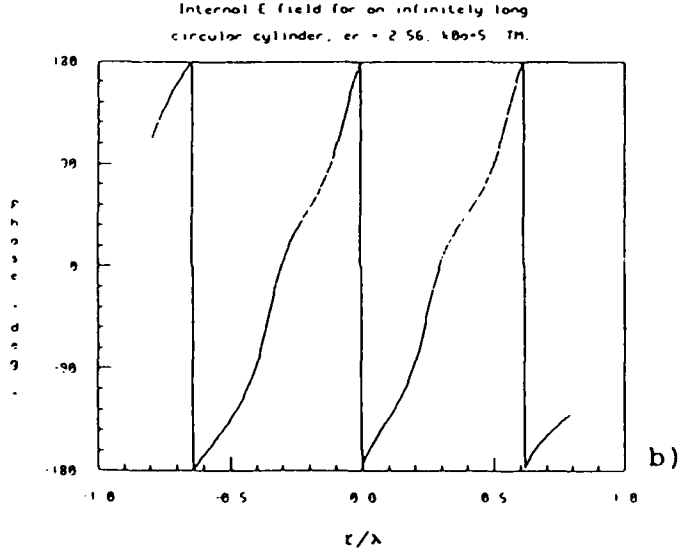

b)

Fig. 11

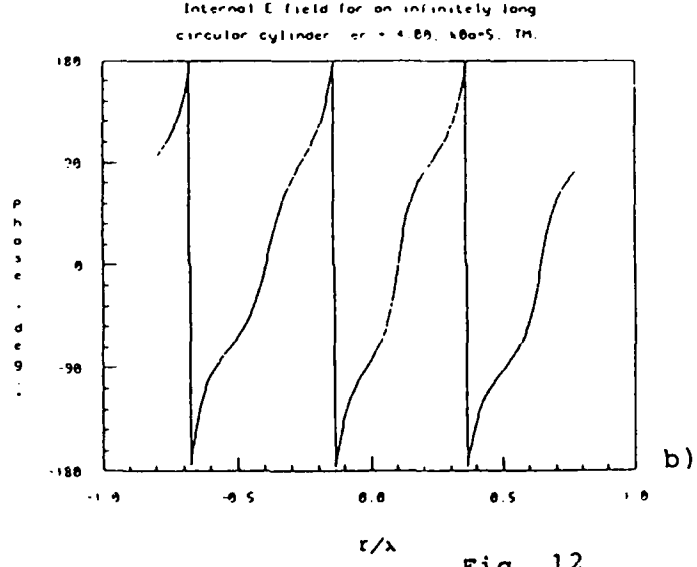

b)

Fig. 12

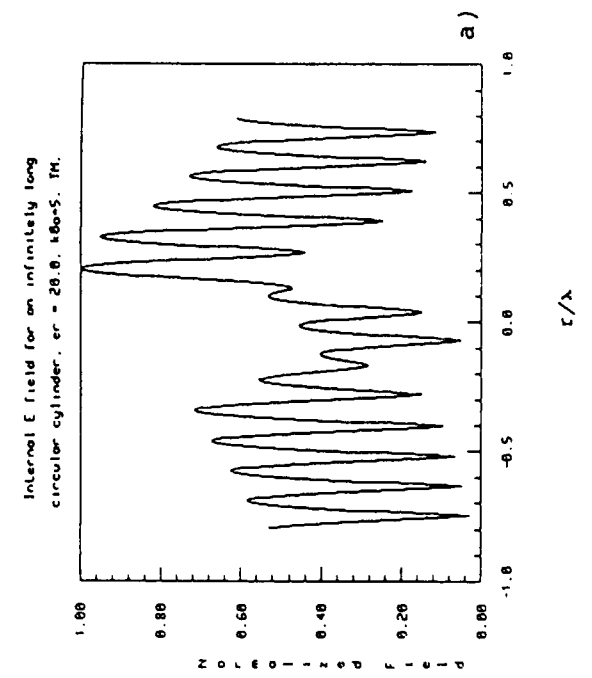
Internal E field for an infinitely long
circular cylinder, er = 20.0, k0a=5, TM.
a)
Normalized Field
r/λ

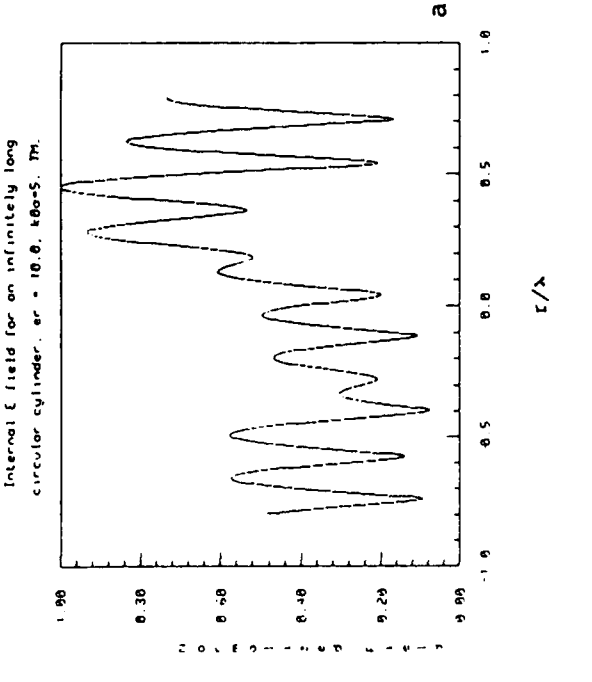
Internal E field for an infinitely long
circular cylinder, er = 10.0, k0a=5, TM.
a)
r/λ

Fig. 13

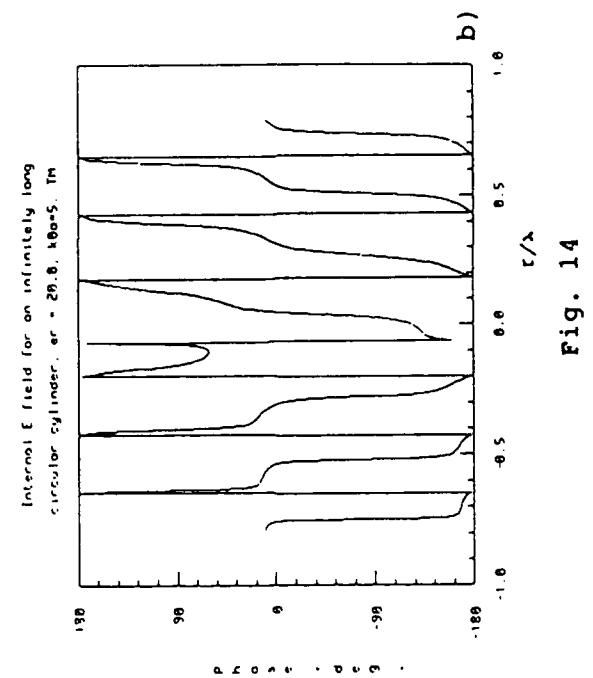
Internal E field for an infinitely long
circular cylinder, er = 20.0, k0a=5, TM
b)
r/λ

Fig. 14

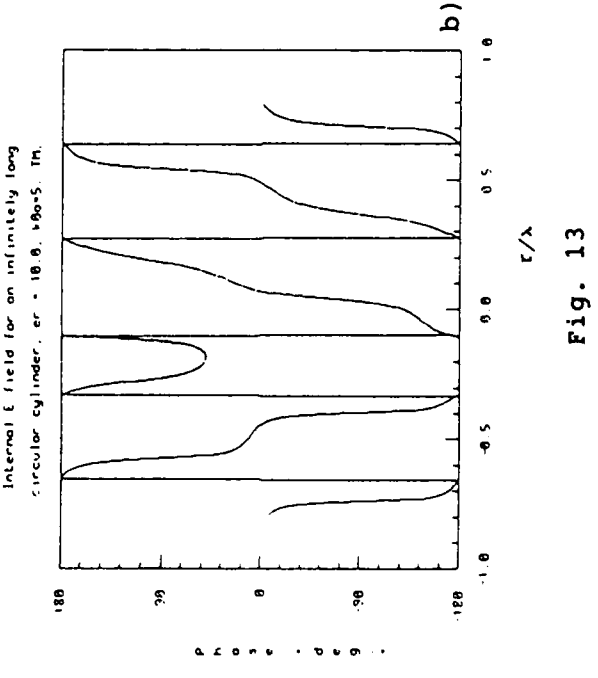
Internal E field for an infinitely long
circular cylinder, er = 10.0, k0a=5, TM.
b)
r/λ

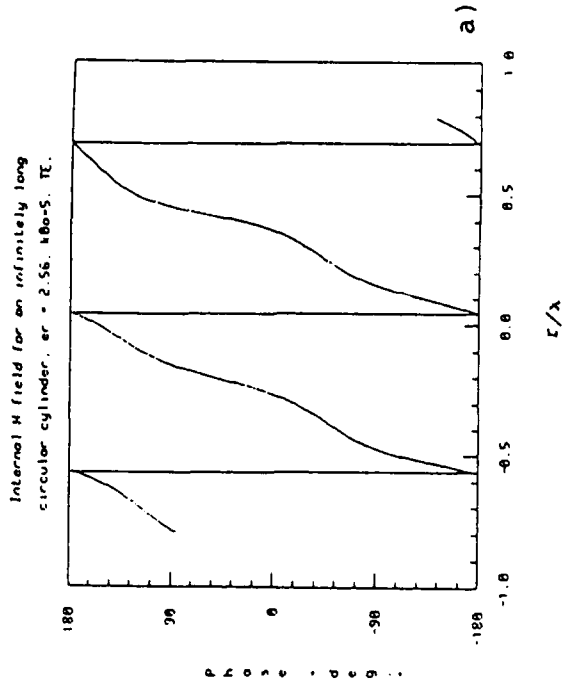
Internal H field for an infinitely long
circular cylinder, er = 2.56, k0a=5, TE.
a)
b)
r/λ
Phase - deg.

Fig. 16

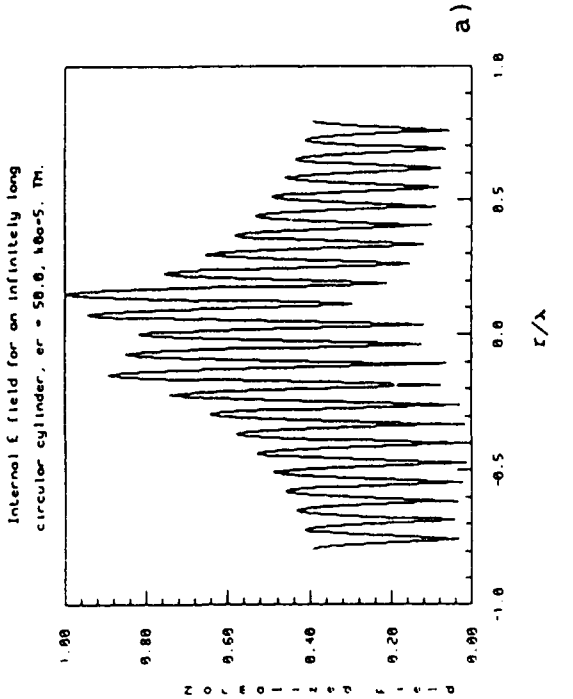
Internal E field for an infinitely long
circular cylinder, er = 50.0, k0a=5, TM.
a)
b)
r/λ
Normalized field

Fig. 15

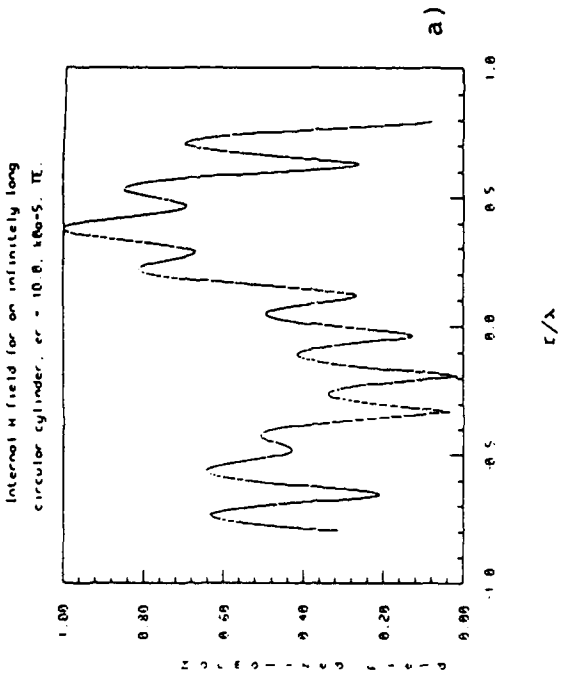
a)
Internal H field for an infinitely long
circular cylinder, er = 10.0, k0a=5, TE.
r/λ

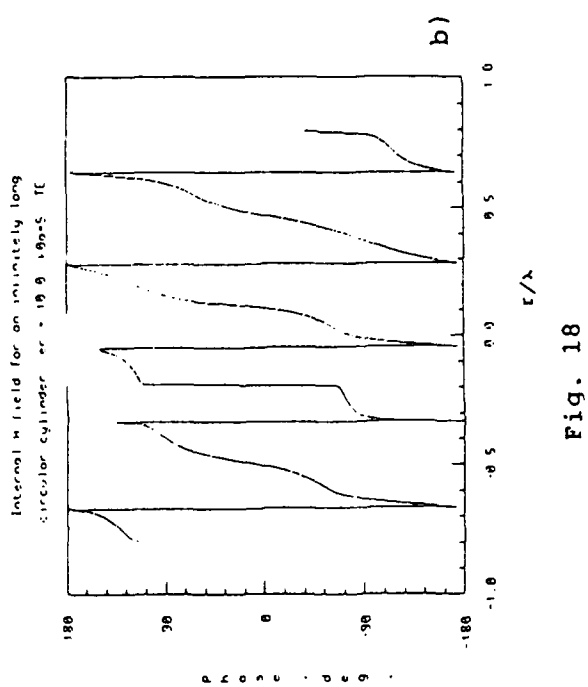
b)
Internal H field for an infinitely long
circular cylinder, er = 10.0, k0a=5, TE.
r/λ

Fig. 18

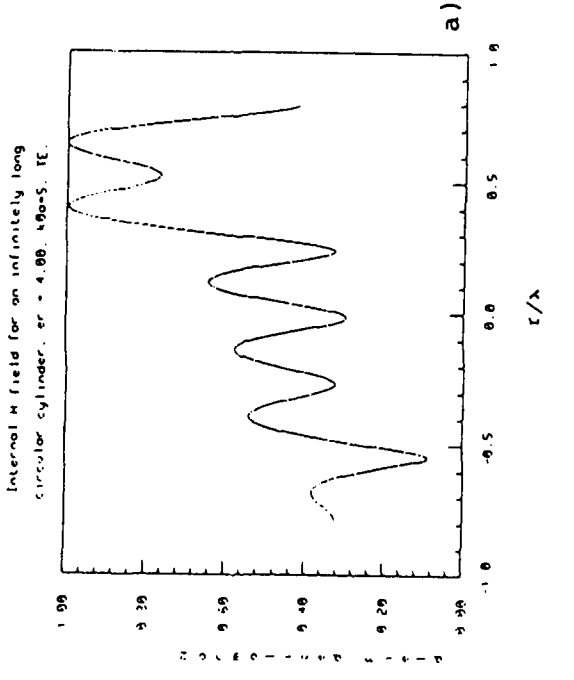
a)
Internal H field for an infinitely long
circular cylinder, er = 4.00, k0a=5, TE.
r/λ

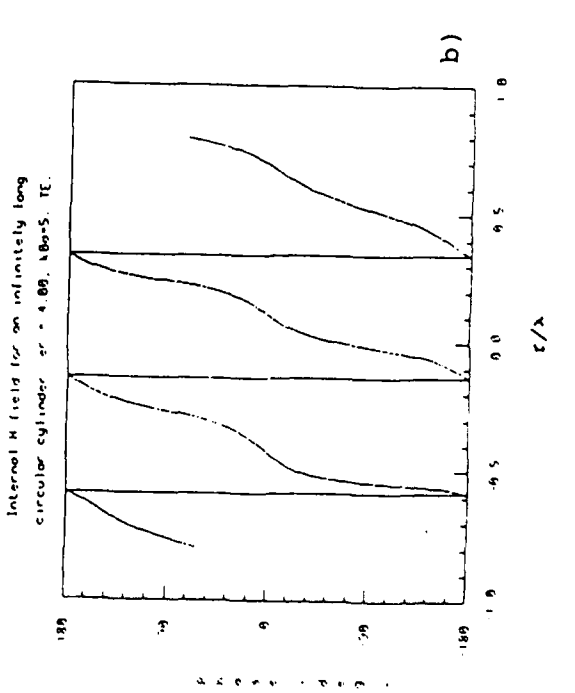
b)
Internal H field for an infinitely long
circular cylinder, er = 4.00, k0a=5, TE.
r/λ

Fig. 17

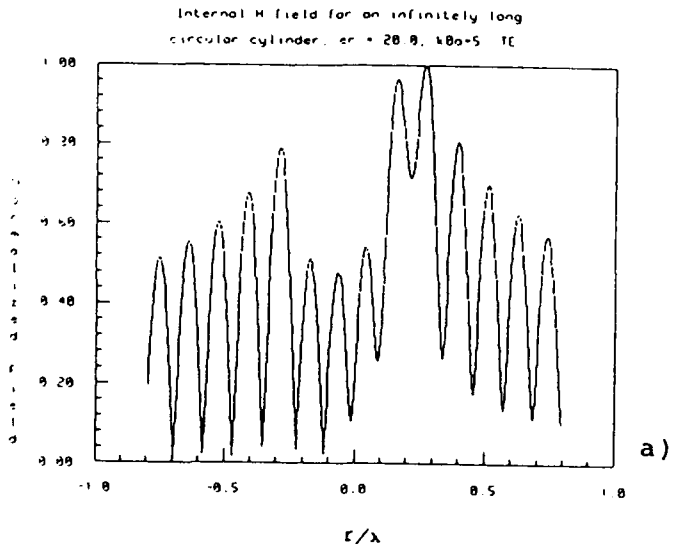

a)

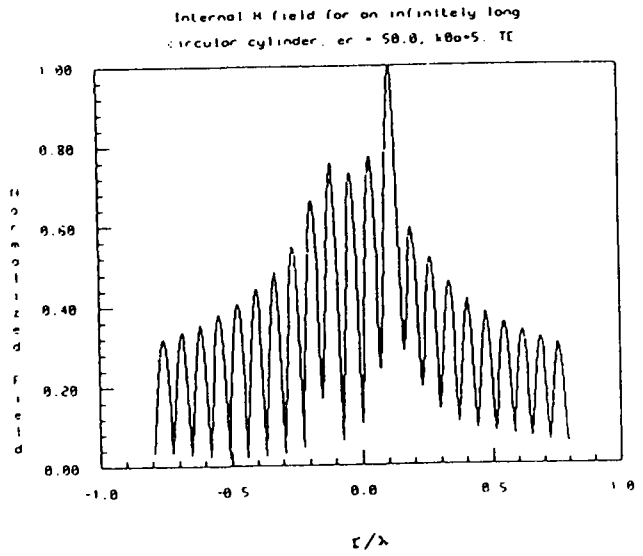

a)

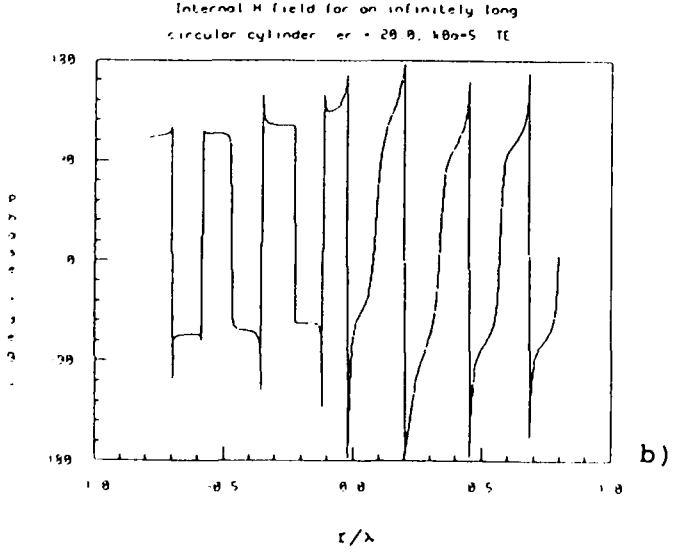

b)

Fig. 19

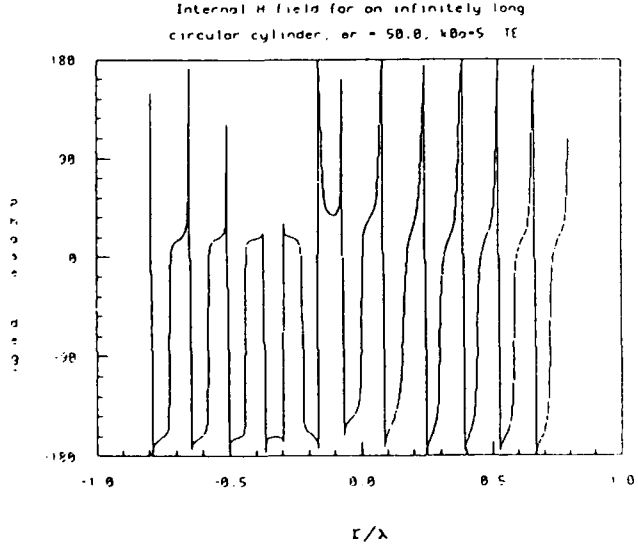

b)

Fig. 20

with various angles (0,45,90,135,180 degrees) and relative permittivities (2.56,4,10,20,50) as a function of distance across the radius of the cylinder for both polarizations. It can be seen that the internal field at 0 degrees when combined with the internal field at 180 degrees give the internal field across the dielctric circular cylinder (see Figs. 11-20).

The purpose of finding the internal fields of the dielectric lossless cylinder with different scattering angles and various permittivities is to see if the internal field varies unexpectedly rapidly near the surface of the large dielectric lossless cylinders. If this were the case, special treatment near the discontinuity or along the edges of the cylinder would be necessary, that is, more cell divisions would be required in our numerical solution. A standing wave pattern can be observed from the figures. Nevertheless, there is no sudden jump nor localization of the internal field near the rim of the large dielectric lossless cylinder. Our results indicate that even though the relative permittivity is large (ϵr=50), the size of the cylinder is still small ($k_o a$=5) enough that the internal fields did not accumulate near

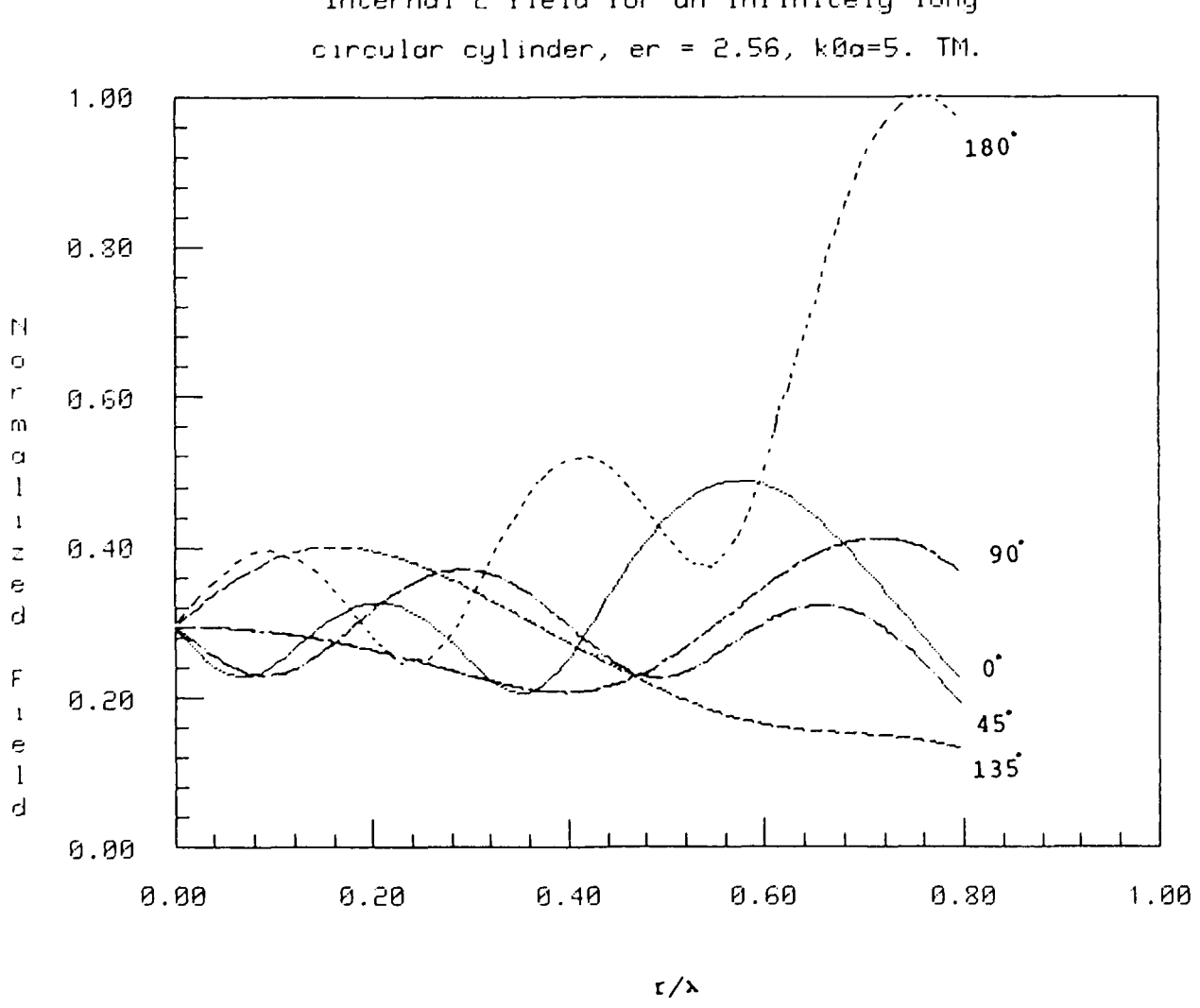
Internal E field for an infinitely long
circular cylinder, er = 2.56, k0a=5. TM.
Normalized Field
1.00
0.80
0.60
0.40
0.20
0.00
0.00
0.20
0.40
0.60
0.80
1.00
r/λ
180°
90°
0°
45°
135°

Fig. 21

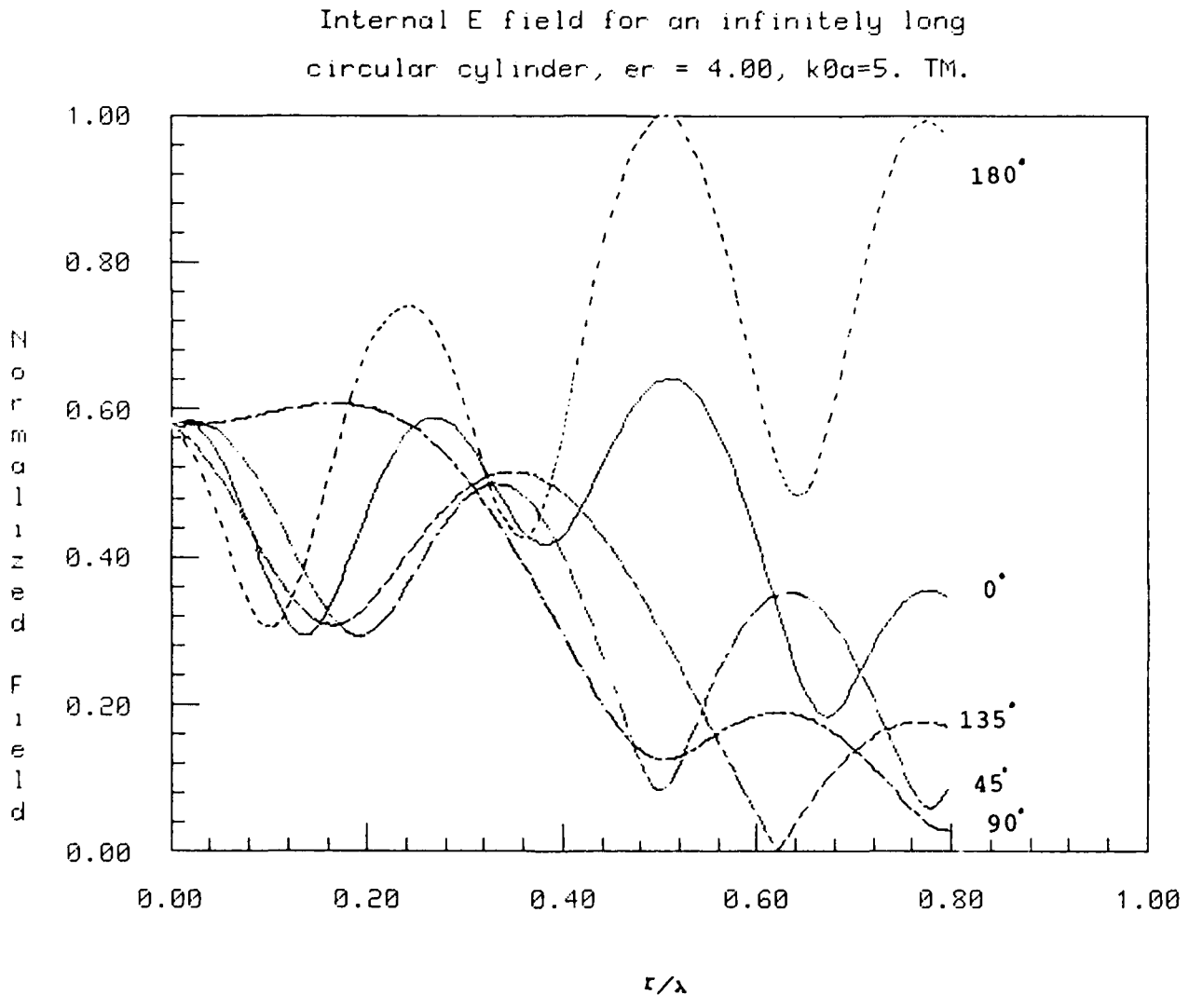
Internal E field for an infinitely long
circular cylinder, er = 4.00, k0a=5. TM.
Normalized Field
1.00
0.80
0.60
0.40
0.20
0.00
0.00
0.20
0.40
0.60
0.80
1.00
r/λ
180°
0°
135°
45°
90°

Fig. 22

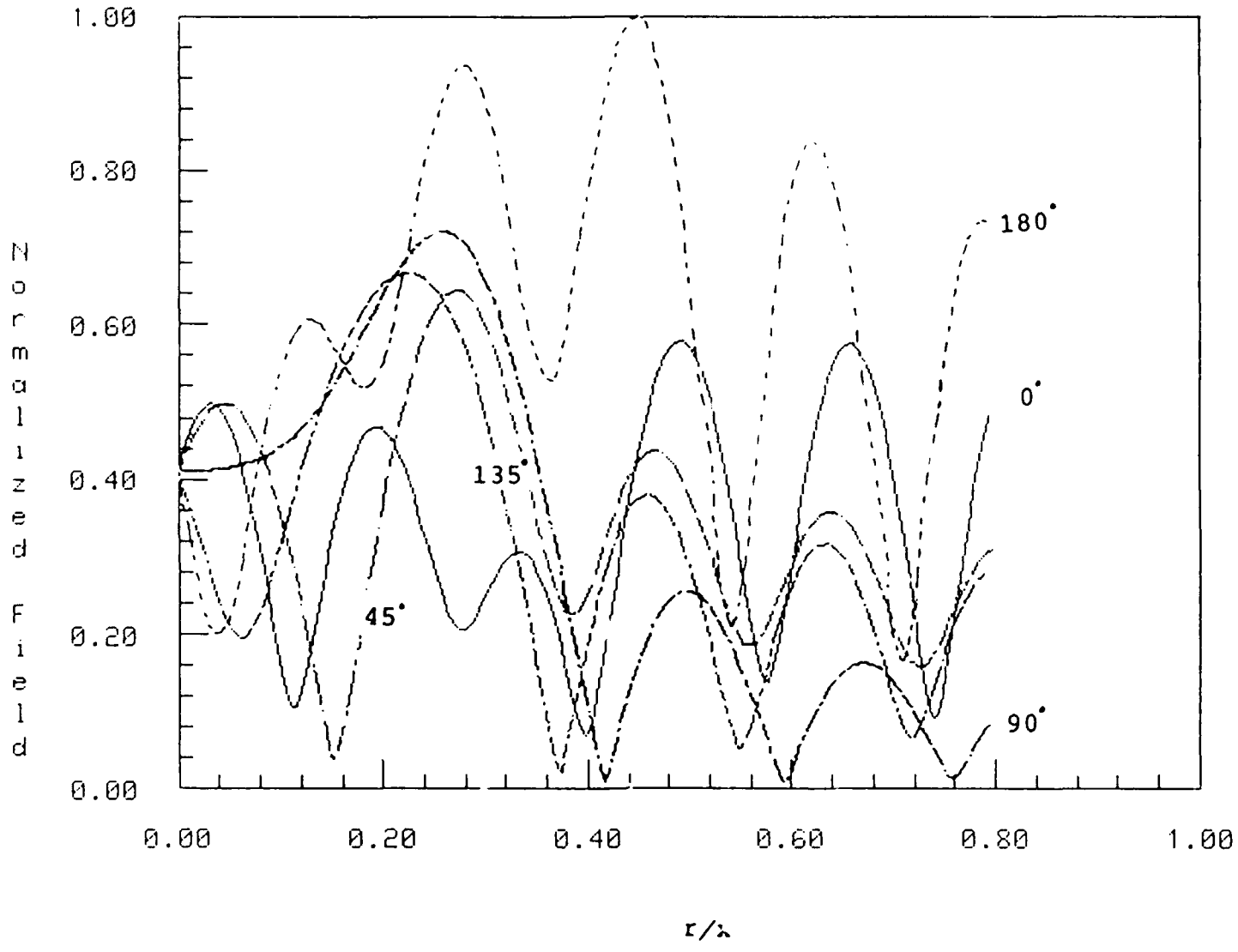
Internal E field for an infinitely long
circular cylinder, er = 10.0, k0a=5. TM.
Normalized Field
1.00
0.80
0.60
0.40
0.20
0.00
0.00
0.20
0.40
0.60
0.80
1.00
r/a
180°
0°
135°
45°
90°

Fig. 23

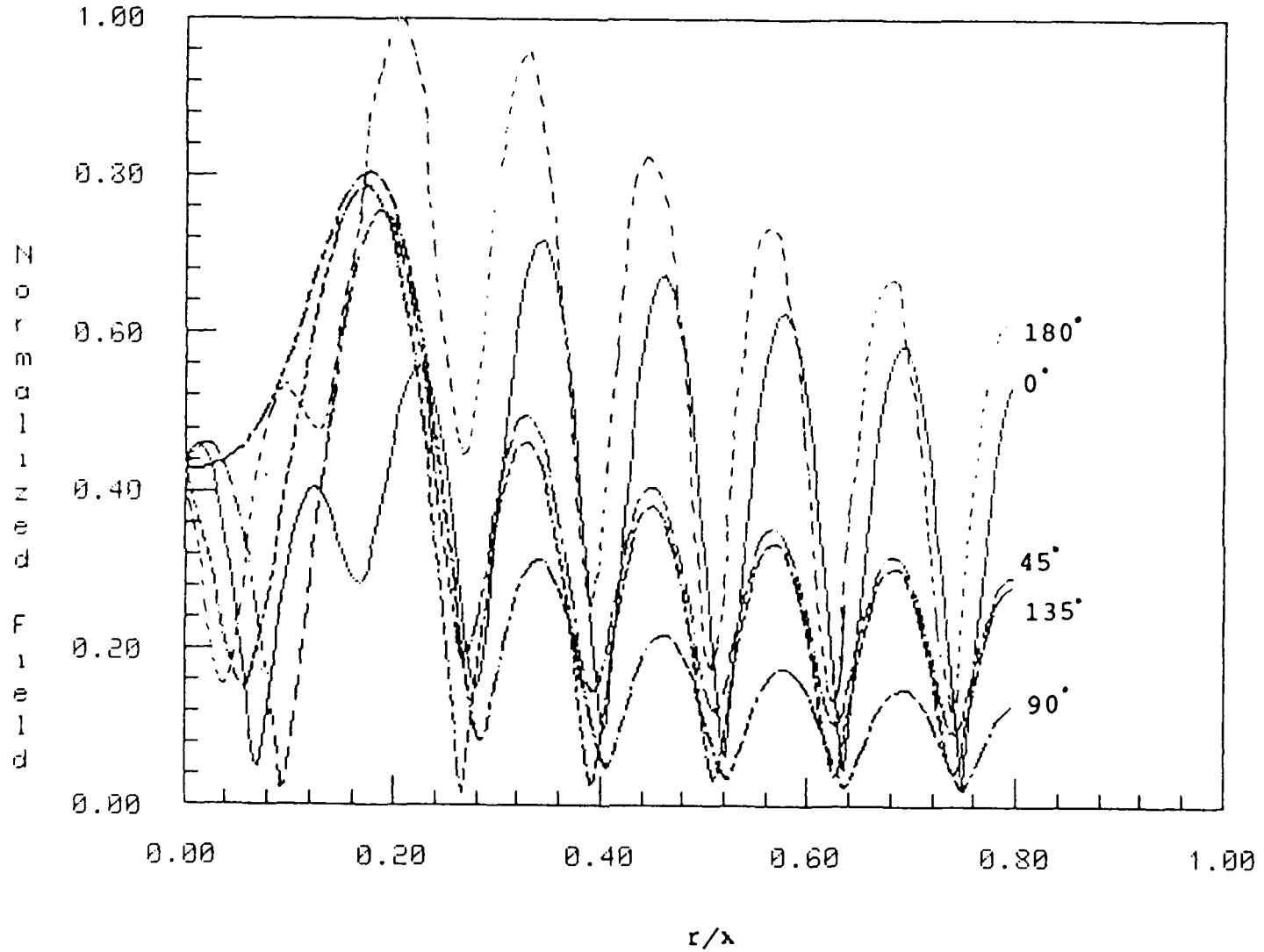
Internal E field for an infinitely long
circular cylinder, er = 20.0, k0a=5. TM.
Normalized field
1.00
0.80
0.60
0.40
0.20
0.00
0.00
0.20
0.40
0.60
0.80
1.00
r/λ
180°
0°
45°
135°
90°

Fig. 24

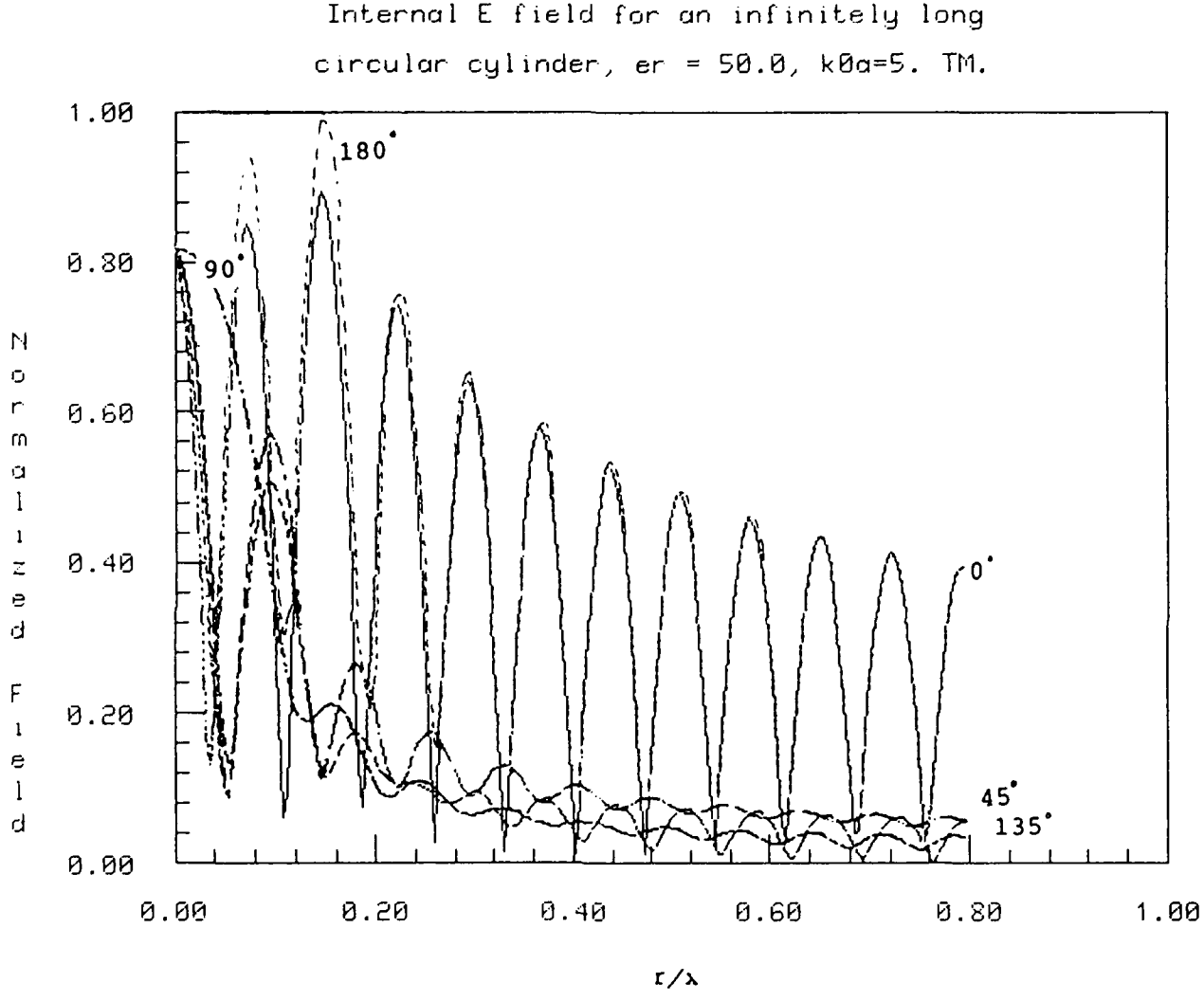
Internal E field for an infinitely long
circular cylinder, er = 50.0, k0a=5. TM.
1.00
0.80
0.60
0.40
0.20
0.00
Normalized Field
180°
90°
0°
45°
135°
0.00
0.20
0.40
0.60
0.80
1.00
r/λ

Fig. 25

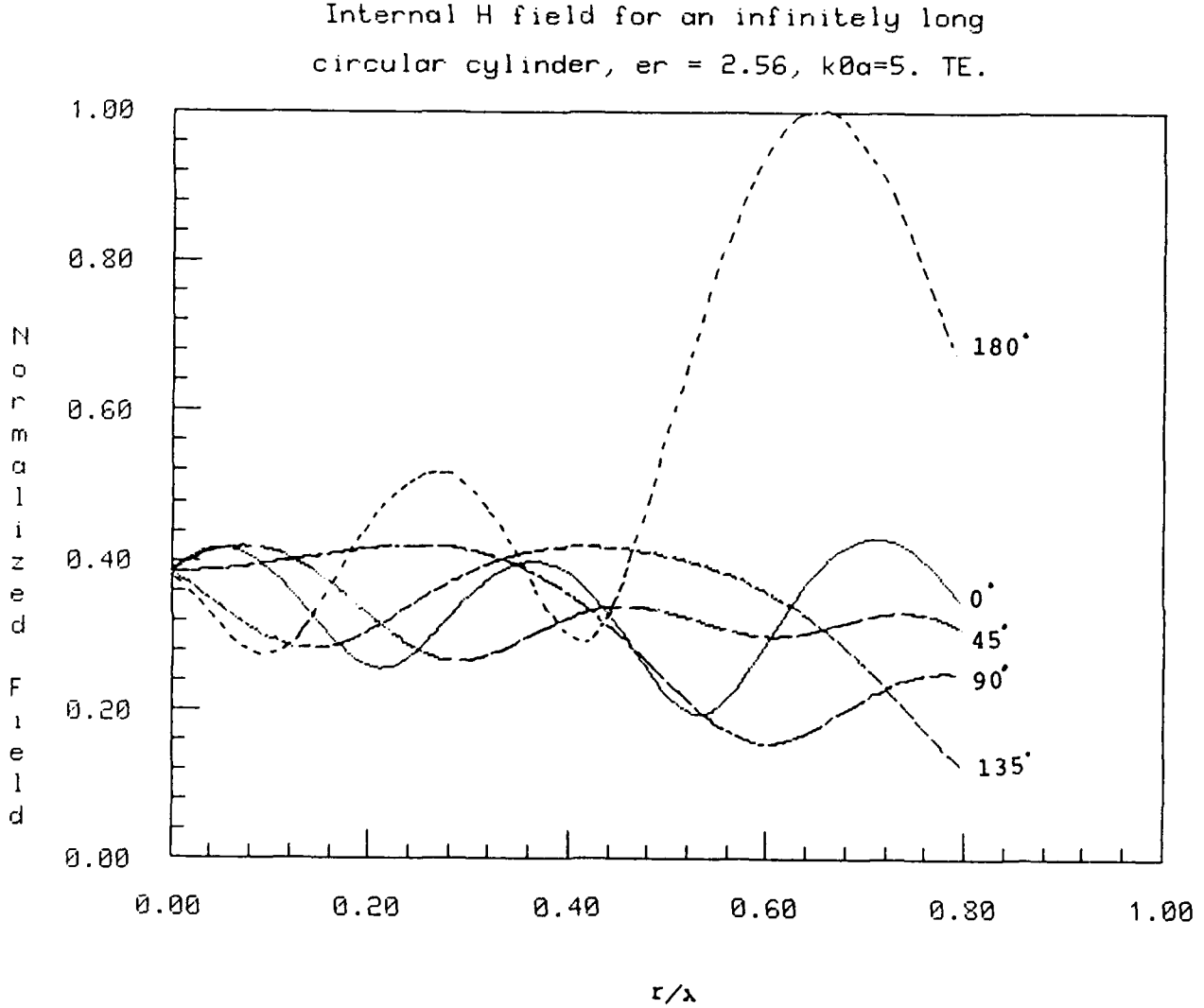
Internal H field for an infinitely long
circular cylinder, er = 2.56, k0a=5. TE.
Normalized Field
1.00
0.80
0.60
0.40
0.20
0.00
0.00
0.20
0.40
0.60
0.80
1.00
r/λ
180°
0°
45°
90°
135°

Fig. 26

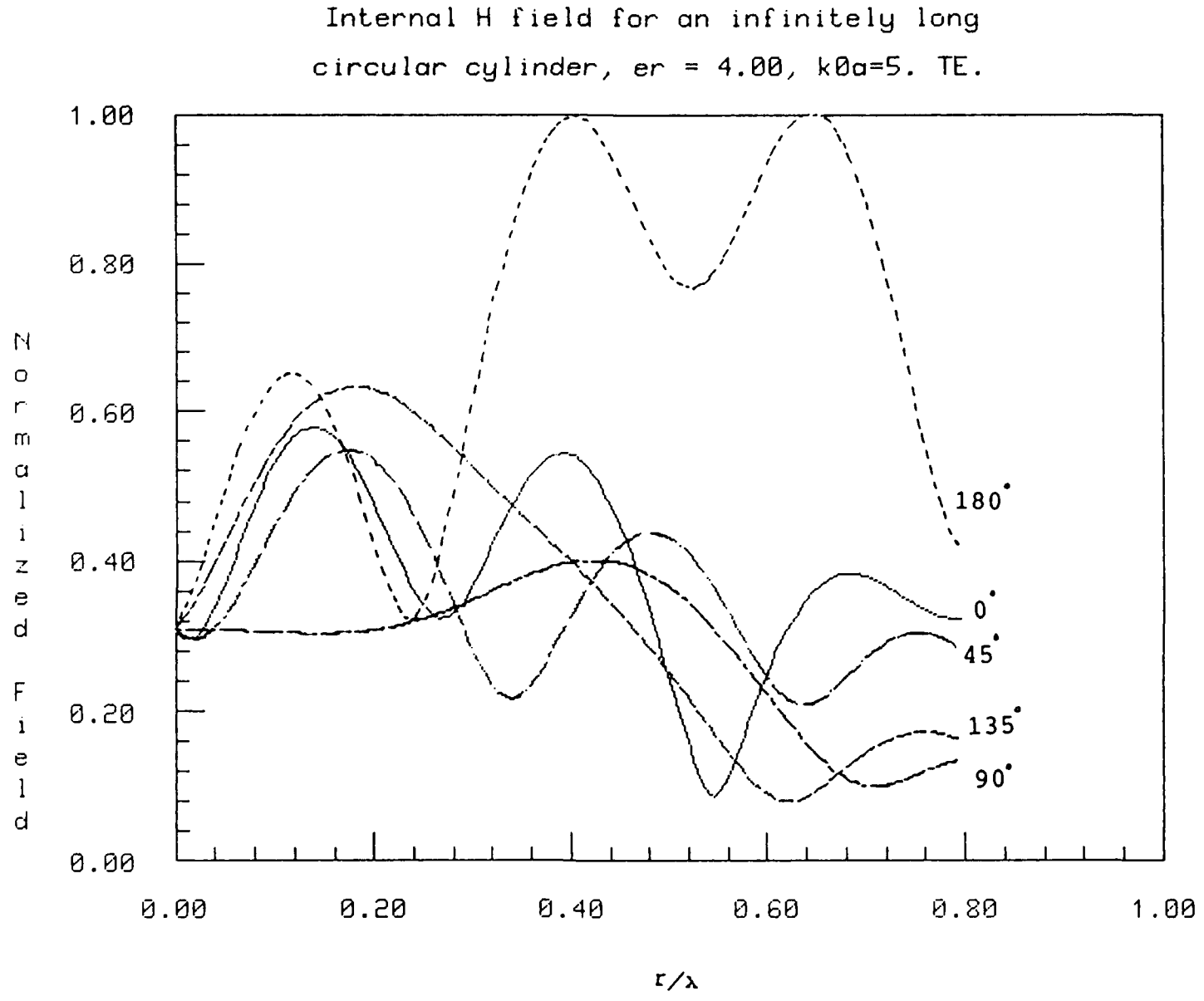
Internal H field for an infinitely long
circular cylinder, er = 4.00, k0a=5. TE.
1.00
0.80
0.60
0.40
0.20
0.00
Normalized Field
0.00
0.20
0.40
0.60
0.80
1.00
r/λ
180°
0°
45°
135°
90°

Fig. 27

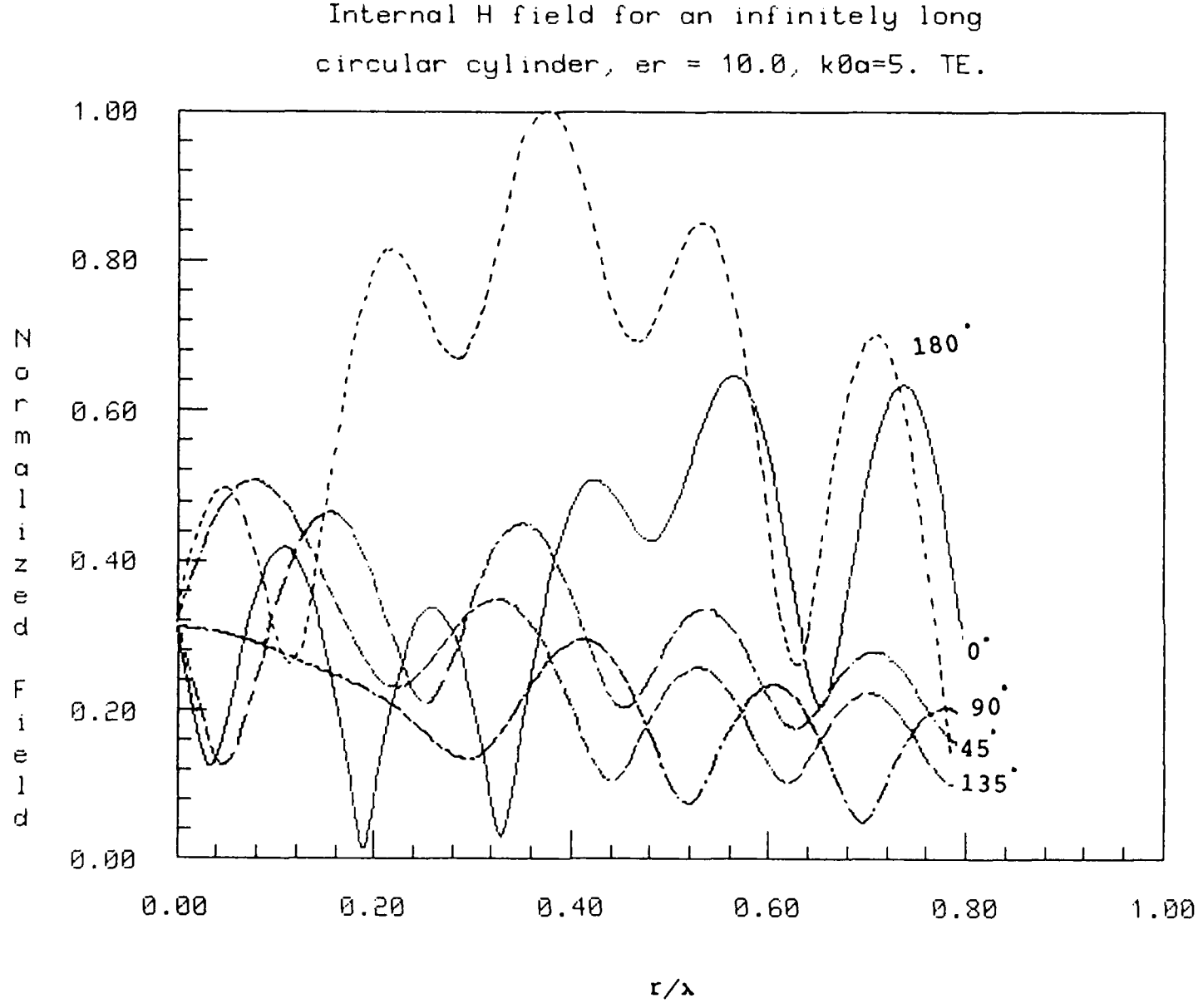
Internal H field for an infinitely long
circular cylinder, er = 10.0, k0a=5. TE.
1.00
0.80
0.60
0.40
0.20
0.00
Normalized Field
180°
0°
90°
45°
135°
0.00
0.20
0.40
0.60
0.80
1.00
r/λ

Fig. 28

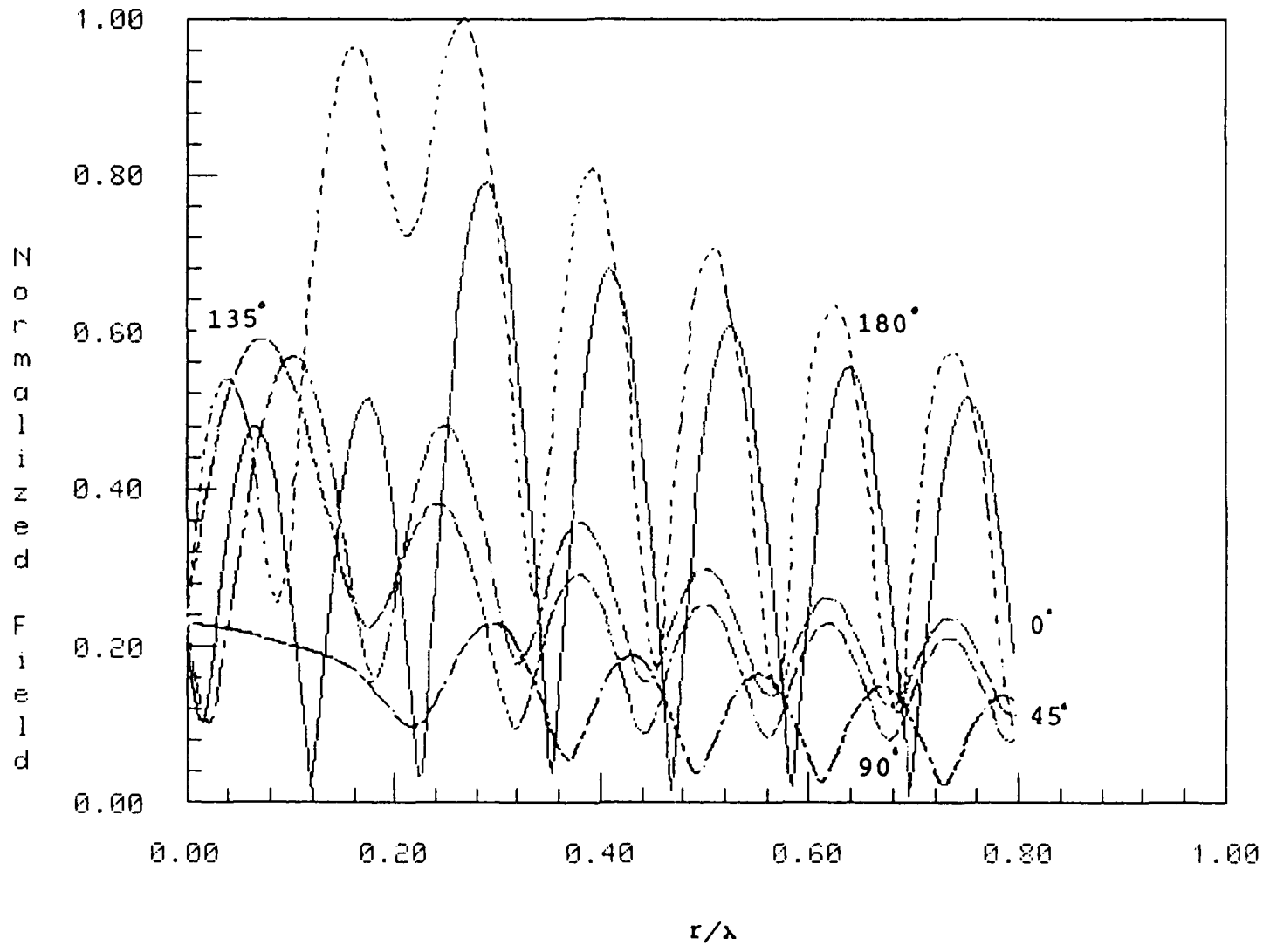
Internal H field for an infinitely long
circular cylinder, er = 20.0, k0a=5. TE.
Normalized Field
1.00
0.80
0.60
0.40
0.20
0.00
0.00
0.20
0.40
0.60
0.80
1.00
r/λ
135°
180°
0°
45°
90°

Fig. 29

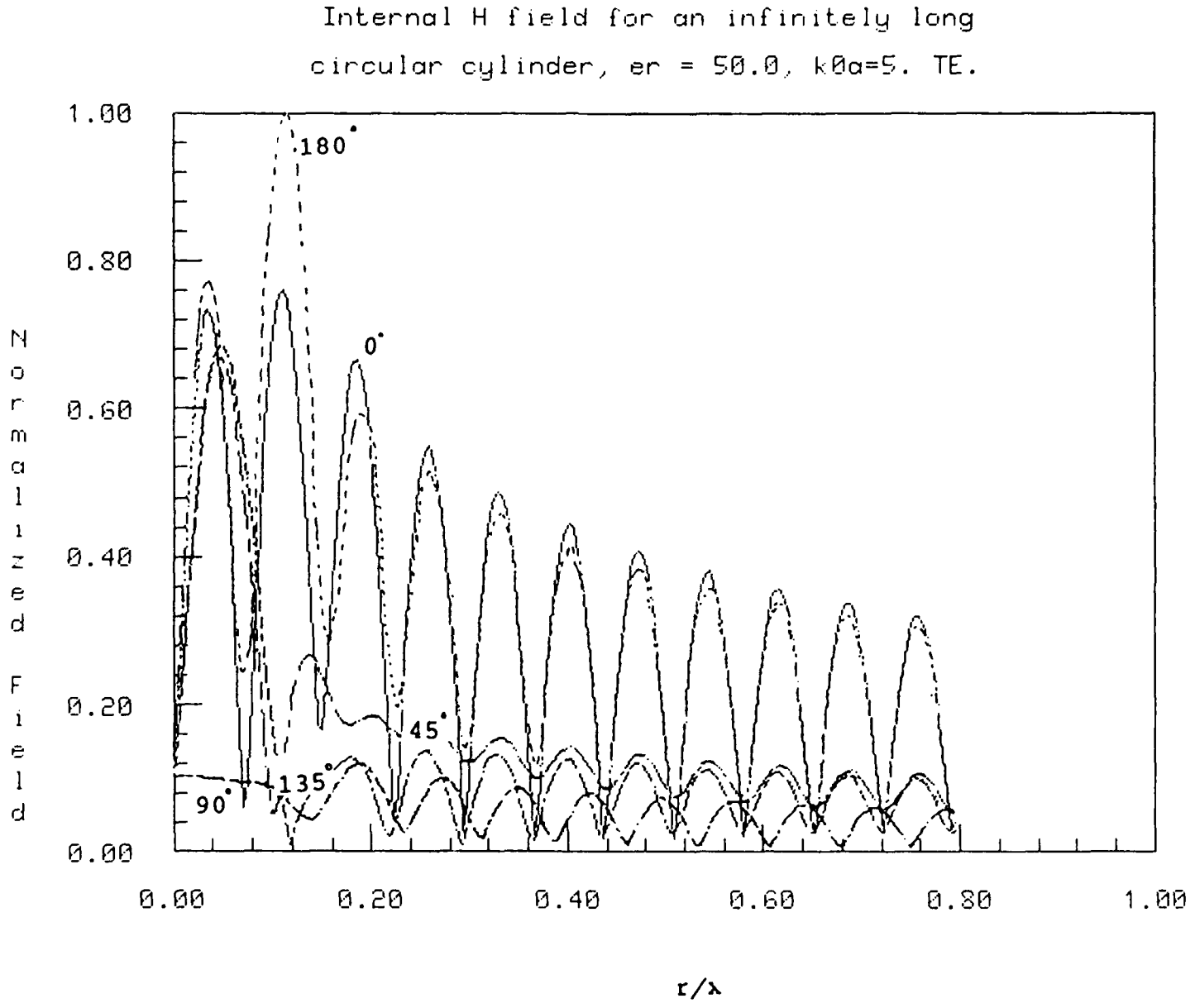
Internal H field for an infinitely long
circular cylinder, er = 50.0, k0a=5. TE.
Normalized Field
1.00
0.80
0.60
0.40
0.20
0.00
0.00
0.20
0.40
0.60
0.80
1.00
r/λ
180°
0°
45°
135°
90°

Fig. 30

the surface. (However, for large cylinders ($k_o a = 45$), the internal fields do localize near the surface [8].) Furthermore, the total number of variations of the internal fields across the cylinder is consistent with the value of the relative permittivity. Since there is no abnormality in the internal fields for the cylinder size and dielectric constants we considered, no special treatment was needed in the numerical solution to take this into account.

5. COMPARISON BETWEEN EXACT SOLUTIONS AND THE MOM NUMERICAL SOLUTIONS USING THE AREA AND LINE INTEGRATION METHODS

The derivation of the area integration method can be found in Marian Silberstein's report, Electromagnetic Scattering from Dielectrics - A Two-Dimensional Integral Equation Solution [14]. This approach uses the method of moments (MOM) with pulse basis functions and point matching to discretize the integral equation into a linear system of equations which is then solved by matrix inversion. That is, the electric field was represented by a constant function within each cell and the equation was enforced at the cell centers. To ensure good accuracy, the size of each cell must be small compared to the dielectric wavelength, (i.e., the number of cells n per dielectric wavelength λ, should be $\geq$ 10). For the circular cylinder, the results are compared to the exact series solution and are shown in Figs. 31-40.

Figs. 31-37 show the normalized bistatic TE scattering from a long circular dielectric cylinder with different relative permittivities and values of $k_o a$. The number of cells per dielectric wavelength is set to 10 and the center point integration method is used. Excellent agreement

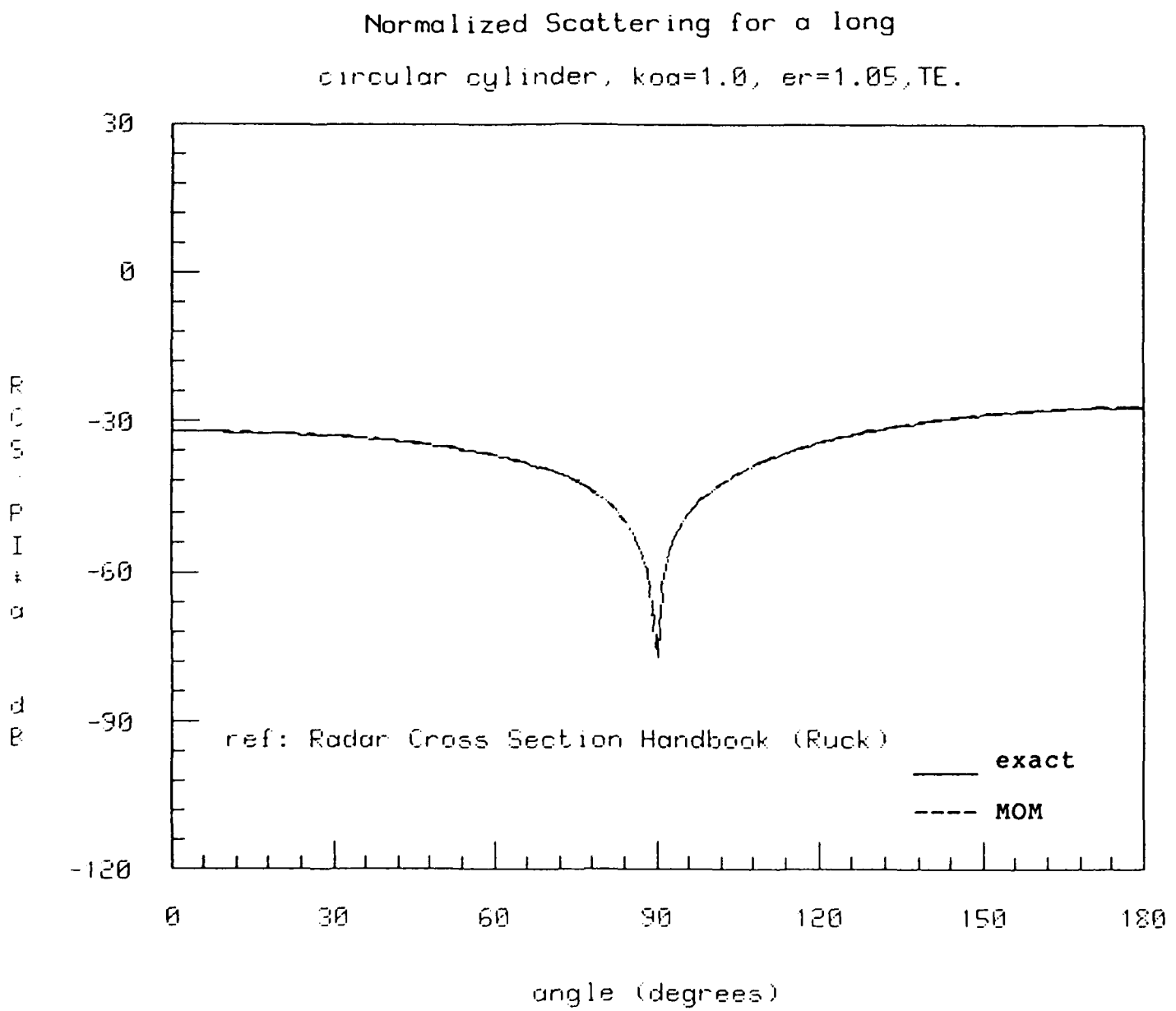
Normalized Scattering for a long
circular cylinder, koa=1.0, er=1.05,TE.
30
0
-30
-60
-90
-120
RCS, PI*a dB
ref: Radar Cross Section Handbook (Ruck)
exact
MOM
0
30
60
90
120
150
180
angle (degrees)

Fig. 31

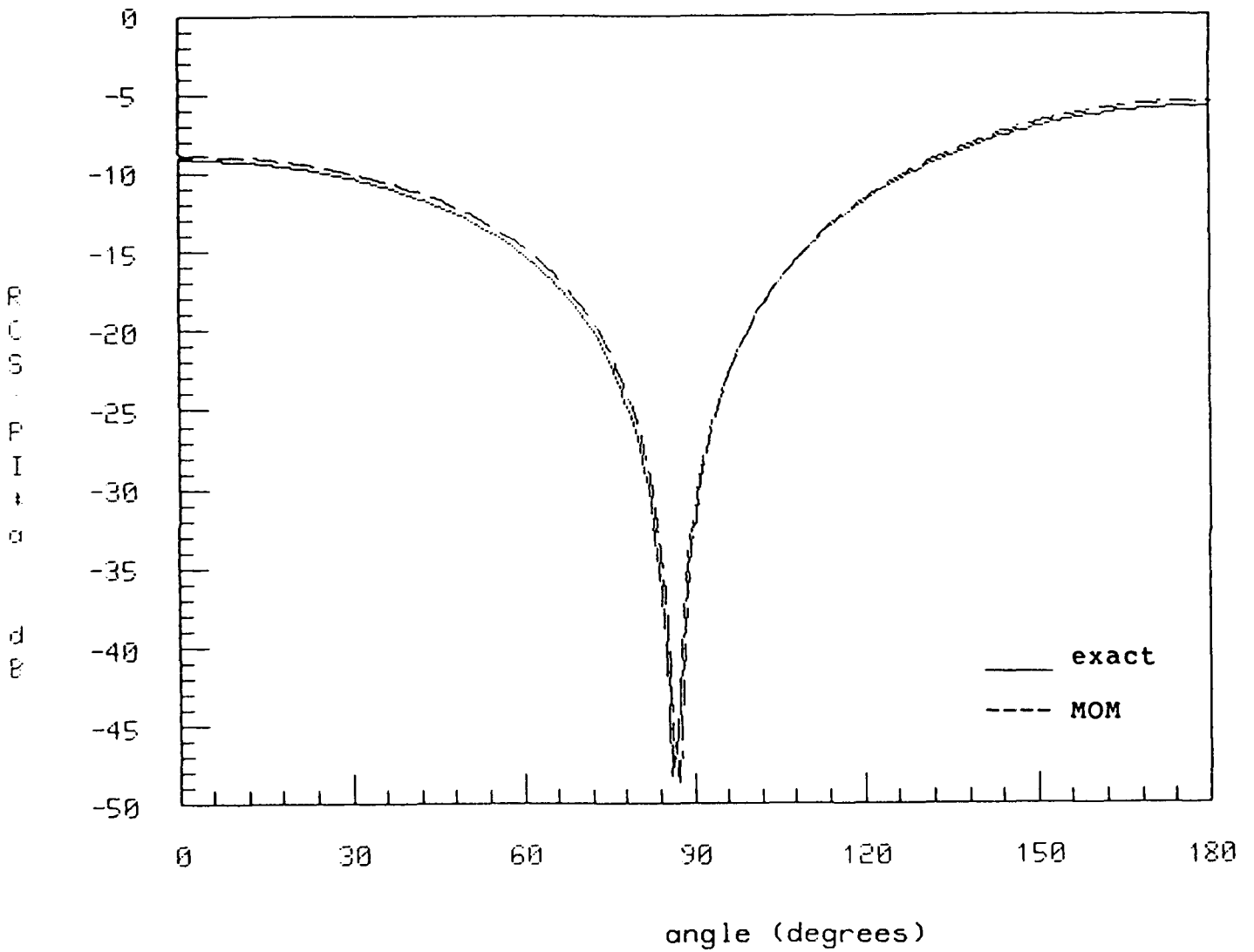
Normalized Scattering for a long
circular cylinder, er=2.56, koa=0.7 TE.
RCS - PI * a
dB
0
-5
-10
-15
-20
-25
-30
-35
-40
-45
-50
0
30
60
90
120
150
180
angle (degrees)
exact
MOM

Fig. 32

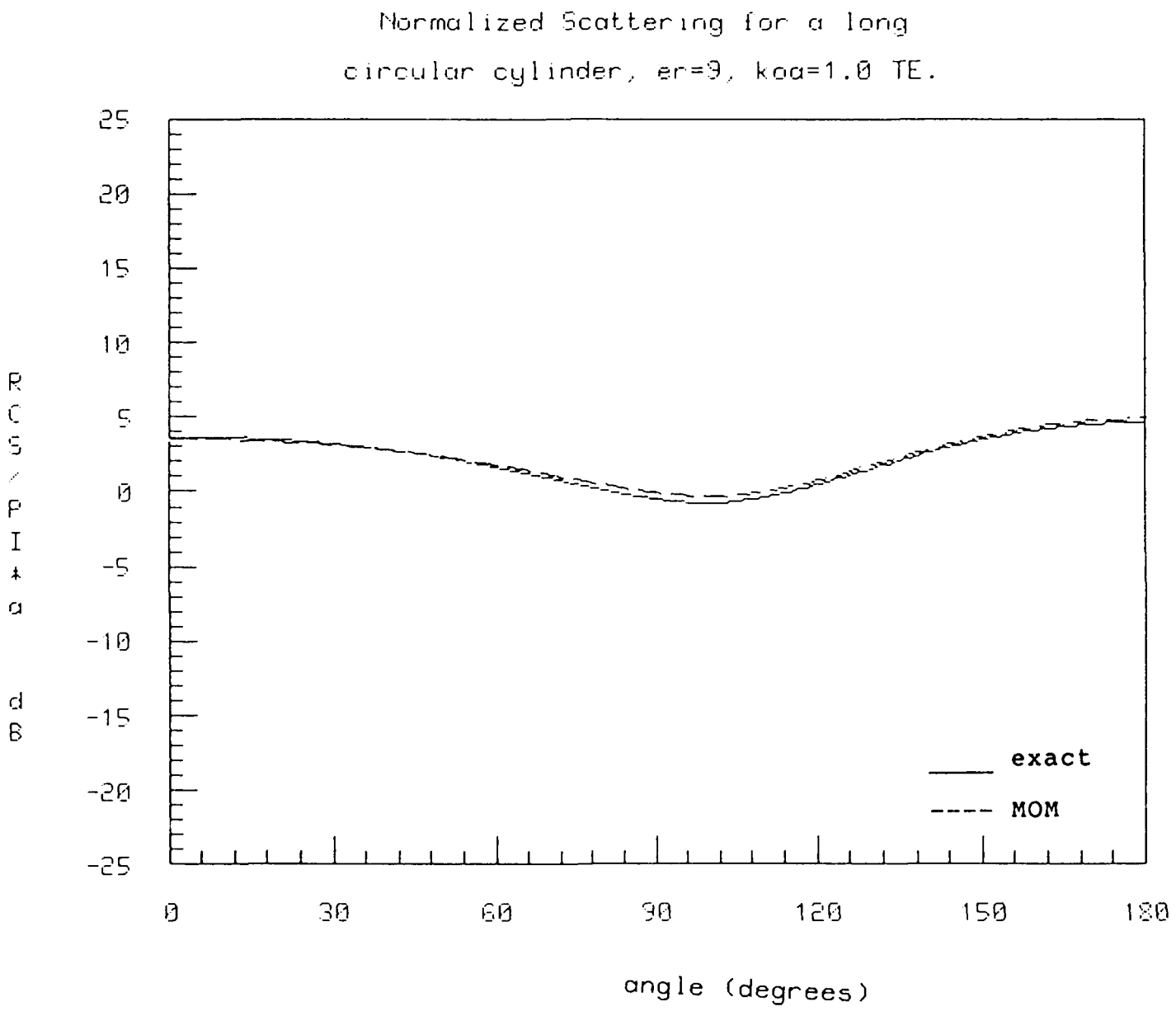
Normalized Scattering for a long
circular cylinder, er=9, koa=1.0 TE.
25
20
15
10
5
0
-5
-10
-15
-20
-25
RCS / PI * a dB
0
30
60
90
120
150
180
angle (degrees)
exact
MOM

Fig. 33

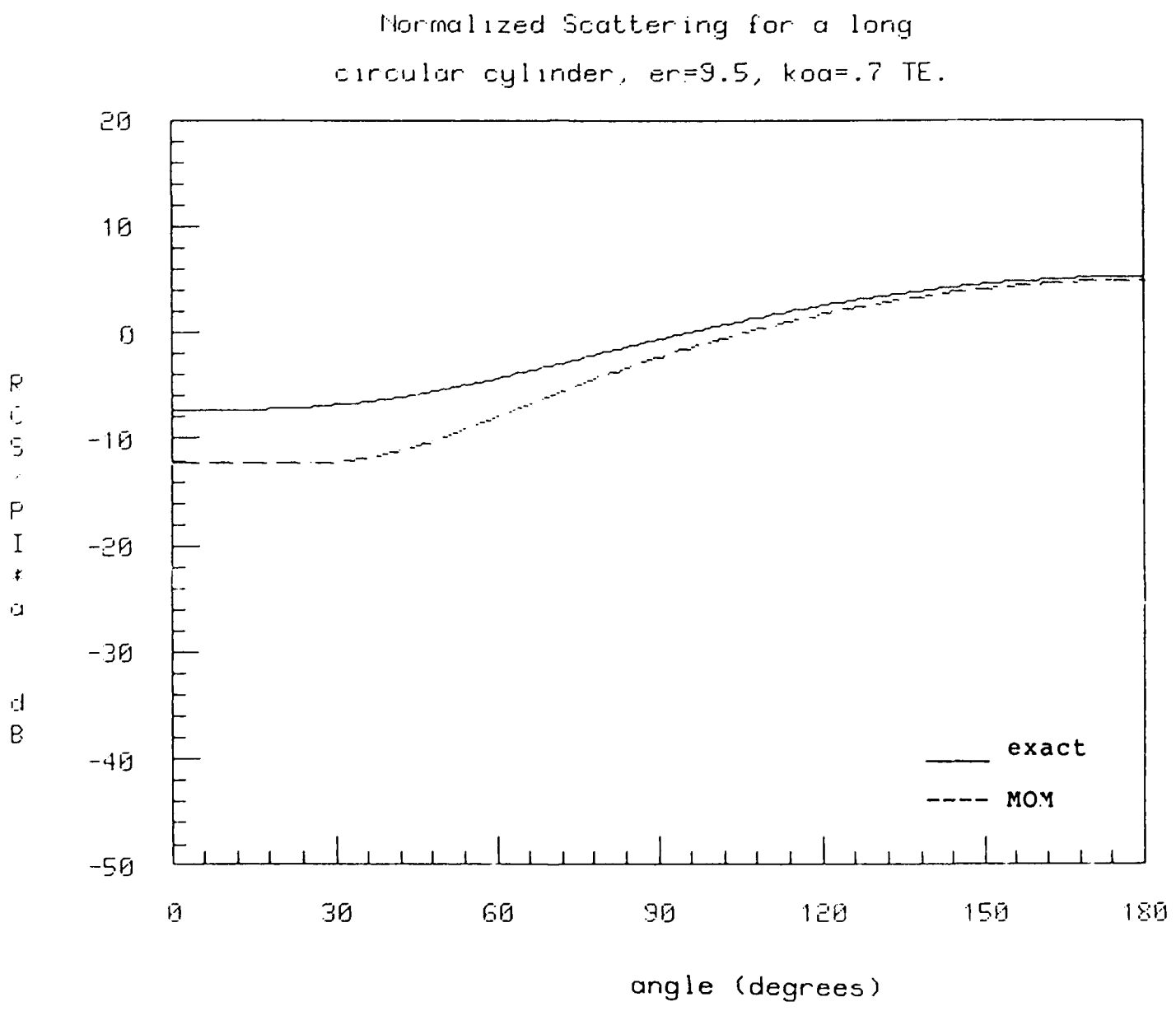
Normalized Scattering for a long
circular cylinder, er=9.5, koa=.7 TE.
20
10
0
-10
-20
-30
-40
-50
RCS/PI*a
dB
0
30
60
90
120
150
180
angle (degrees)
exact
MOM

Fig. 34

is observed with the exact series solution when the relative permittivity or size of the cylinder is small (see Figs. 31-33 and Figs. 35-37).

Figs. 34 shows the TE bistatic scattering from a circular cylinder versus scattering angles for $k_o a = 0.7$ and a large relative permittivity of 9.5. As seen from the figure, the MOM solution tends to deviate from the exact solution for large relative permittivity.

For TM polarization, the normalized bistatic scattering from a long dielectric circular cylinder is shown in the Figs. 38-40. Fig. 38 shows the normalized bistatic scattering cross section from a long circular dielectric cylinder with $\epsilon_r = 2.56$ and $k_o a = 0.7$. Figs. 39-40 show that even with large relative permittivities, the agreement between the computed solution and the reference solution is good.

The following figures show the comparison between the exact solution and the integral equation solution using the center point integration method for a circular cylinder with varying $k_o a$. Relative permittivities of 2.56,4, and 10 are chosen. Both TM and TE polarization

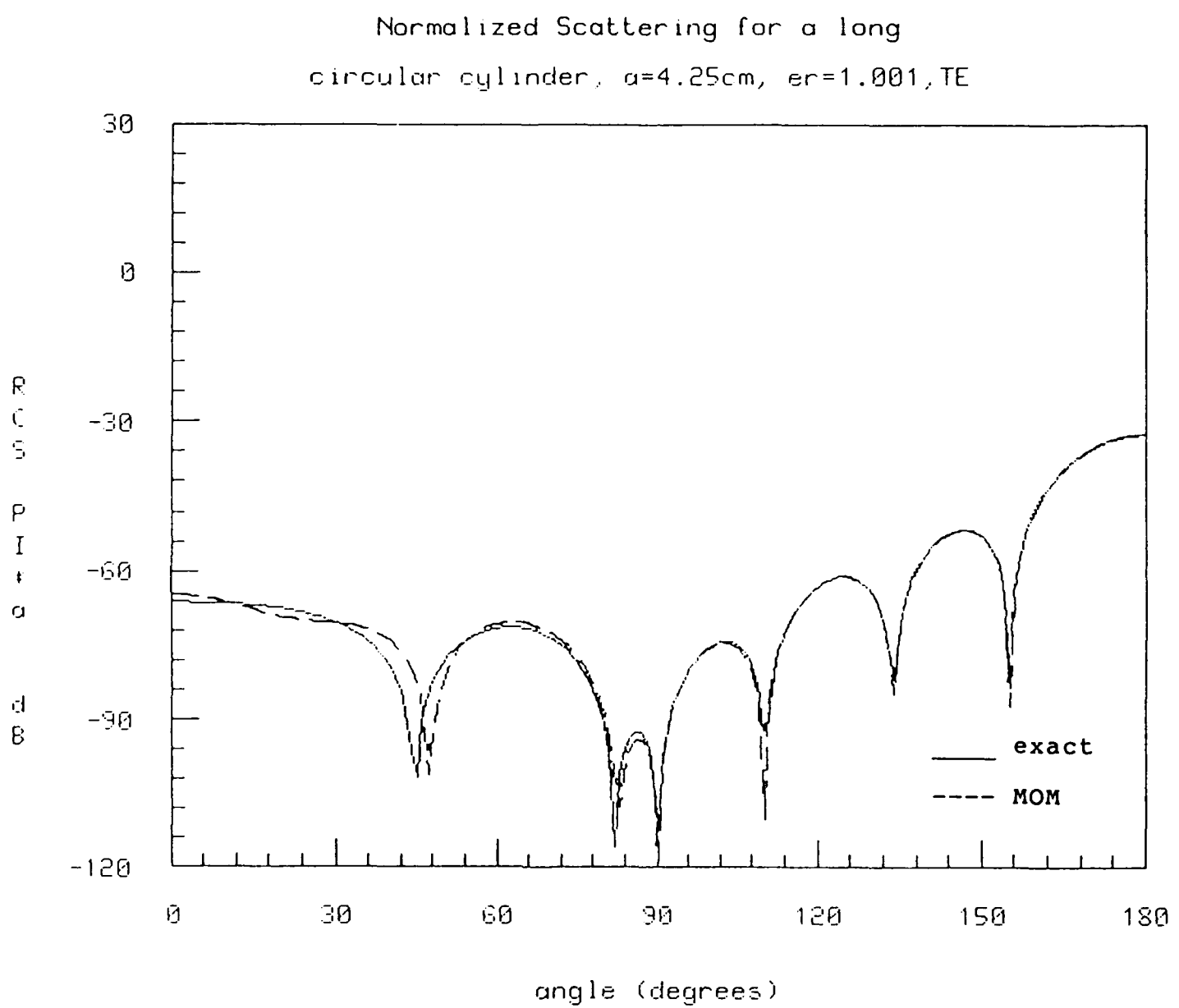
Normalized Scattering for a long
circular cylinder, a=4.25cm, er=1.001, TE
30
0
-30
-60
-90
-120
RCS PI*a dB
0
30
60
90
120
150
180
angle (degrees)
exact
MOM

Fig. 35

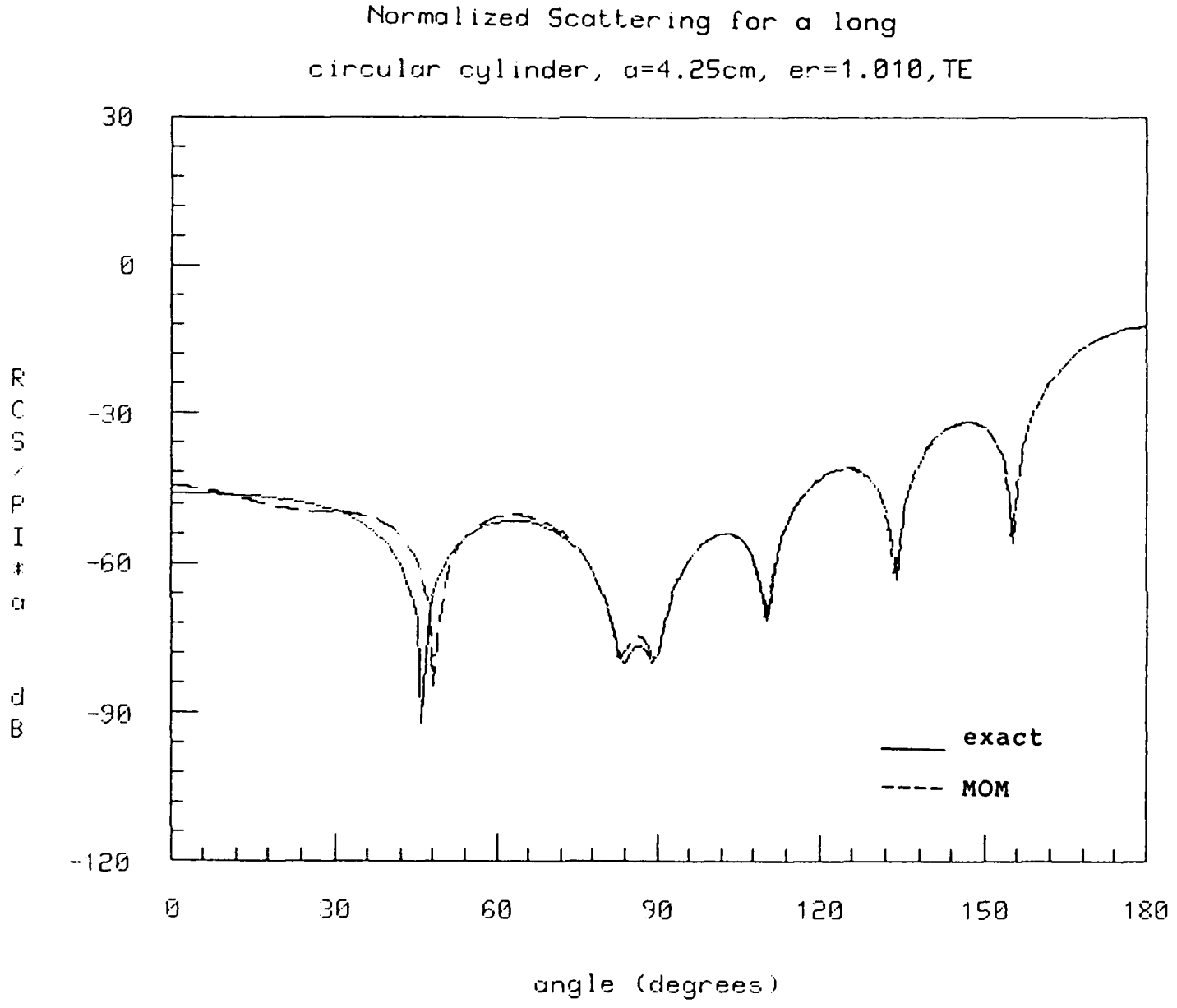
Normalized Scattering for a long
circular cylinder, a=4.25cm, er=1.010,TE
30
0
-30
-60
-90
-120
RCS/PI*a
dB
0
30
60
90
120
150
180
angle (degrees)
exact
MOM

Fig. 36

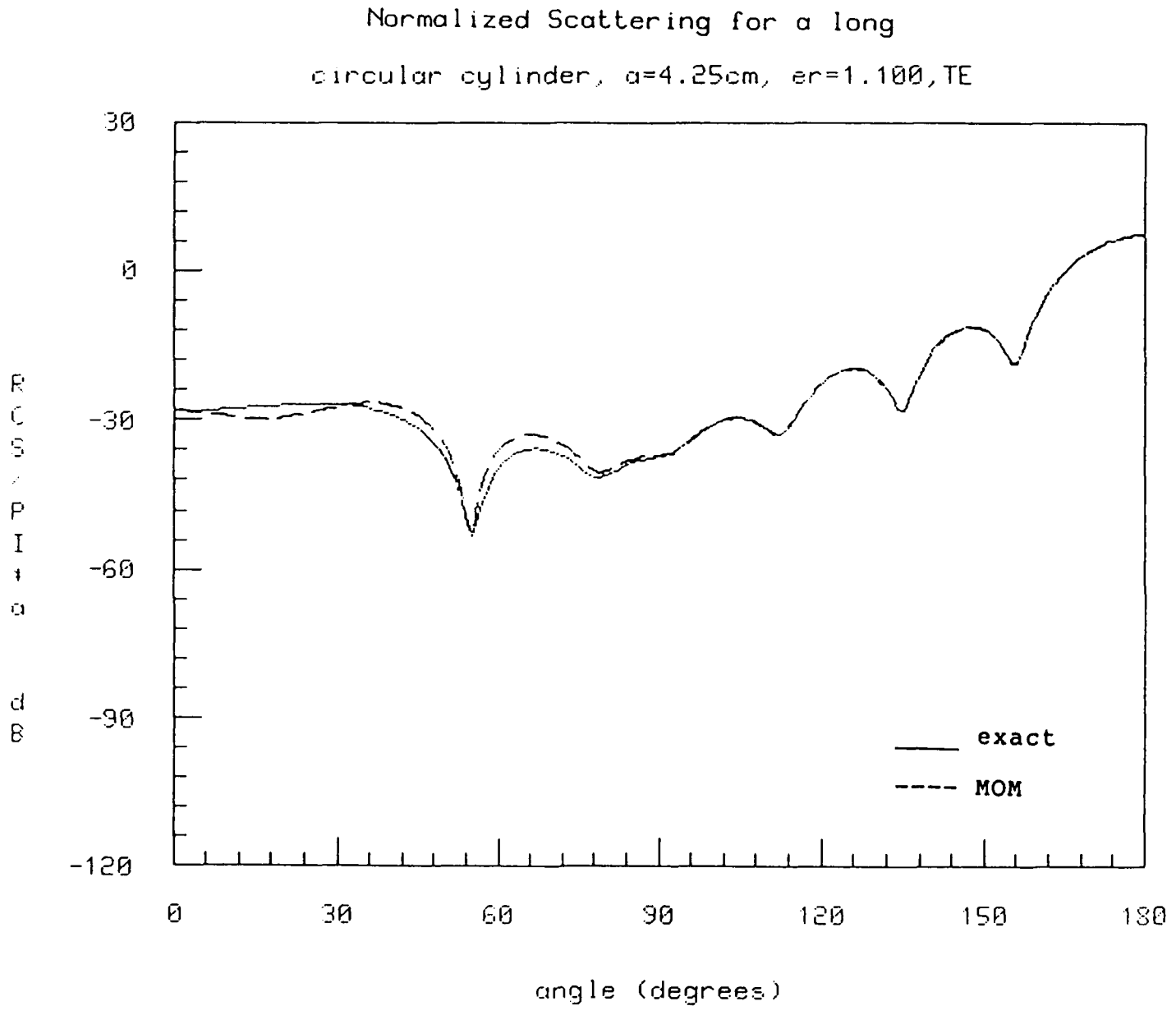
Normalized Scattering for a long
circular cylinder, a=4.25cm, er=1.100,TE
30
0
-30
-60
-90
-120
RCS/PI*a
dB
exact
MOM
0
30
60
90
120
150
180
angle (degrees)

Fig. 37

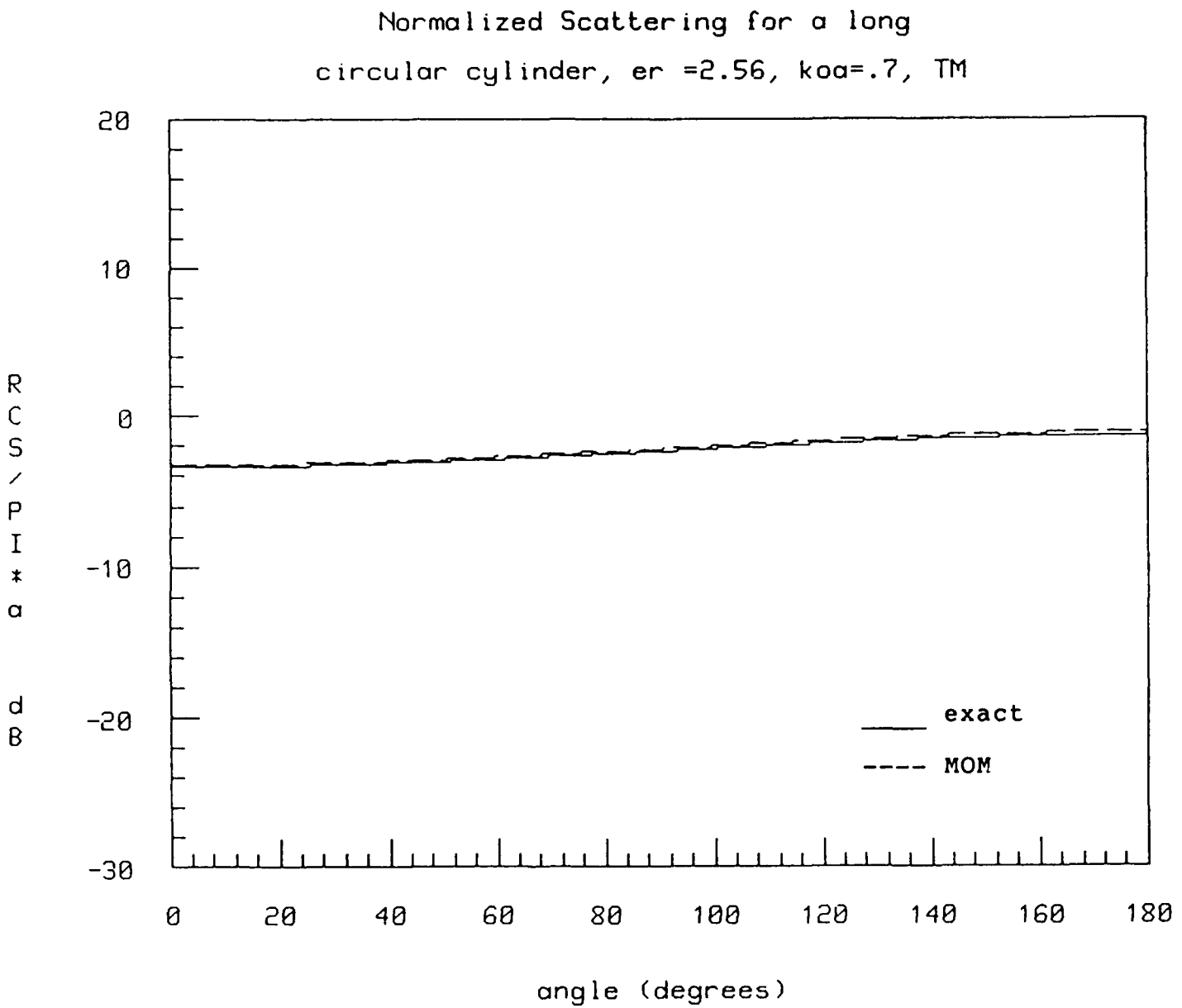
Normalized Scattering for a long
circular cylinder, er =2.56, koa=.7, TM
RCS/PI*a dB
20
10
0
-10
-20
-30
0
20
40
60
80
100
120
140
160
180
exact
MOM
angle (degrees)

Fig. 38

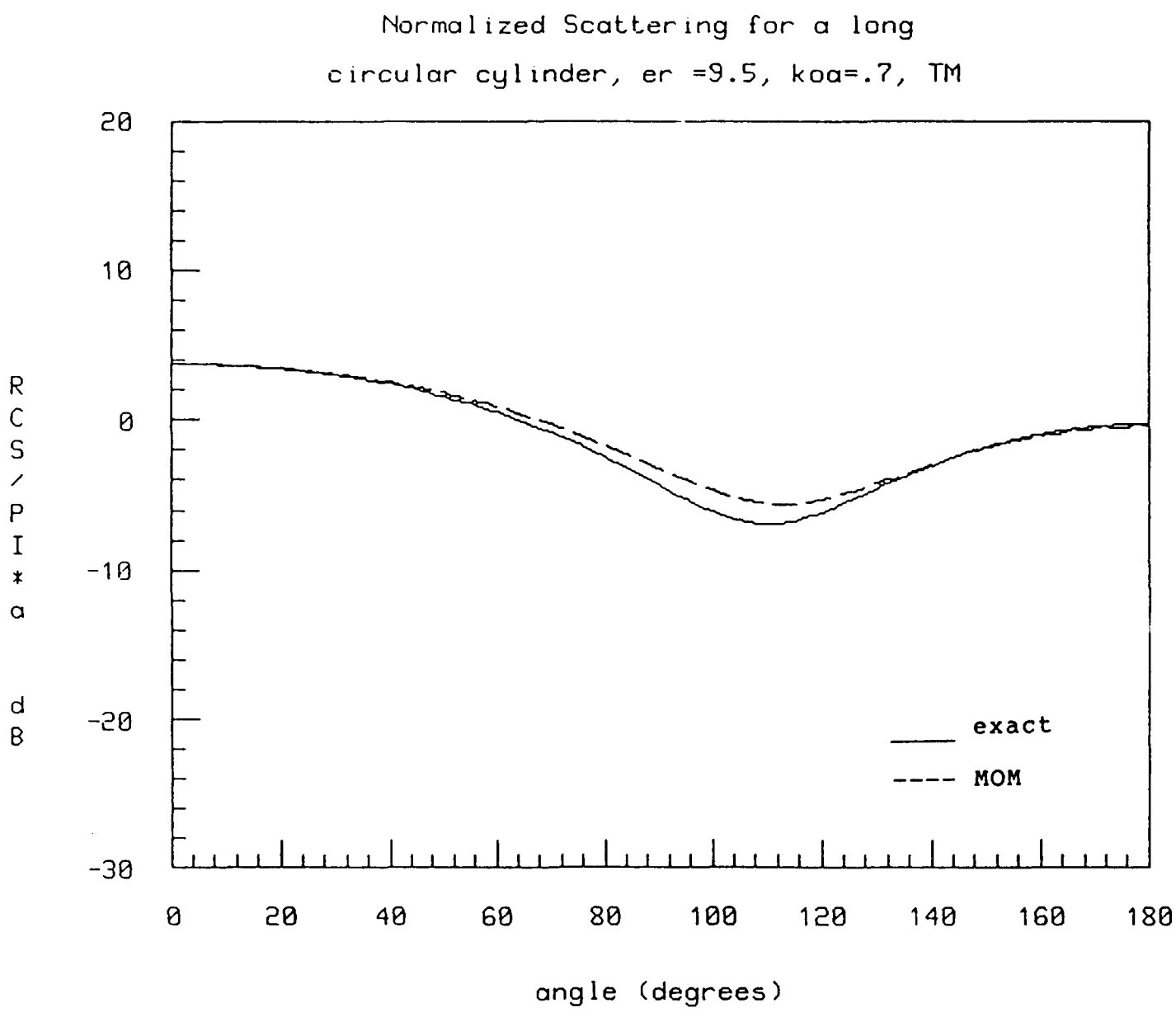
Normalized Scattering for a long
circular cylinder, er =9.5, koa=.7, TM
RCS/PI*a
dB
20
10
0
-10
-20
-30
0
20
40
60
80
100
120
140
160
180
angle (degrees)
exact
MOM

Fig. 39

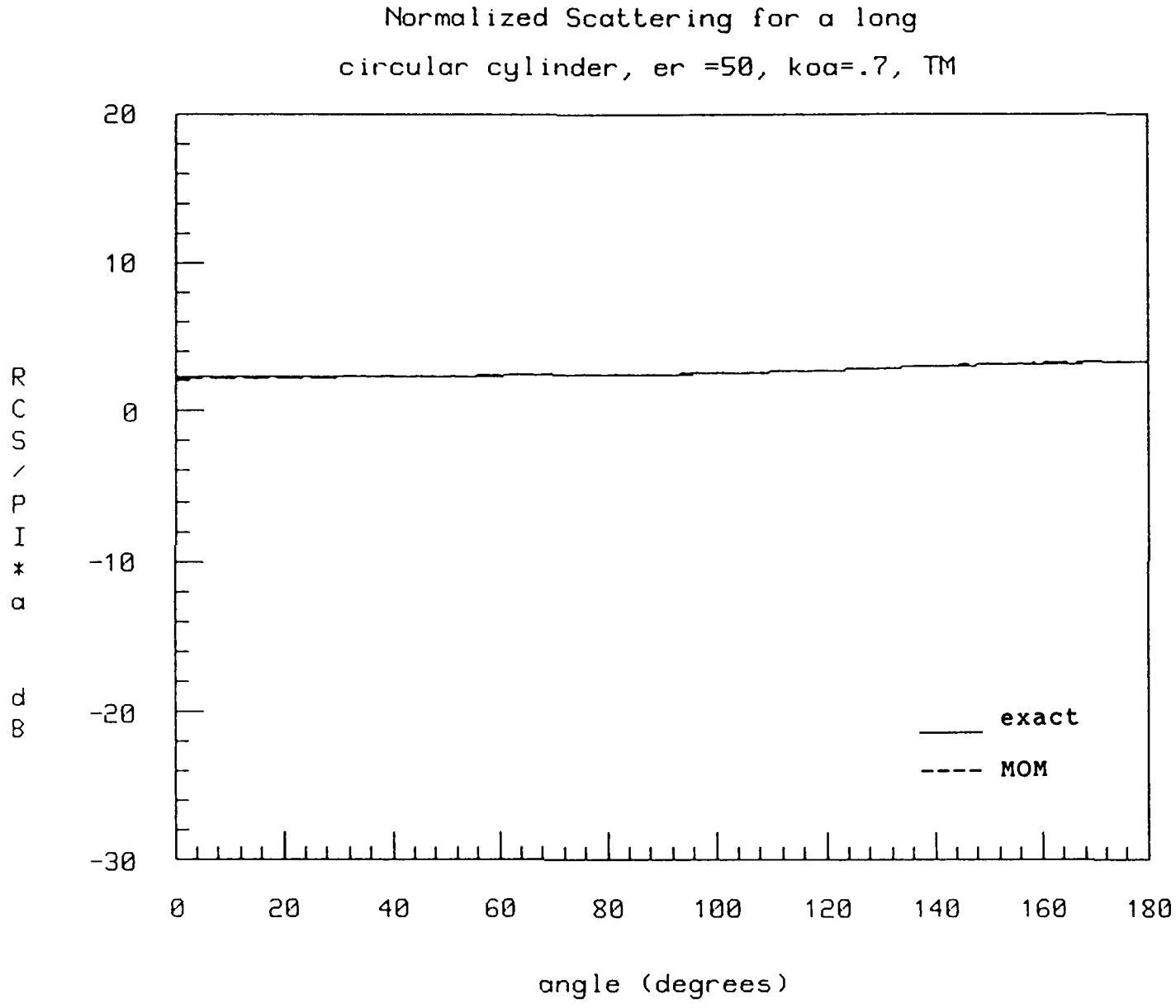
Normalized Scattering for a long
circular cylinder, er =50, koa=.7, TM
20
10
0
-10
-20
-30
RCS/PI*a
dB
exact
MOM
0
20
40
60
80
100
120
140
160
180
angle (degrees)

Fig. 40

are considered. We used three different methods of approximation for evaluating the self cell terms to compare their efficiency. First, the self cell term is approximated by using a constant area with one center point. For case 2, the number of integration points are increased to 25 points using the same approximation method. Thirdly, the self cell term is evaluated by using the line integral method with 80 points.

Figs. 41-43 show the forward scattering from a circular cylinder versus $k_o a$ for relative permittivity = 2.56,4 and 10, respectively, for the TM polarization, the solid curve represents the exact solutions. The exact solution uses 1200 $k_o a$ points. In our numerical computations, the number of cells per dielectric wavelength is set to 10. Due to limitations of computer time, only 120 $k_o a$ points are used in our numerical evaluation. Figs. 44-46 show the back scattering. Good agreement is obtained between the three different numerical methods and the exact solution. However, for ϵr=10, better agreement can be attained if more $k_o a$ points (N > 120) and the number of cells (n/λ) per dielectric wavelength are increased in the computation.

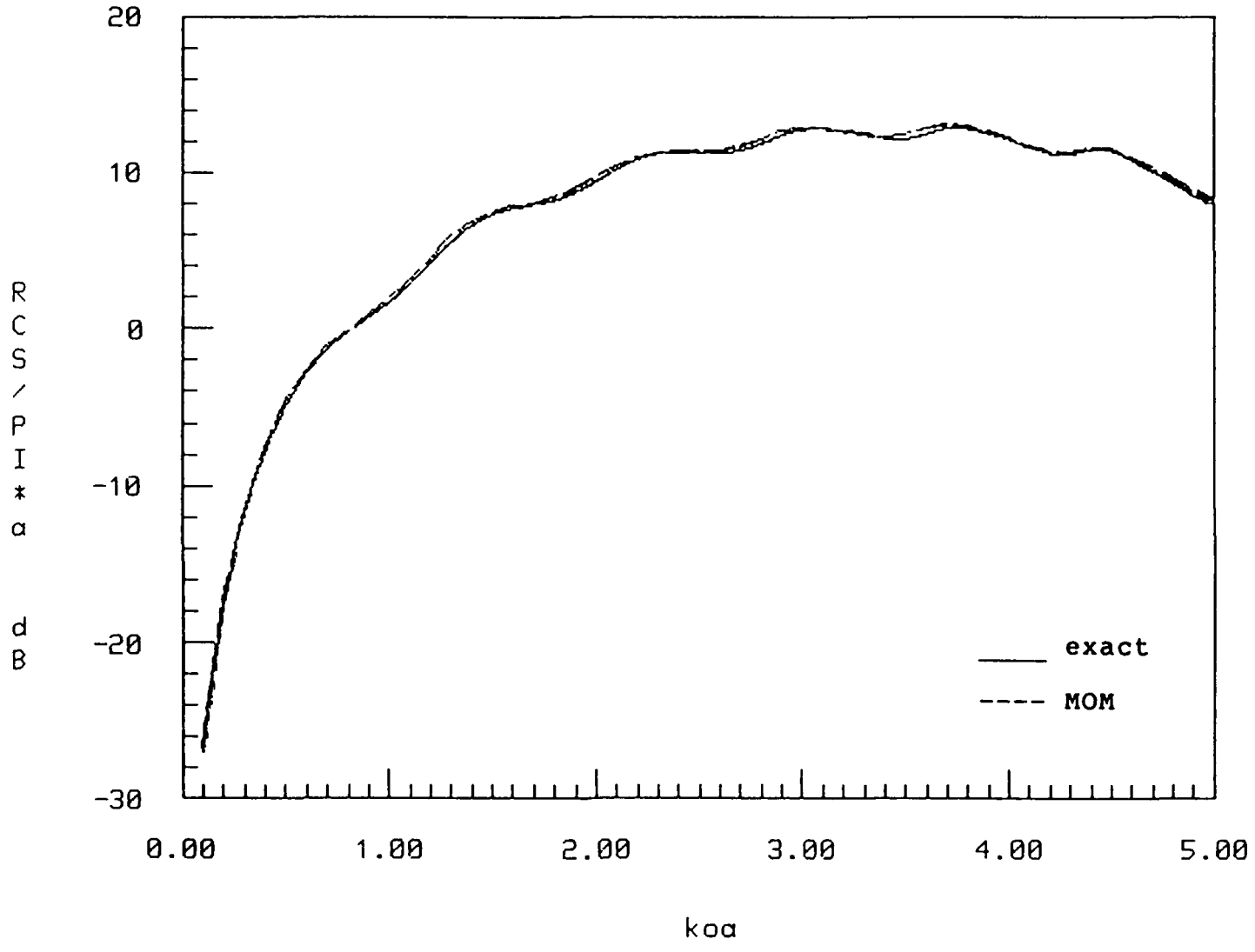
Forward Scattering for a long circular
cylinder, er = 2.56, n/λ = 10, TM
20
10
0
-10
-20
-30
RCS/PI*a
dB
0.00
1.00
2.00
3.00
4.00
5.00
koa
exact
MOM

Fig. 41

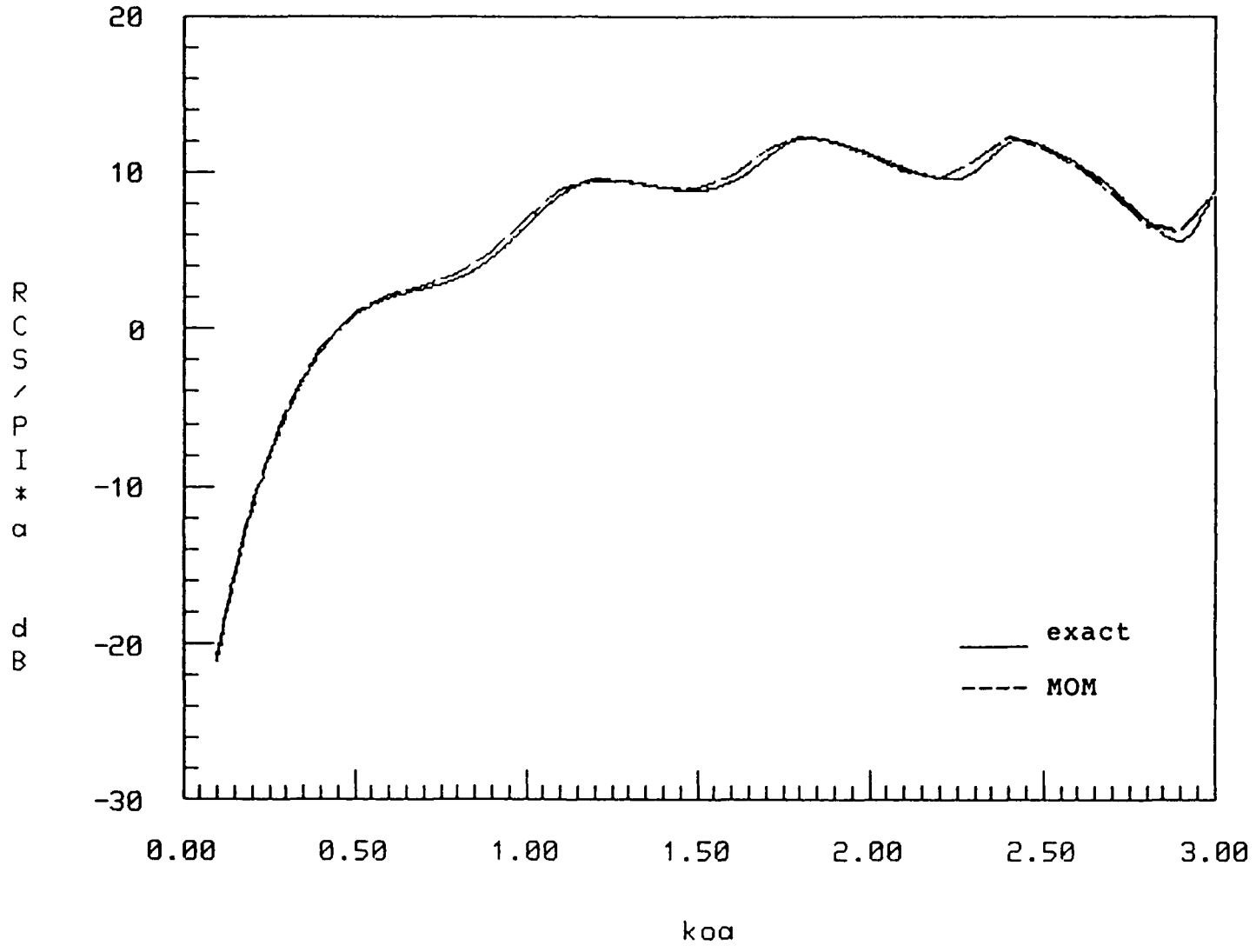
Forward Scattering for a long circular cylinder, er = 4.00, n/λ = 10, TM
RCS/PI*a dB
20
10
0
-10
-20
-30
0.00
0.50
1.00
1.50
2.00
2.50
3.00
koa
exact
MOM

Fig. 42

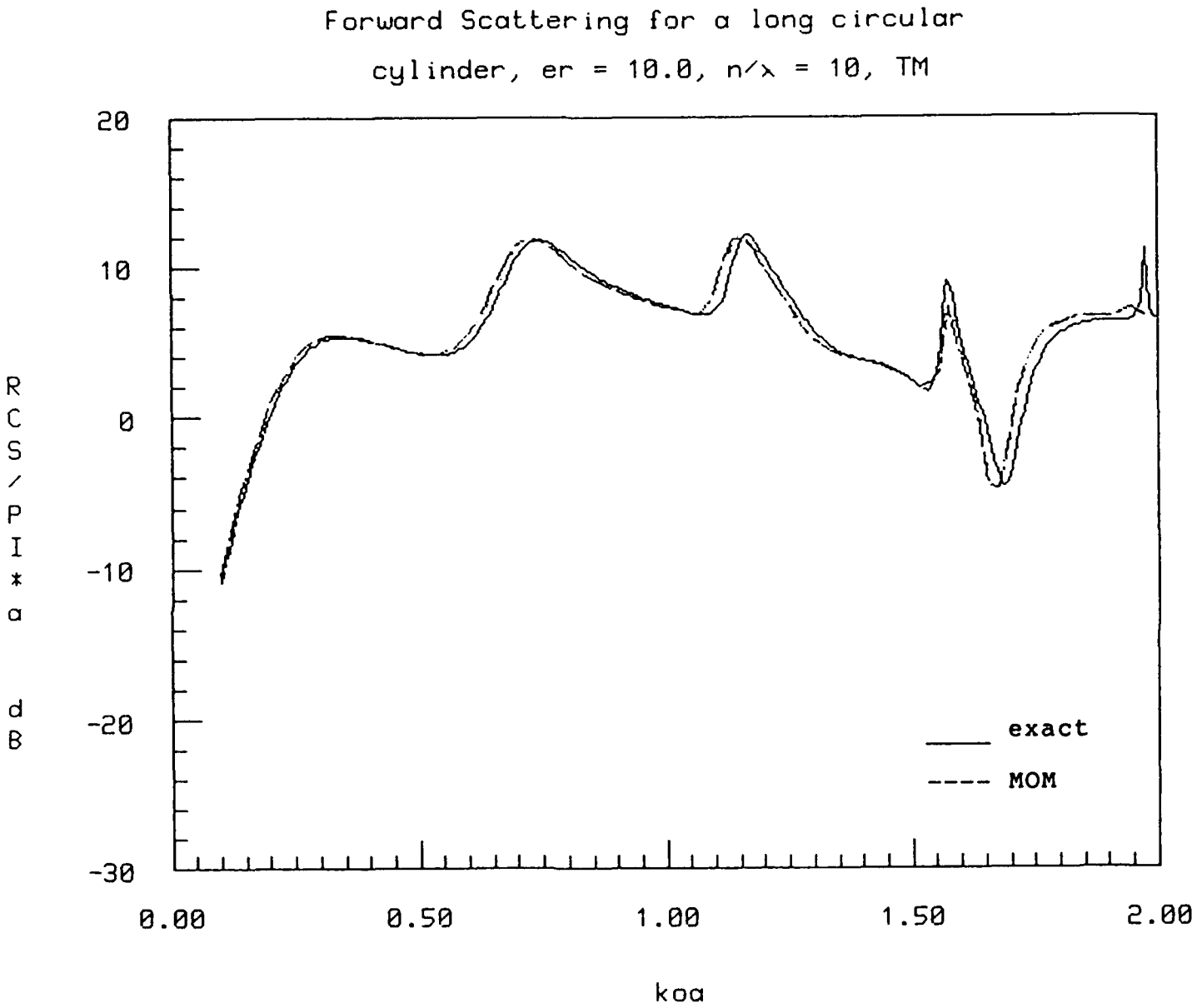
Forward Scattering for a long circular
cylinder, er = 10.0, n/λ = 10, TM
RCS/PI*a
dB
20
10
0
-10
-20
-30
0.00
0.50
1.00
1.50
2.00
koa
exact
MOM

Fig. 43

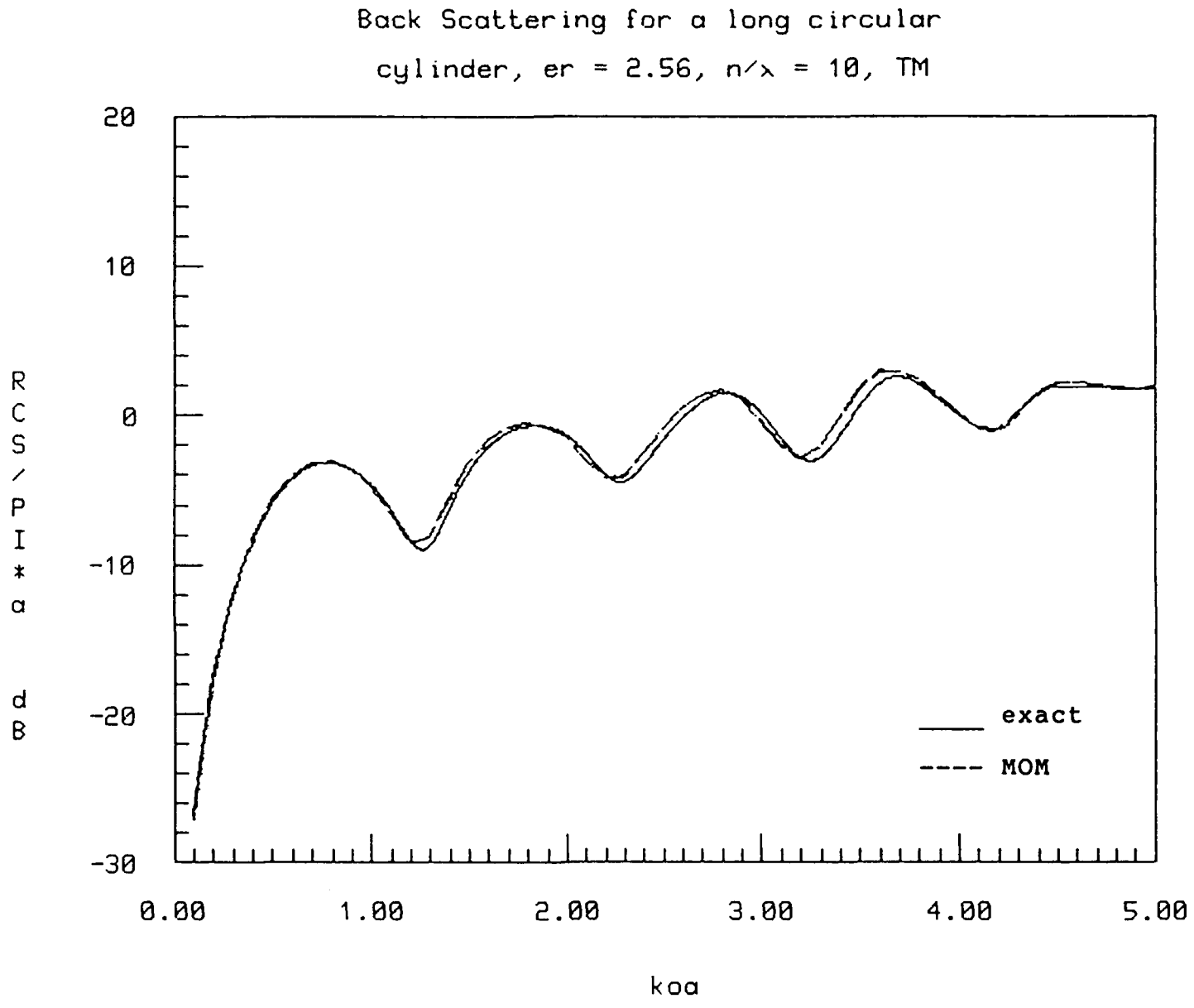
Back Scattering for a long circular
cylinder, er = 2.56, n/λ = 10, TM
20
10
0
-10
-20
-30
RCS/PI*a
dB
0.00
1.00
2.00
3.00
4.00
5.00
koa
exact
MOM

Fig. 44

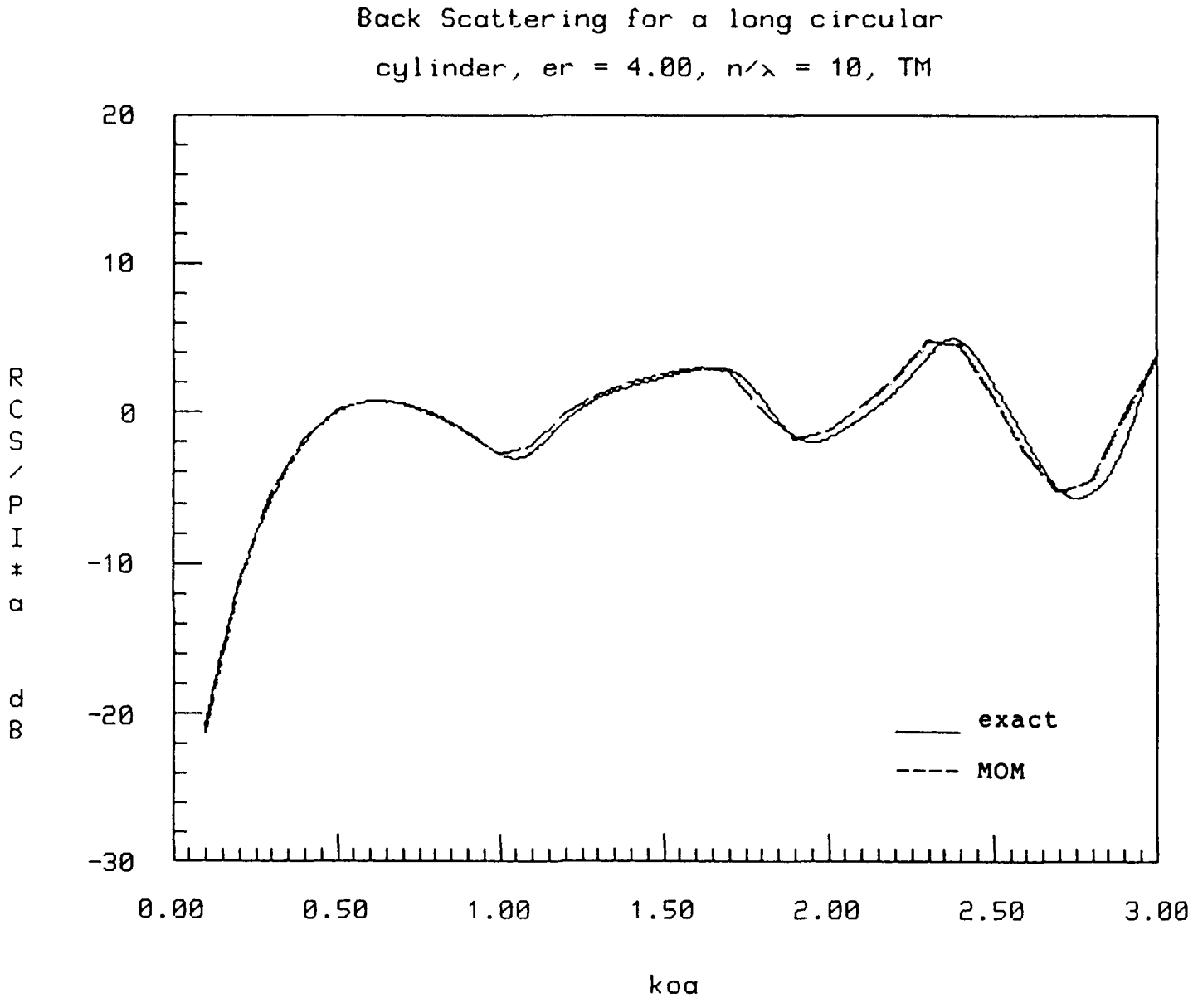
Back Scattering for a long circular
cylinder, er = 4.00, n/λ = 10, TM
20
10
0
-10
-20
-30
RCS/PI*a
dB
0.00
0.50
1.00
1.50
2.00
2.50
3.00
koa
exact
MOM

Fig. 45

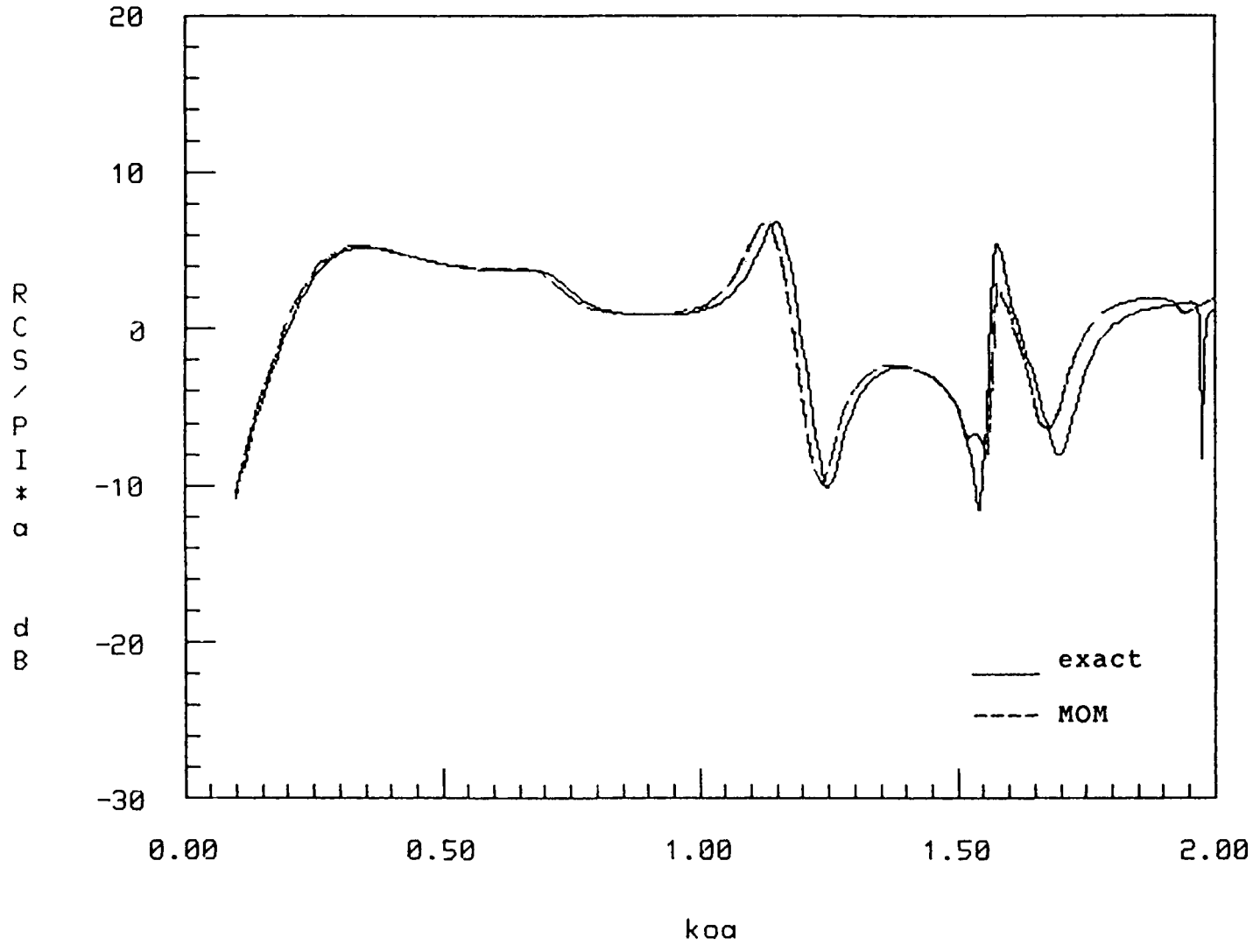
Back Scattering for a long circular
cylinder, er = 10.0, n/λ = 10, TM
20
10
0
-10
-20
-30
RCS/PI*a
dB
0.00
0.50
1.00
1.50
2.00
koa
exact
MOM

Fig. 46

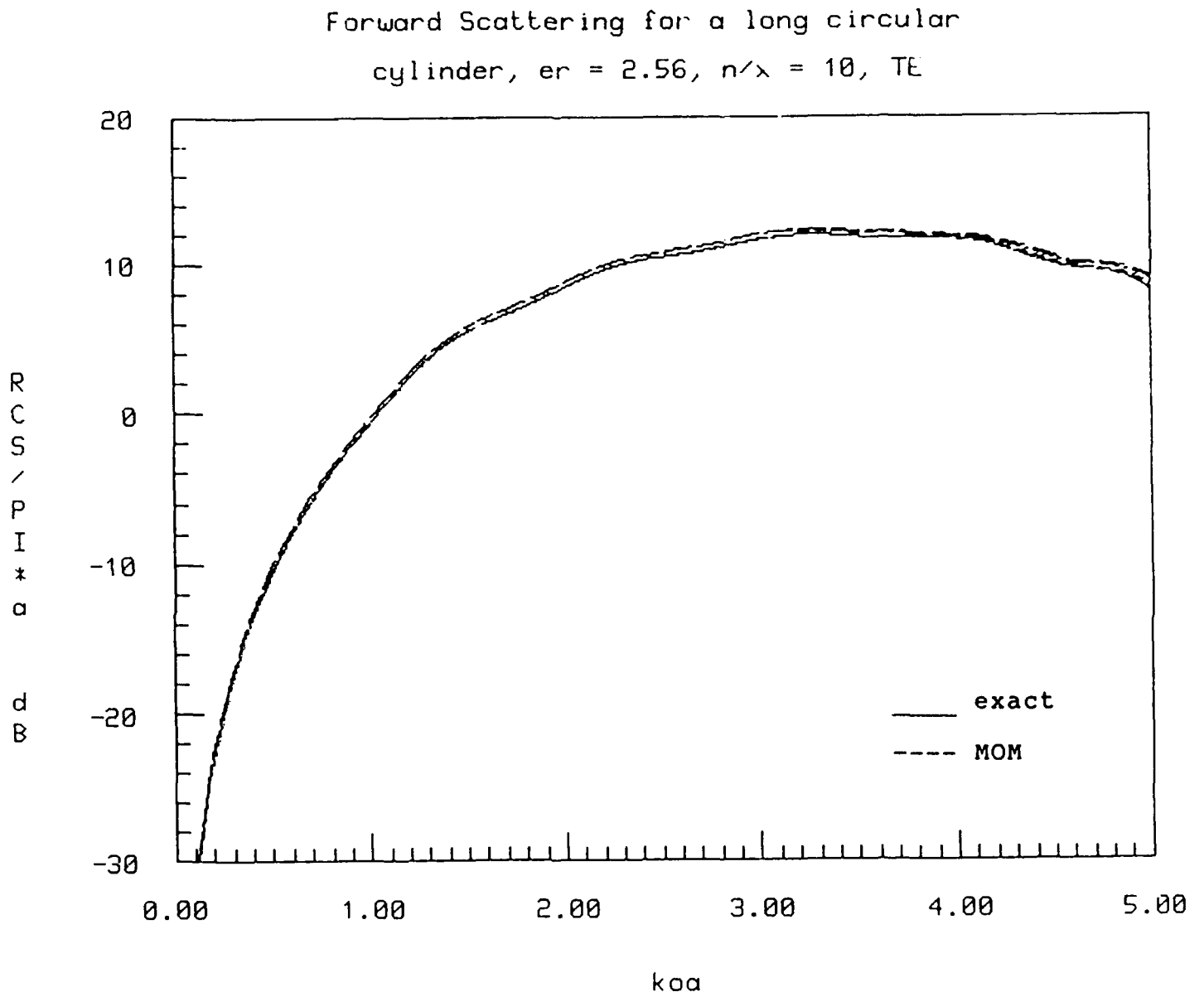
Forward Scattering for a long circular
cylinder, er = 2.56, n/λ = 10, TE
20
10
0
-10
-20
-30
RCS/PI*a
dB
0.00
1.00
2.00
3.00
4.00
5.00
koa
exact
MOM

Fig. 47

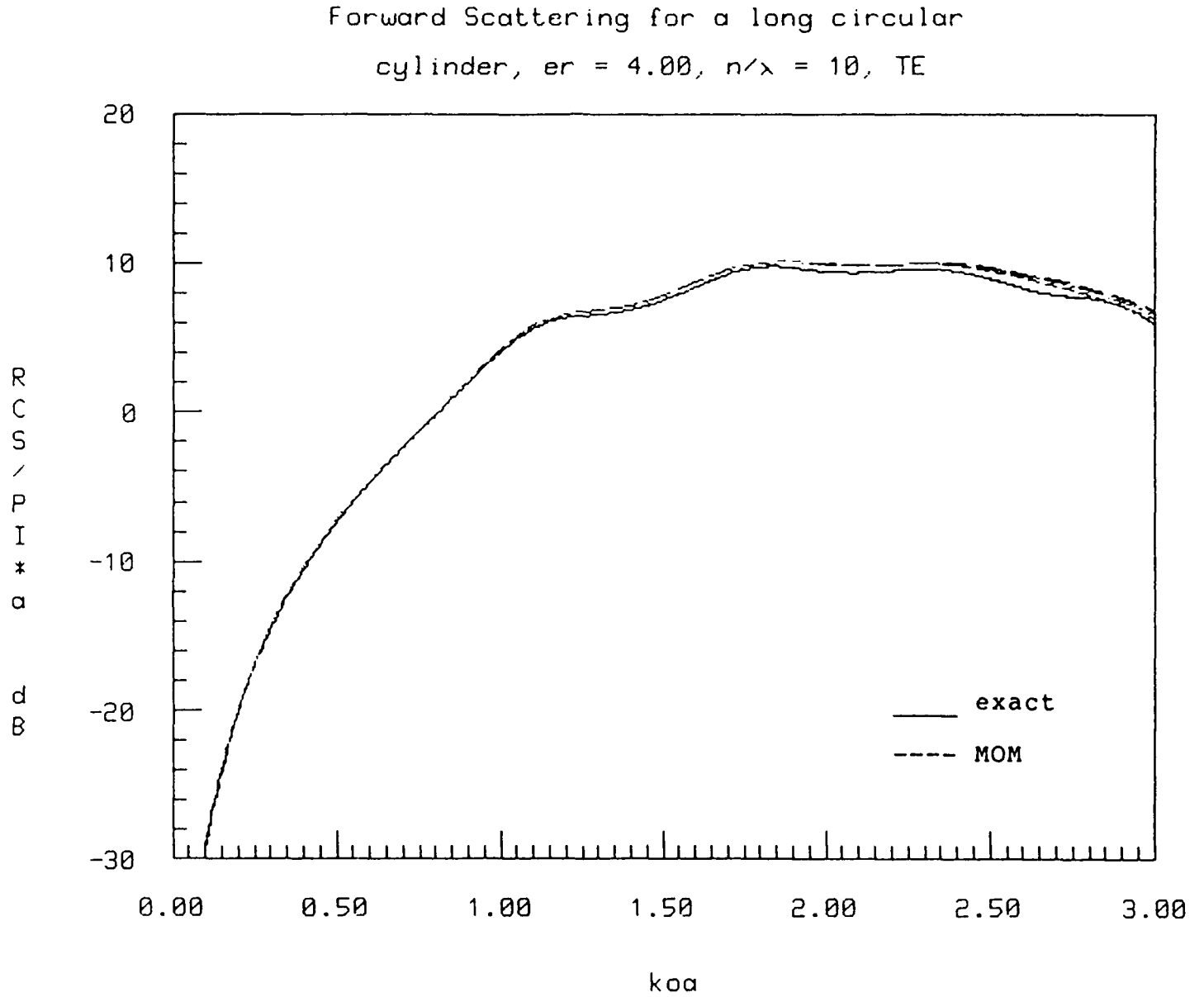
Forward Scattering for a long circular
cylinder, er = 4.00, n/λ = 10, TE
20
10
0
-10
-20
-30
RCS/PI*a
dB
0.00
0.50
1.00
1.50
2.00
2.50
3.00
koa
exact
MOM

Fig. 48

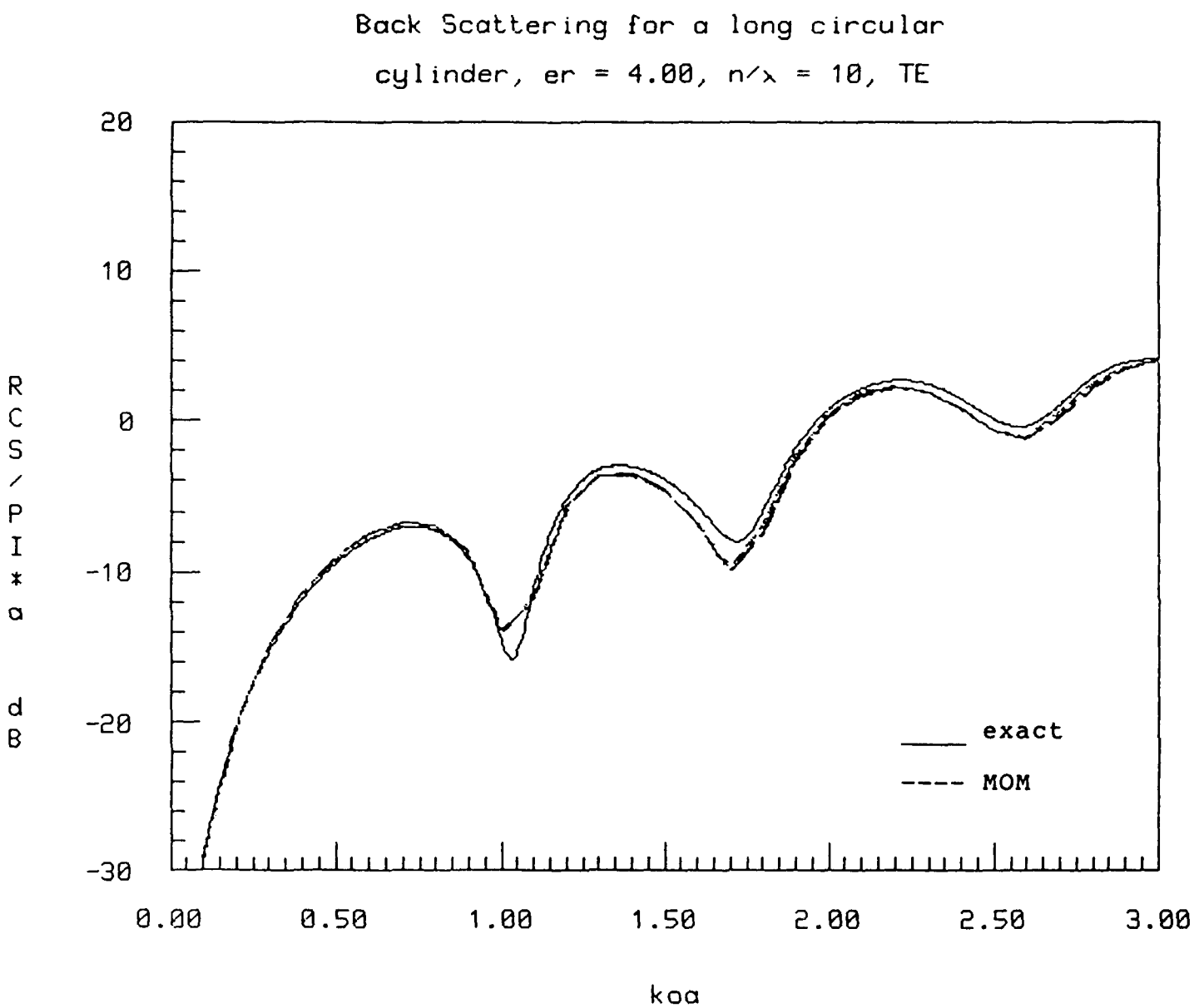
Back Scattering for a long circular
cylinder, er = 4.00, n/λ = 10, TE
RCS/PI*a dB
20
10
0
-10
-20
-30
0.00
0.50
1.00
1.50
2.00
2.50
3.00
koa
exact
MOM

Fig. 49

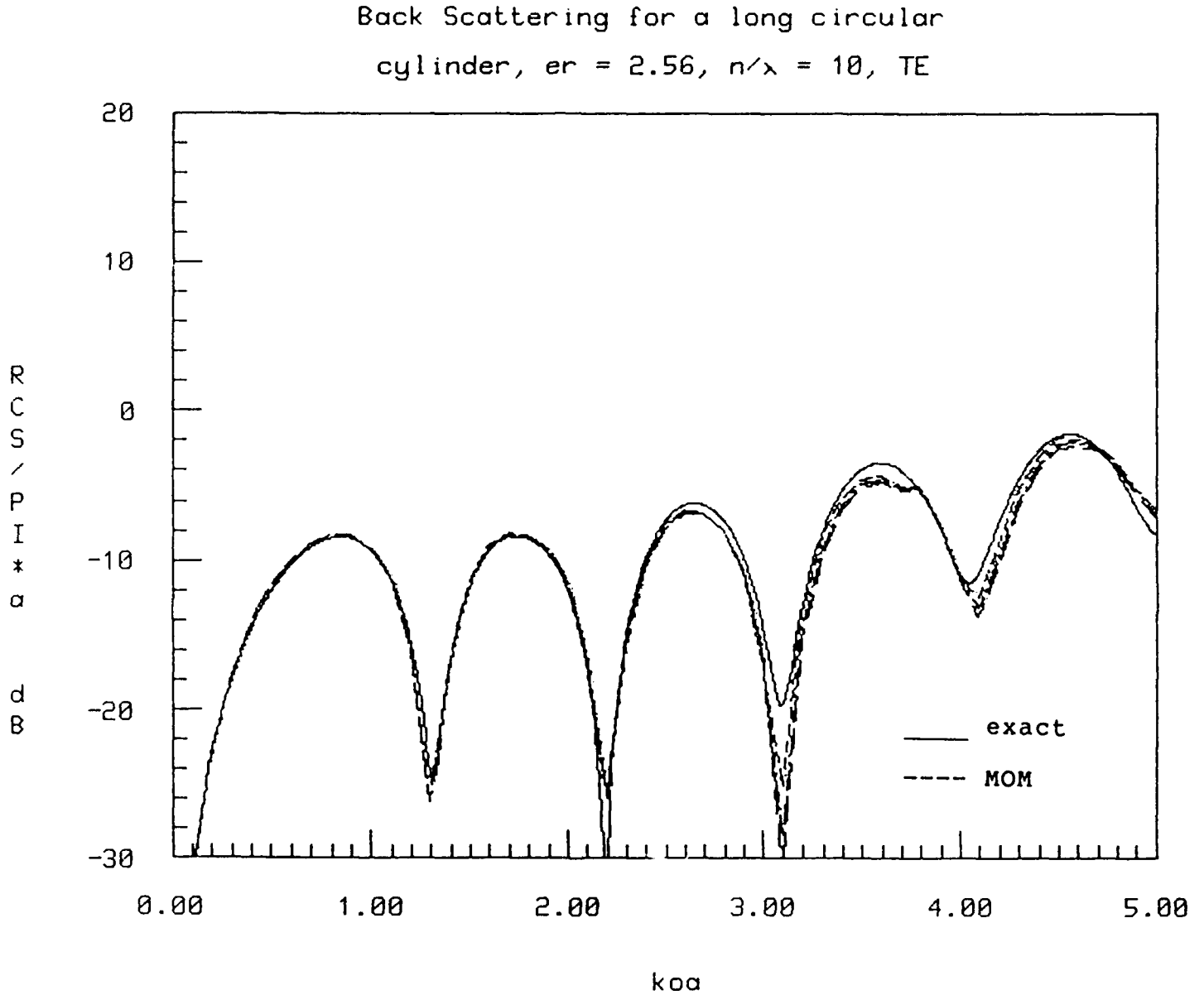
Back Scattering for a long circular
cylinder, er = 2.56, n/λ = 10, TE
20
10
0
-10
-20
-30
RCS/PI*a
dB
0.00
1.00
2.00
3.00
4.00
5.00
koa
exact
MOM

Fig. 50

Figs. 47-50 show the forward and back scattering from the dielectric circular cylinder versus $k_o a$ with relative permittivities of 2.56 and 4 respectively for TE polarization. Good agreement exists between the different methods (120 $k_o a$ points) and the exact series solution (1200 $k_o a$ points). These is no significant distinction between the exact solution and the three methods when the relative permittivity is small.

However, as the permittivity is increased, the computed solution deviates from the exact solution. This is especially true for the TE case when the relative permittivity is increased to 10. Shown in Fig. 51 is the forward scattering from a long lossless circular cylinder versus $k_o a$ with two different methods, the single center point area integral and the line integral method. The number of segments per dielectric wavelength is set to 15. The curves begin to deviate from the exact solution (the solid curve) when $k_o a > 0.5$. Fig. 52 shows the back scattering . Even though, the two numerical methods produce curves that differ somewhat, the line integral method for evaluating the self cell terms deviates less than the center point area integral method. It is noted

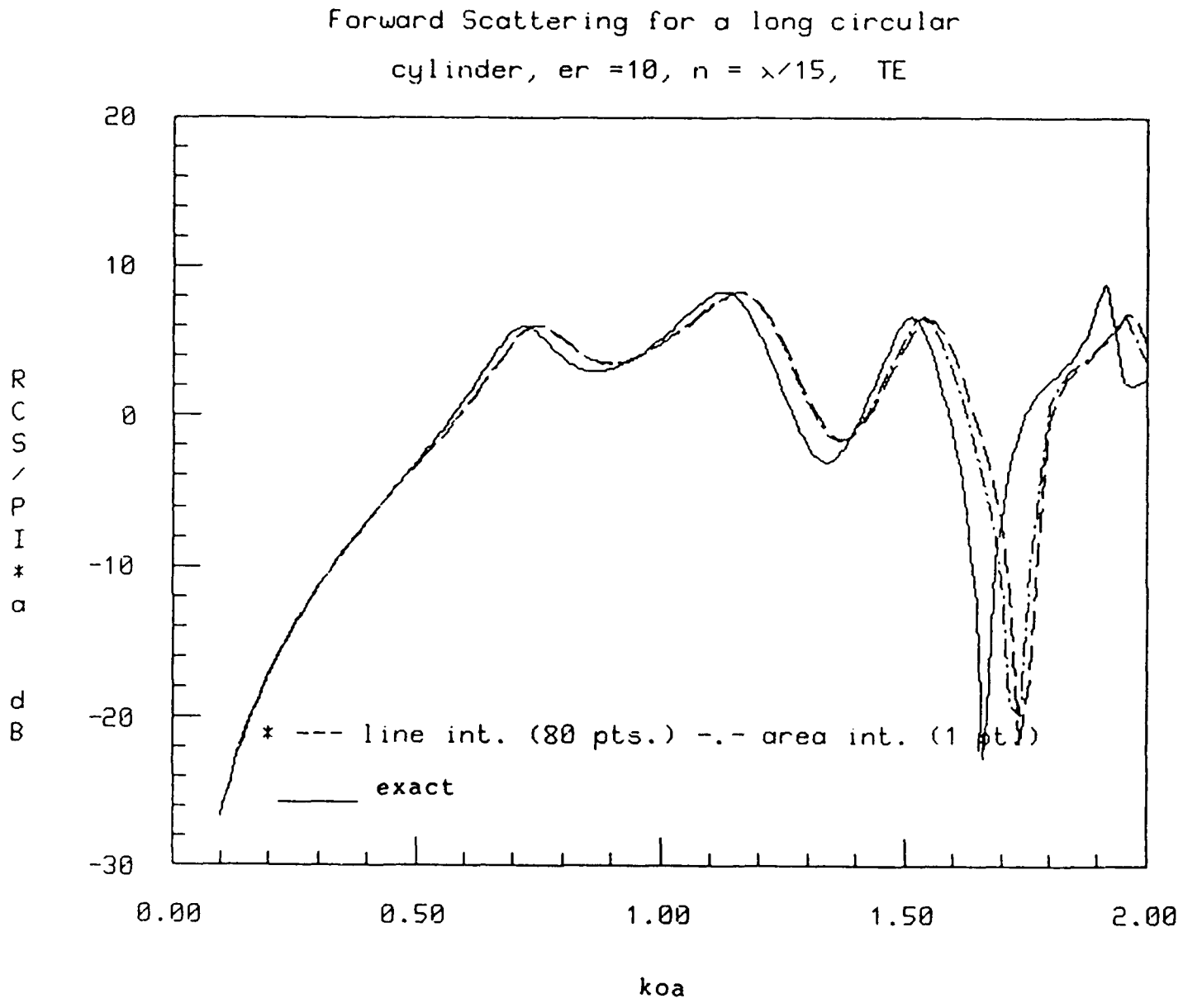
Forward Scattering for a long circular
cylinder, er =10, n = λ/15, TE
20
10
0
-10
-20
-30
RCS/PI*a
dB
* --- line int. (80 pts.) -.- area int. (1 pt.)
exact
0.00
0.50
1.00
1.50
2.00
koa

Fig. 51

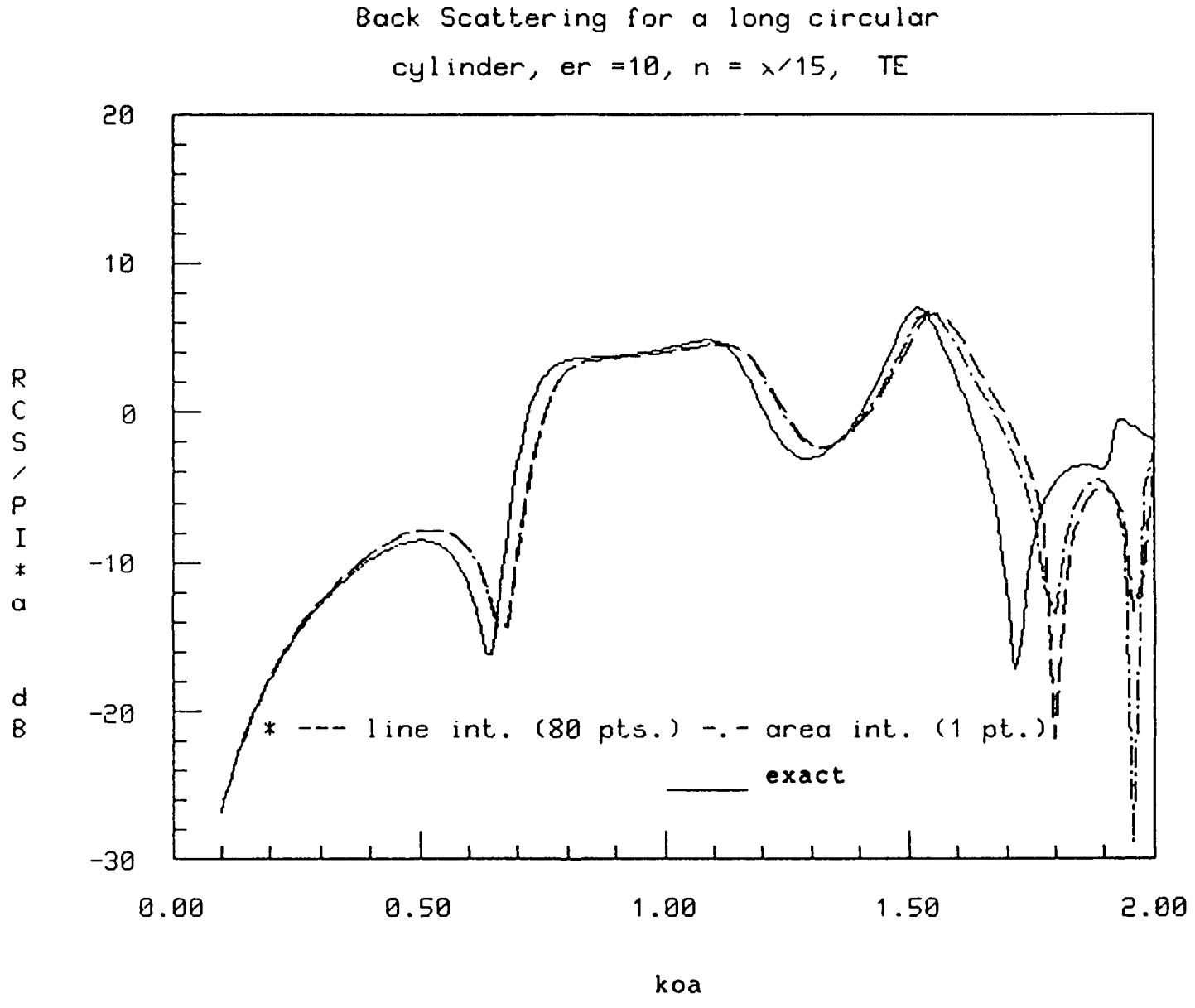
Back Scattering for a long circular
cylinder, er =10, n = λ/15, TE
20
10
0
-10
-20
-30
RCS/PI*a dB
* --- line int. (80 pts.) -.- area int. (1 pt.)
exact
0.00
0.50
1.00
1.50
2.00
koa

Fig. 52

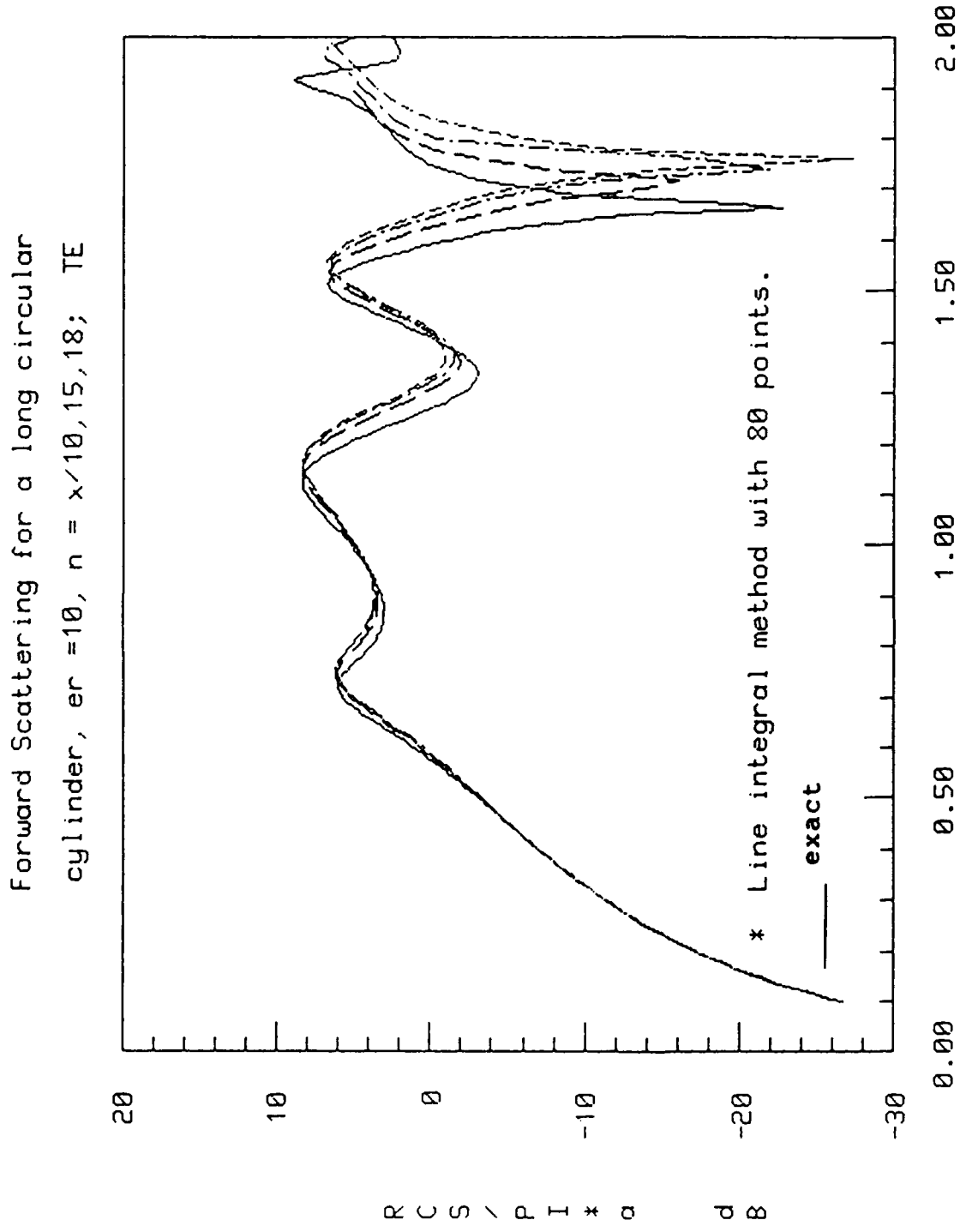
Forward Scattering for a long circular
cylinder, er =10, n = x/10,15,18; TE
RCS/PI*a dB
20
10
0
-10
-20
-30
0.00
0.50
1.00
1.50
2.00
koa
* Line integral method with 80 points.
exact

Fig. 53

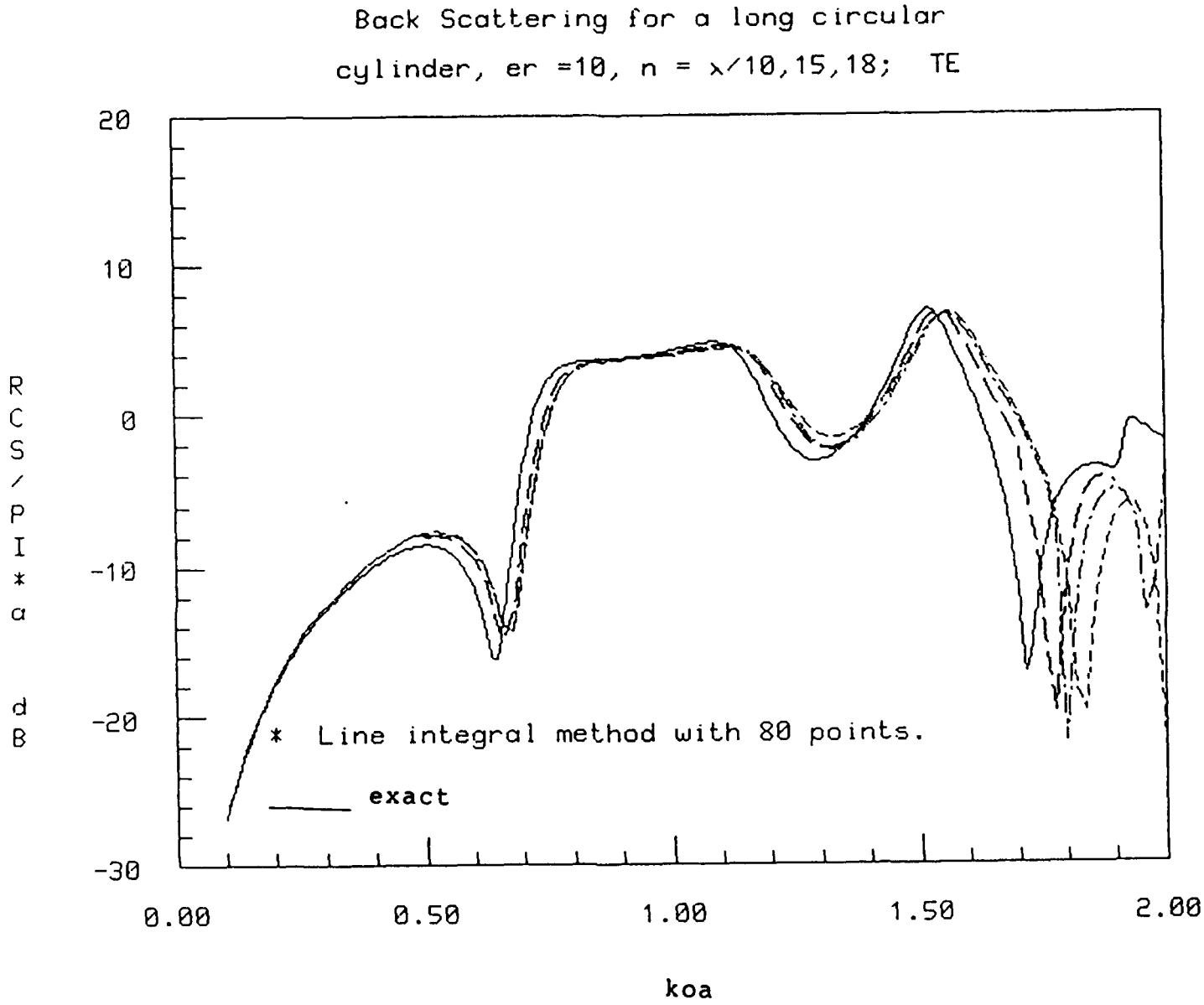
Back Scattering for a long circular
cylinder, er =10, n = λ/10,15,18; TE
20
10
0
-10
-20
-30
RCS/PI*a
dB
* Line integral method with 80 points.
exact
0.00
0.50
1.00
1.50
2.00
koa

Fig. 54

that a sharp drop occurs at $k_o a = 1.95$ in the solution with center point area integral method that is not found in the exact solution or with the line integral.

Figs. 53-54 shows a slight improvement when the number of cells per dielectric wavelength is increased. However, the curves seem to converge more slowly. The closest match is the curve where the number of cells per dielectric wavelength is set to 18. The greatest mismatch is found when it is set to 10. Due to the limitation of computer time and storage, the maximum size $k_o a$ of the cylinder is set to 1.8 for $n/\lambda = 18$. This gave an 1800 x 1800 matrix.

From Figs. 53 and 54, we select three points to observe the scattering from the dielectric circular cylinder versus scattering angles. The three points are $k_o a = 0.5$ (good agreement with exact solution), 1.5 (slight disagreement with exact solution) and 1.7 (poor agreement with exact solution). Figs. 55-57 show the normalized scattering from a lossless dielectric circular cylinder when $\epsilon r = 10$, and $k_o a = 0.5, 1.5, 1.7$ respectively. The number of segments per dielectric wavelength is set to 10. As seen from figures, the curves of scattering versus angle confirm the agreement at the single

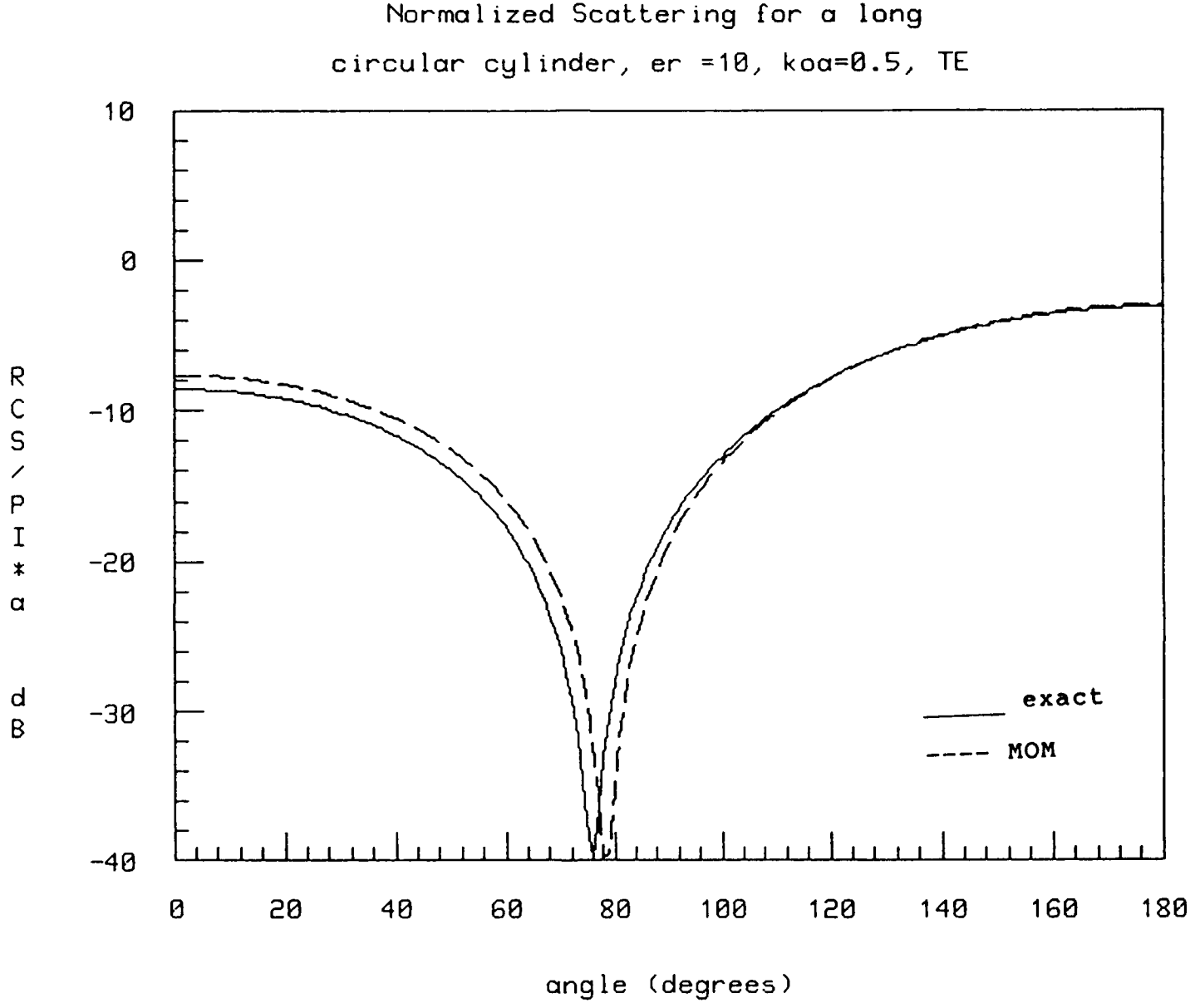
Normalized Scattering for a long
circular cylinder, er =10, koa=0.5, TE
10
0
-10
-20
-30
-40
RCS/PI*a dB
0
20
40
60
80
100
120
140
160
180
angle (degrees)
exact
MOM

Fig. 55

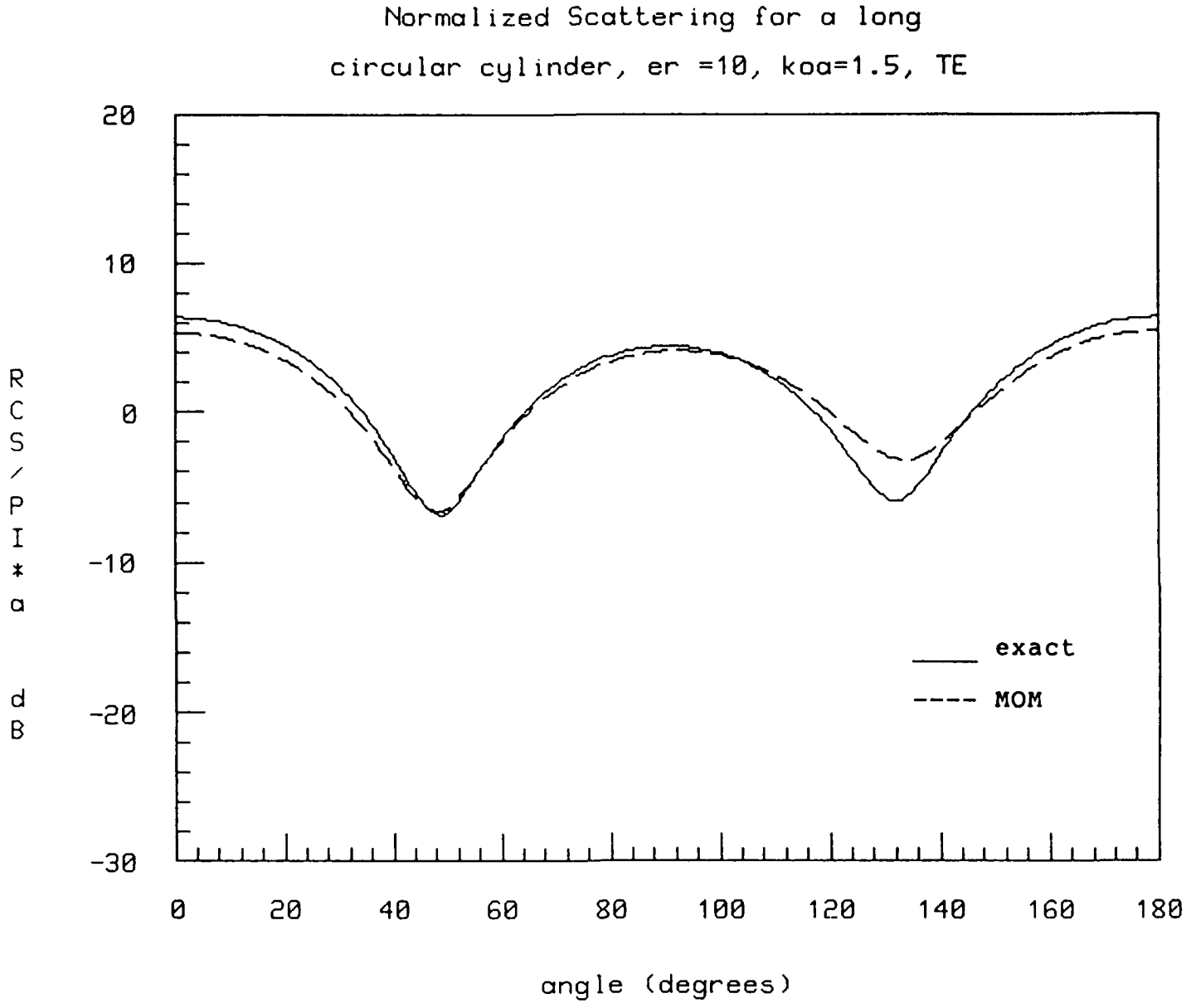
Normalized Scattering for a long
circular cylinder, er =10, koa=1.5, TE
20
10
0
-10
-20
-30
RCS/PI*a
dB
0
20
40
60
80
100
120
140
160
180
angle (degrees)
exact
MOM

Fig. 56

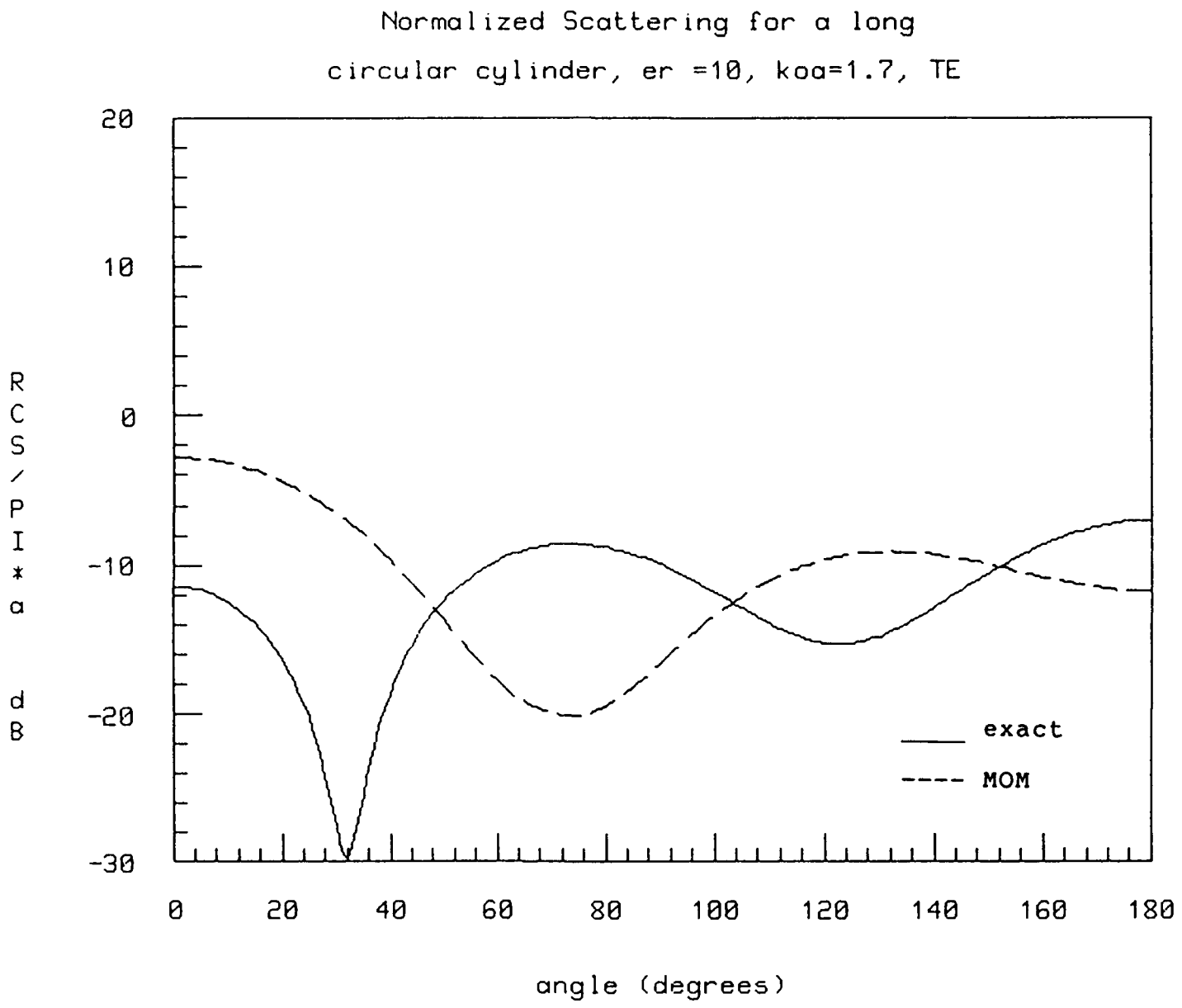
Normalized Scattering for a long
circular cylinder, er =10, koa=1.7, TE
RCS/PI*a dB
20
10
0
-10
-20
-30
0
20
40
60
80
100
120
140
160
180
angle (degrees)
exact
MOM

Fig. 57

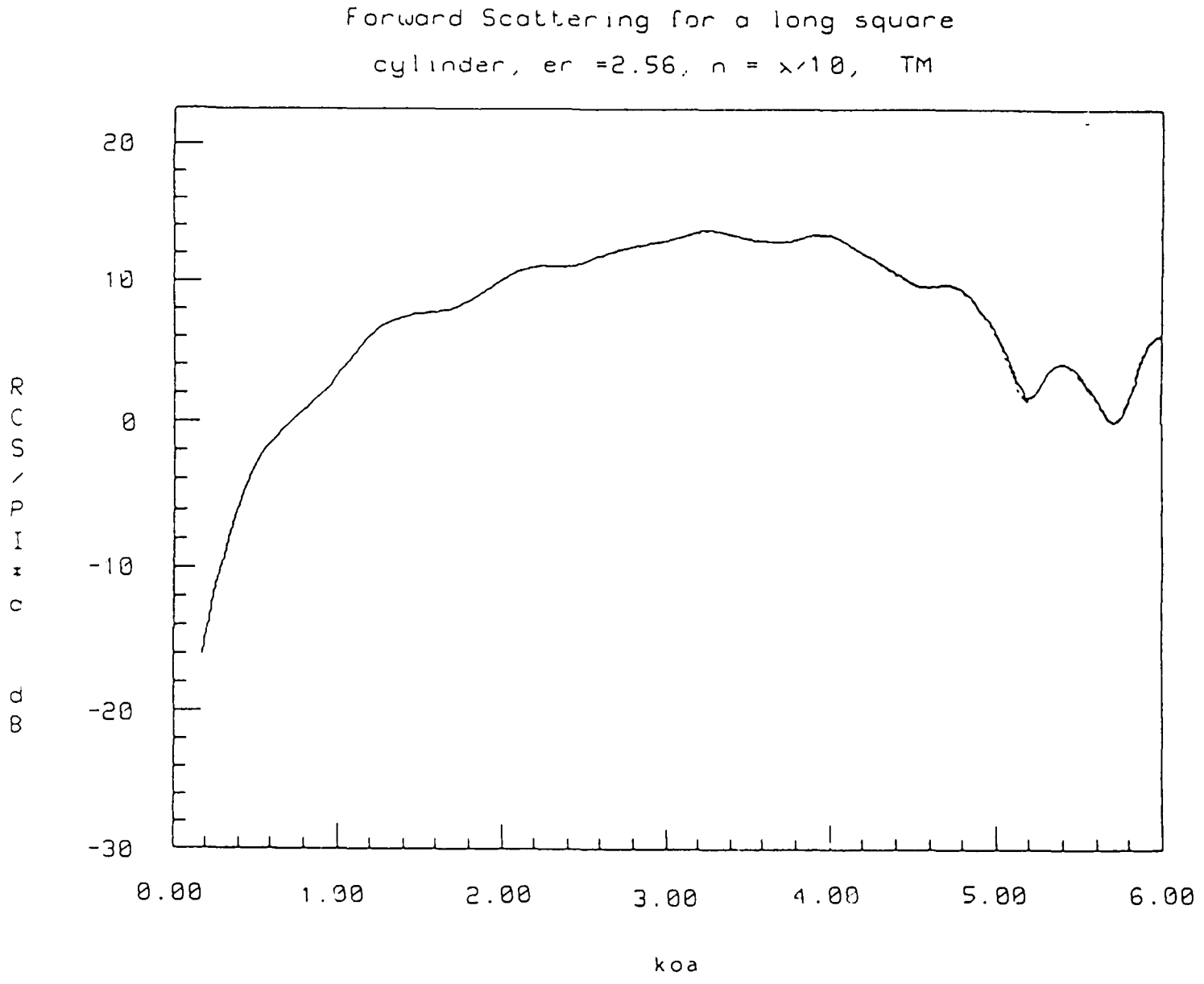
Forward Scattering for a long square
cylinder, er =2.56, n = λ/10, TM
RCS/PI*c dB
20
10
0
-10
-20
-30
0.00
1.00
2.00
3.00
4.00
5.00
6.00
koa

Fig. 58

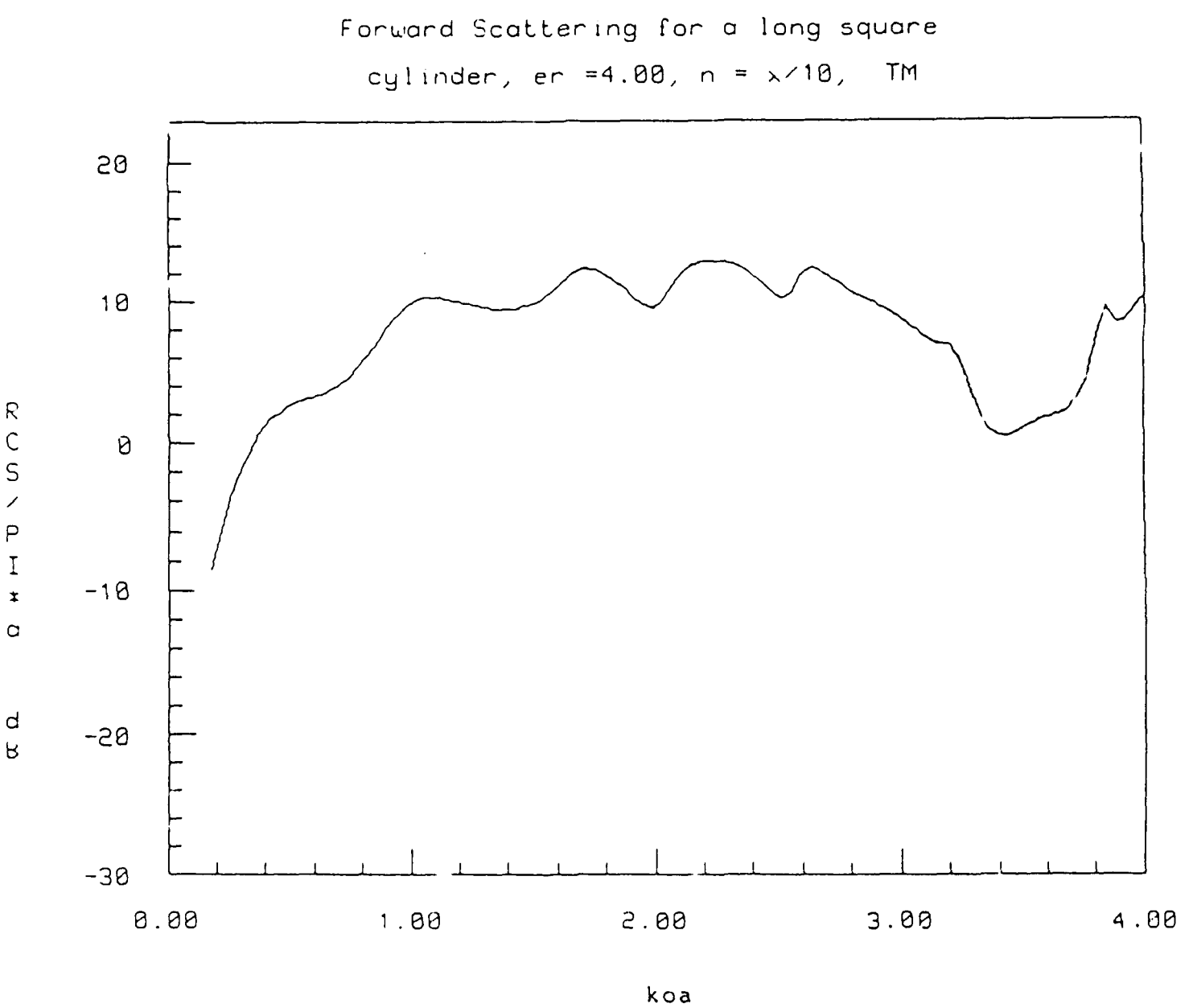
Forward Scattering for a long square
cylinder, er =4.00, n = λ/10, TM
20
10
0
-10
-20
-30
0.00
1.00
2.00
3.00
4.00
koa

Fig. 59

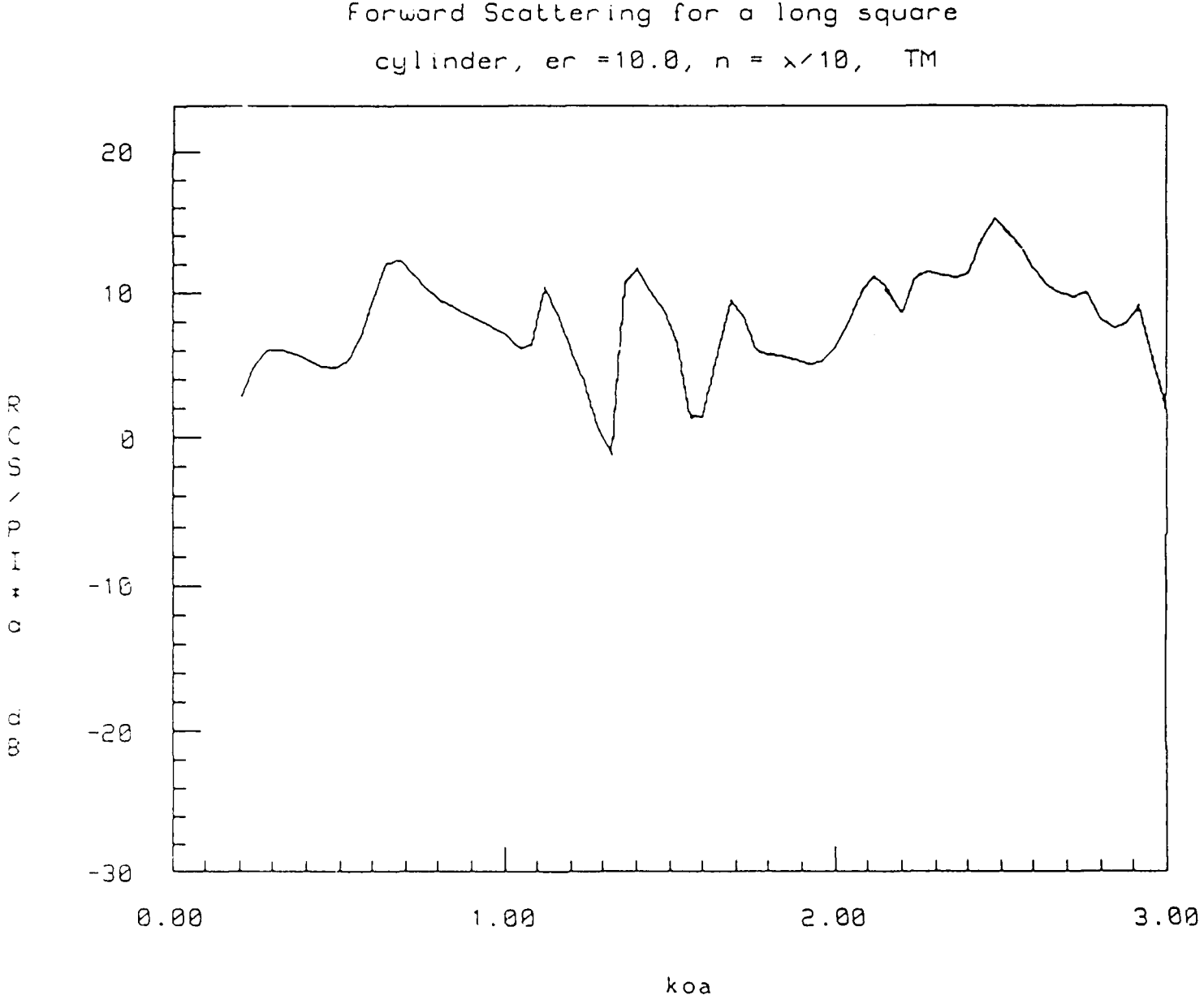
Forward Scattering for a long square
cylinder, er =10.0, n = λ/10, TM
20
10
0
-10
-20
-30
RCS / PI * a
dB
0.00
1.00
2.00
3.00
koa

Fig. 60

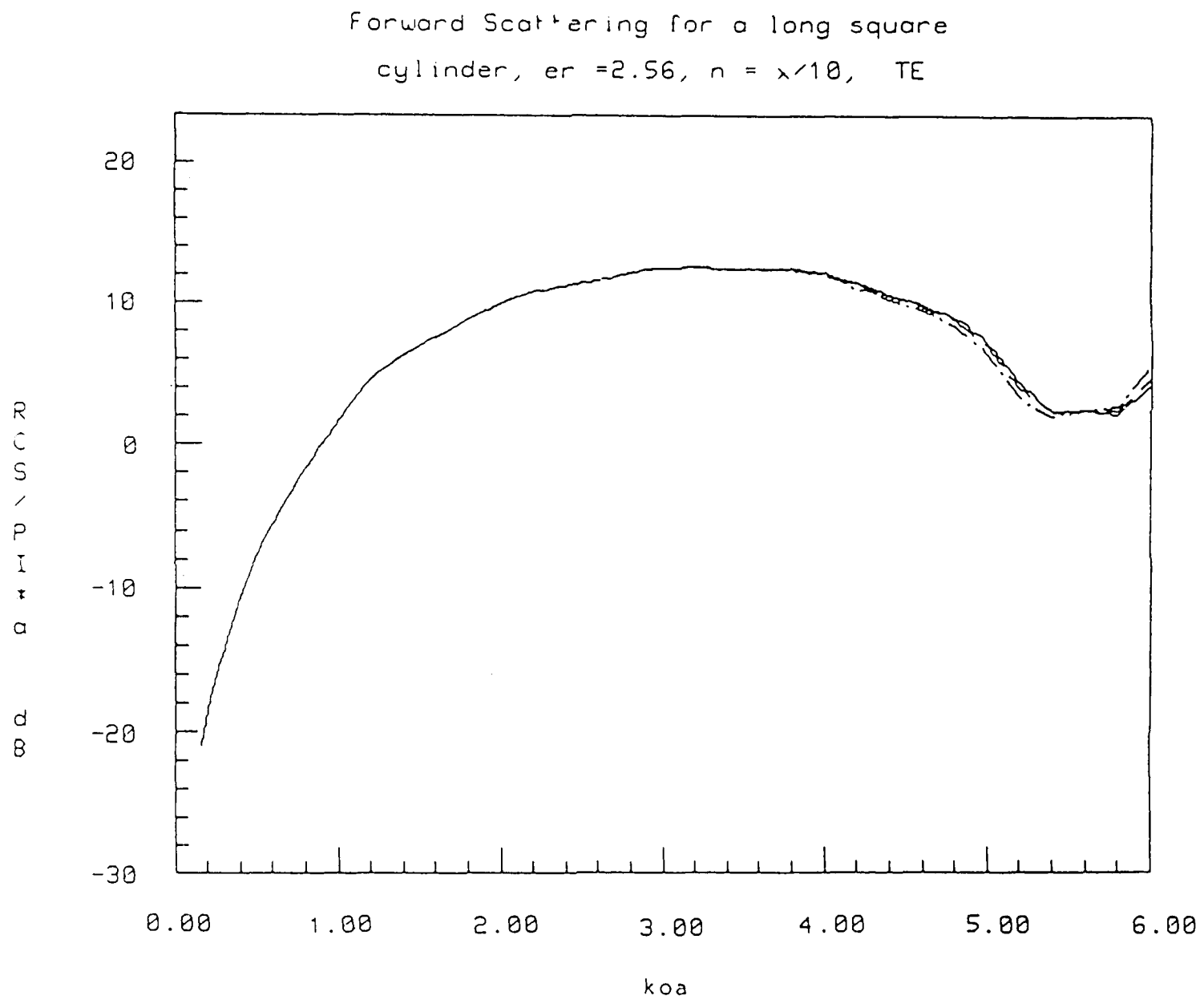
Forward Scattering for a long square
cylinder, er =2.56, n = λ/10, TE
RCS/PI*a dB
20
10
0
-10
-20
-30
0.00
1.00
2.00
3.00
4.00
5.00
6.00
koa

Fig. 61

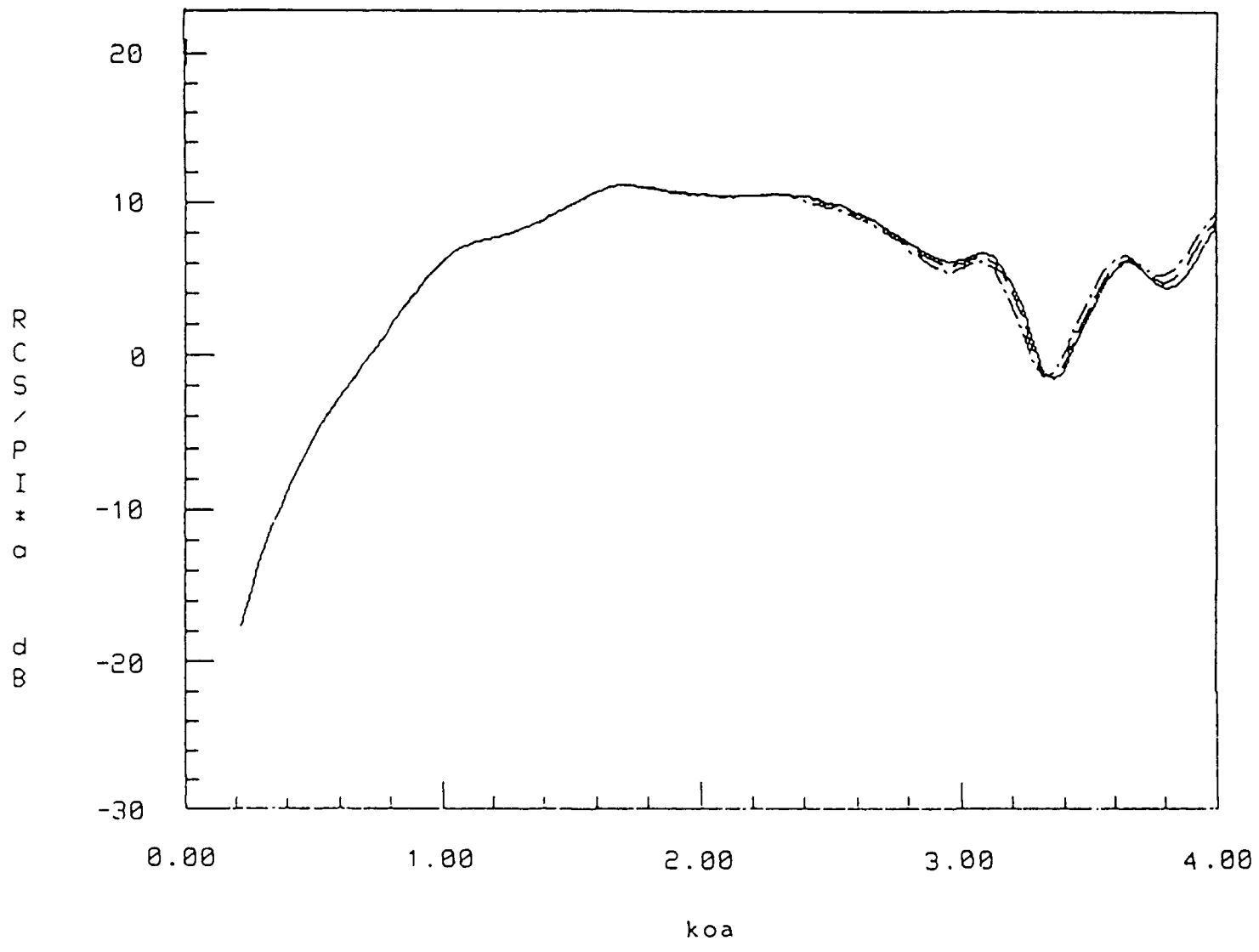
Forward Scattering for a long square
cylinder, er =4.00, n = λ/10, TE
20
10
0
-10
-20
-30
RCS/PI*a
dB
0.00
1.00
2.00
3.00
4.00
koa

Fig. 62

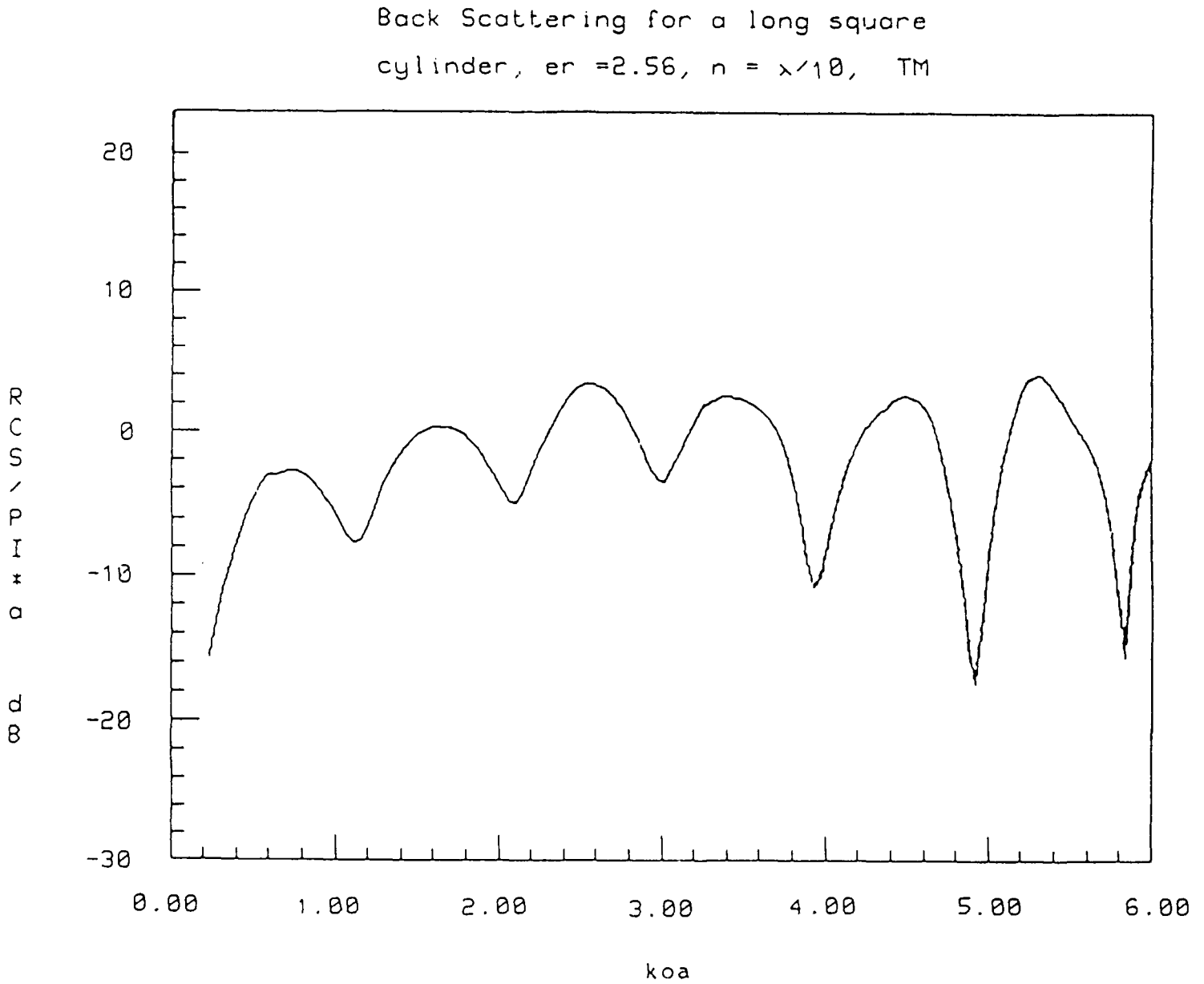
Back Scattering for a long square
cylinder, er =2.56, n = λ/10, TM
RCS/PI*a
dB
20
10
0
-10
-20
-30
0.00
1.00
2.00
3.00
4.00
5.00
6.00
koa

Fig. 63

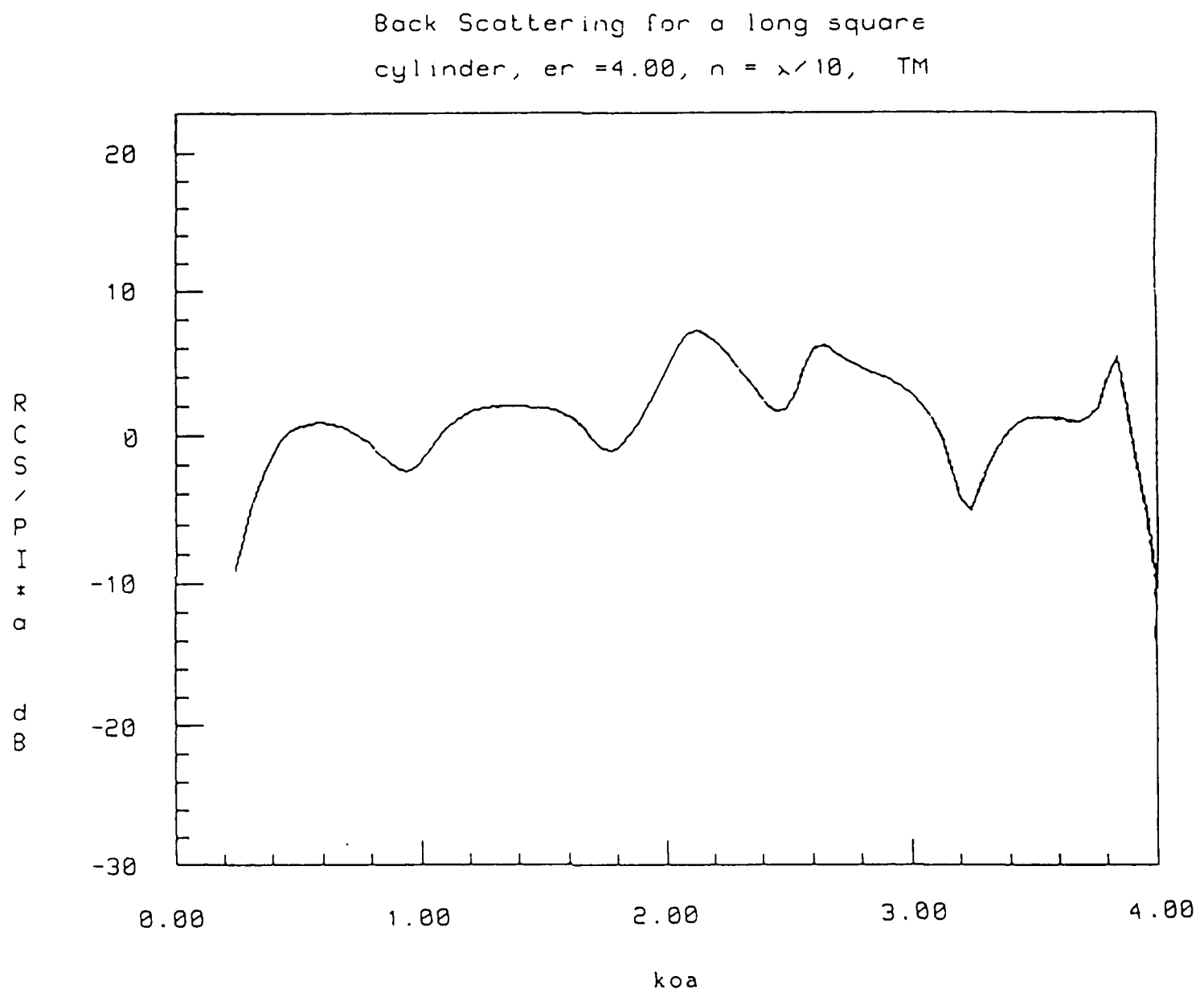
Back Scattering for a long square
cylinder, er =4.00, n = λ/10, TM
RCS/PI*a dB
20
10
0
-10
-20
-30
0.00
1.00
2.00
3.00
4.00
koa

Fig. 64

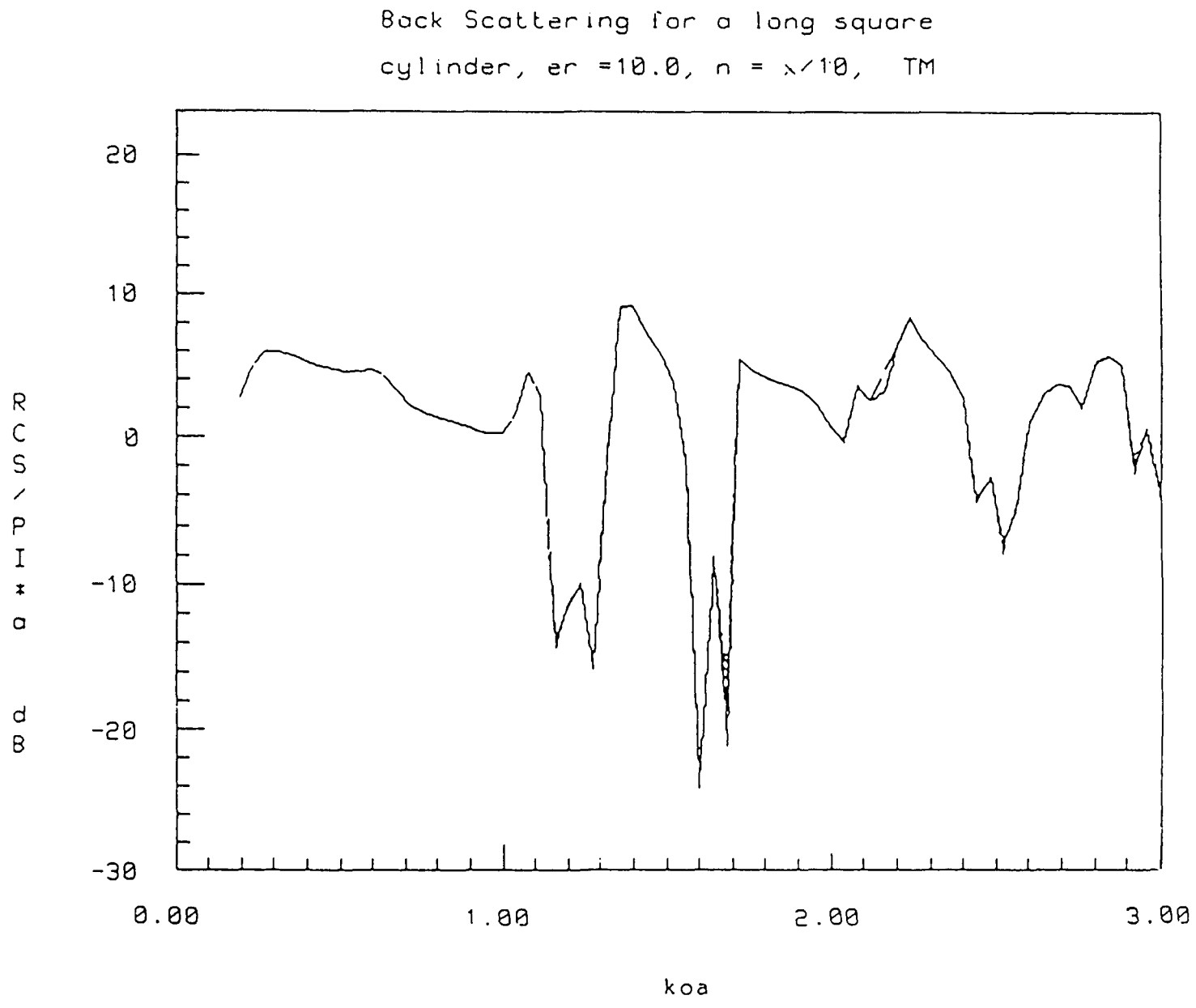
Back Scattering for a long square
cylinder, er =10.0, n = λ/10, TM
20
10
0
-10
-20
-30
RCS/PI*a
dB
0.00
1.00
2.00
3.00
koa

Fig. 65

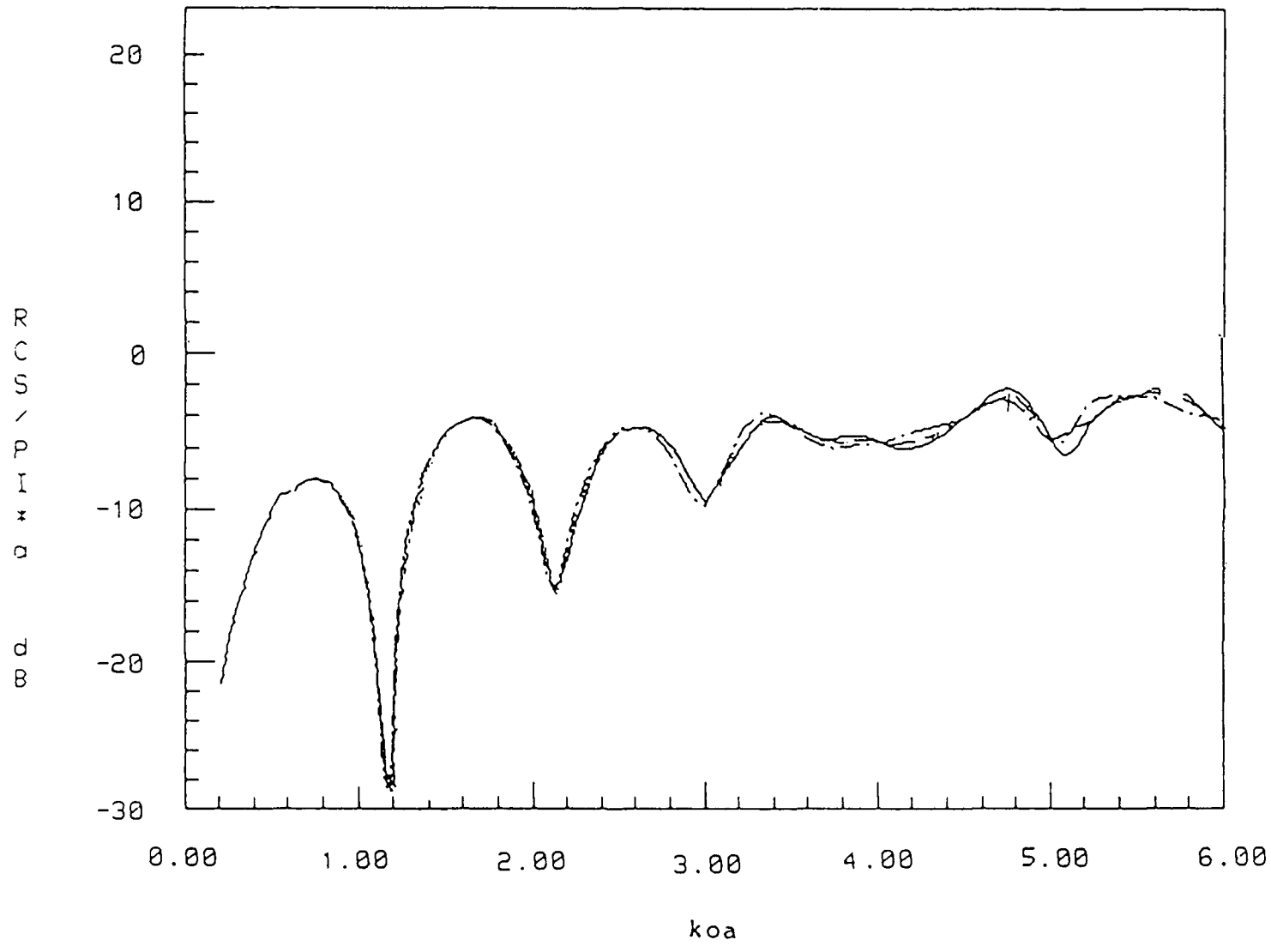
Back Scattering for a long square
cylinder, er =2.56, n = λ/10, TE
20
10
0
-10
-20
-30
RCS/PI*a
dB
0.00
1.00
2.00
3.00
4.00
5.00
6.00
koa

Fig. 66

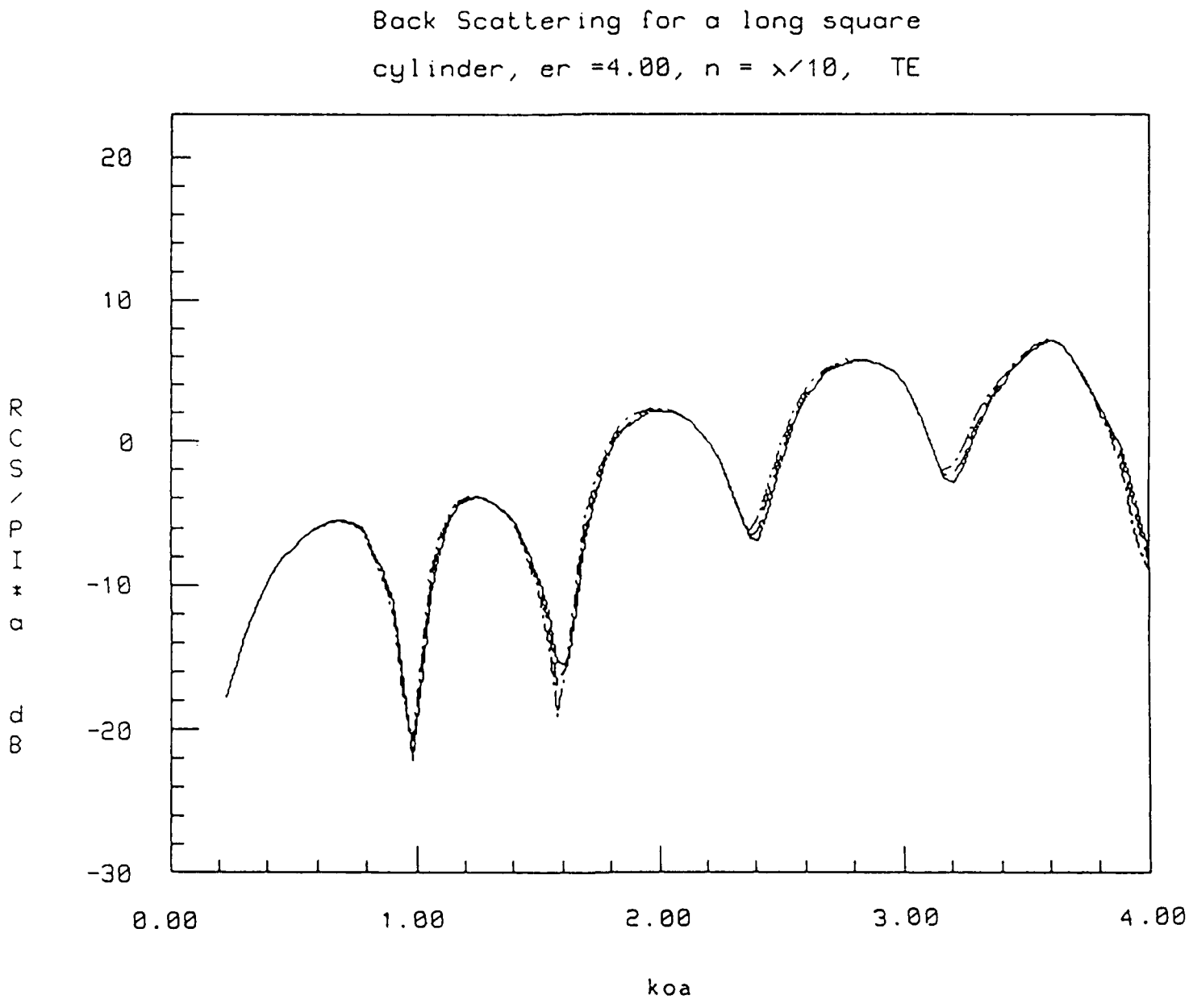
Back Scattering for a long square
cylinder, er =4.00, n = λ/10, TE
RCS/PI*a dB
20
10
0
-10
-20
-30
0.00
1.00
2.00
3.00
4.00
koa

Fig. 67

points. That is, Fig. 55 shows a close match to the exact solution, and Fig. 56 shows a slight mismatch from the exact solution, and Fig. 57 shows a complete mismatch.

The next set of figures (Figs. 58-62) represent the forward scattering from a long square dielectric lossless cylinder, with relative permittivities of 2.56,4,and 10 for TM polarization, and 2.56 and 4 for TE polarization. The number of cells per dielectric wavelength is set to 10 to ensure more accuracy. As before, three methods of integrating the Green's function over the cells are used. The back scattering is shown in Figs. 63-67. As seen from the figures, there is no significant difference between the results of the three methods.

Figs. 68-69 show the TE forward and back scattering from a dielectric square cylinder with relative permittivity of 10 for the three different methods. The number of cells per dielectric wavelength is set to 10. The total number of $k_o a$ points used is 100. As seen from these curves, the three methods give results that vary slightly from each other. The solid curve represents the line integral approximation of the cells, the single dotted line curve represents the

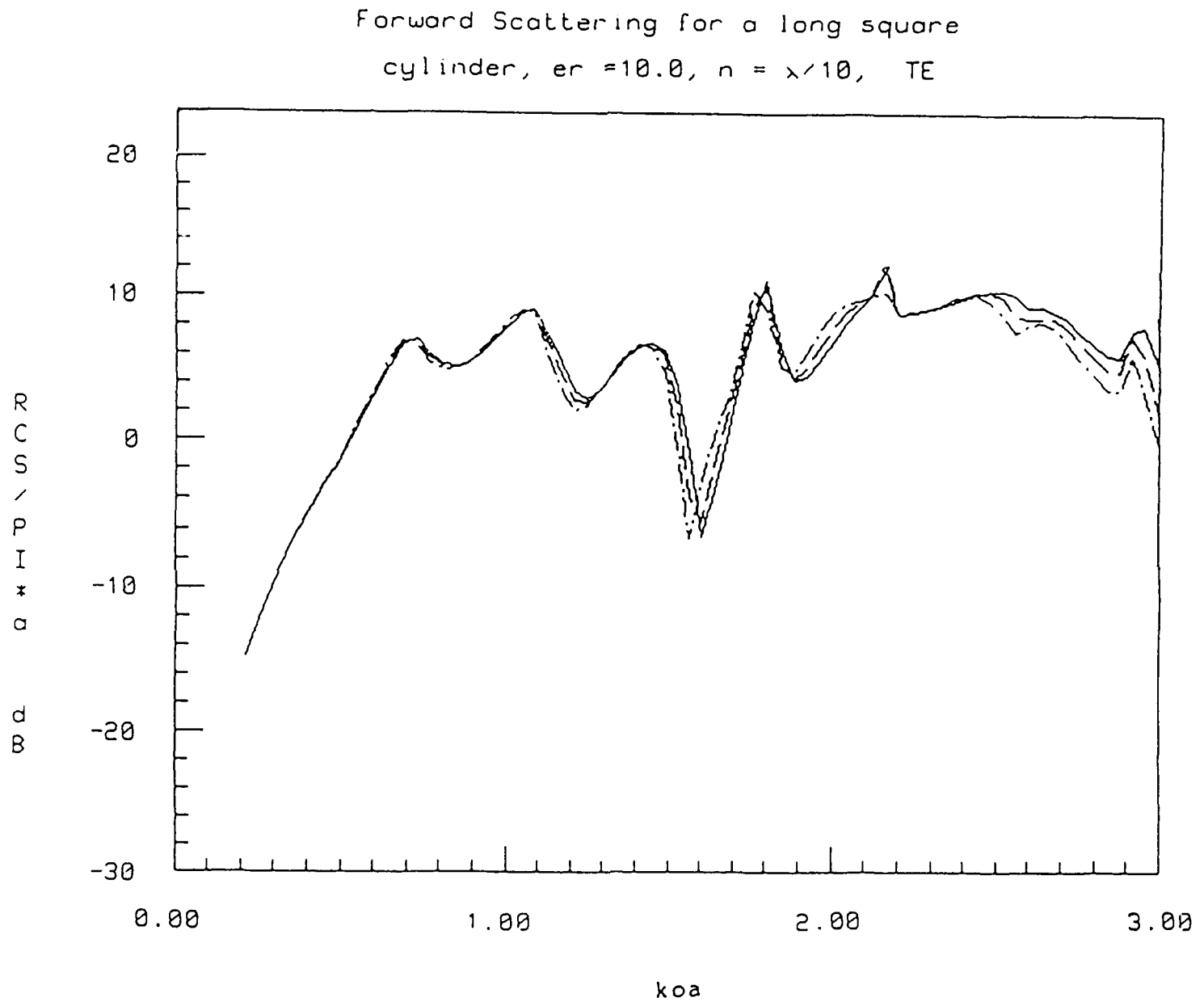
Forward Scattering for a long square
cylinder, er =10.0, n = λ/10, TE
RCS/PI*a
dB
20
10
0
-10
-20
-30
0.00
1.00
2.00
3.00
koa

Fig. 68

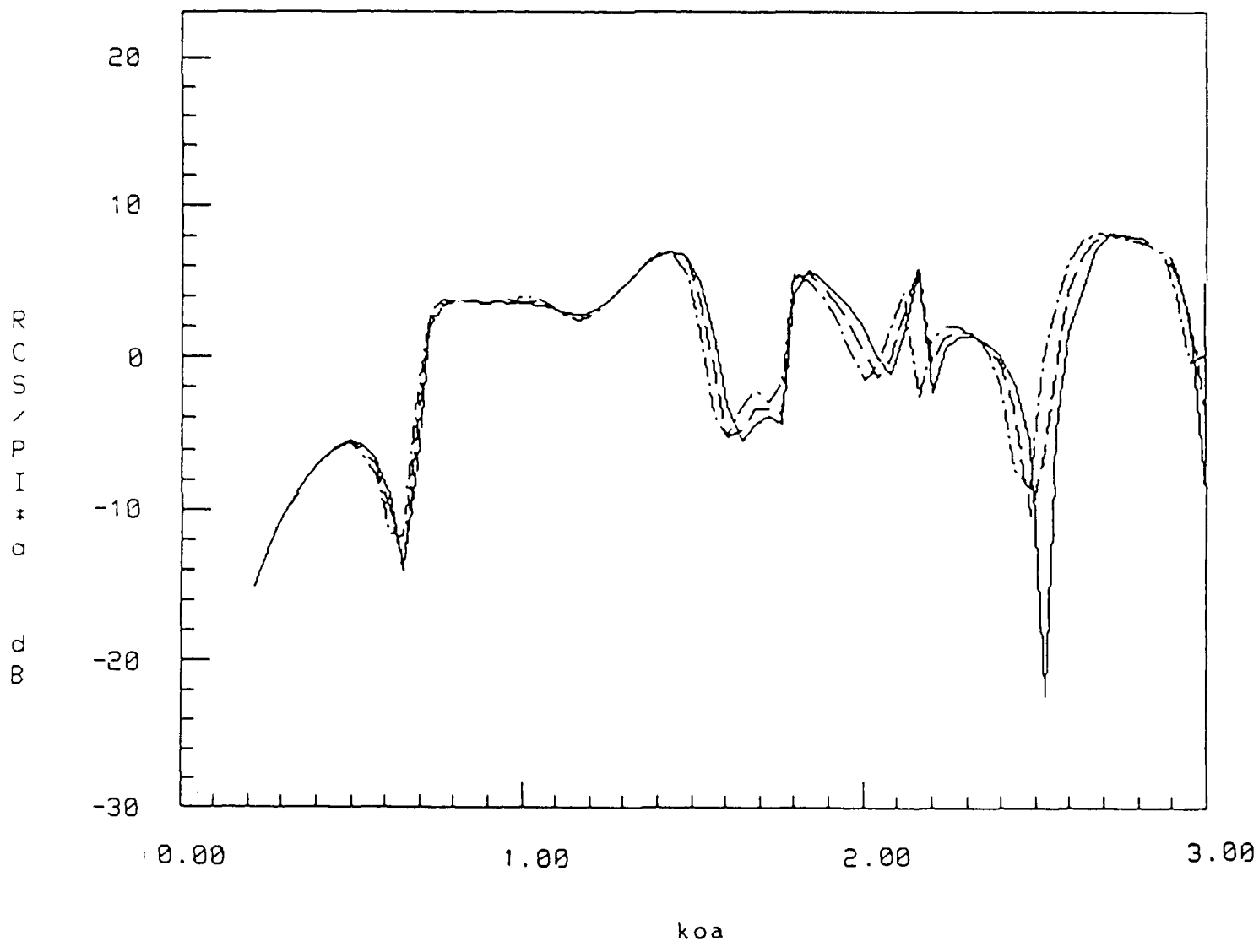
Back Scattering for a long square
cylinder, er =10.0, n = λ/10, TE
20
10
0
-10
-20
-30
dB σ*PI\RCS
0.00
1.00
2.00
3.00
koa

Fig. 69

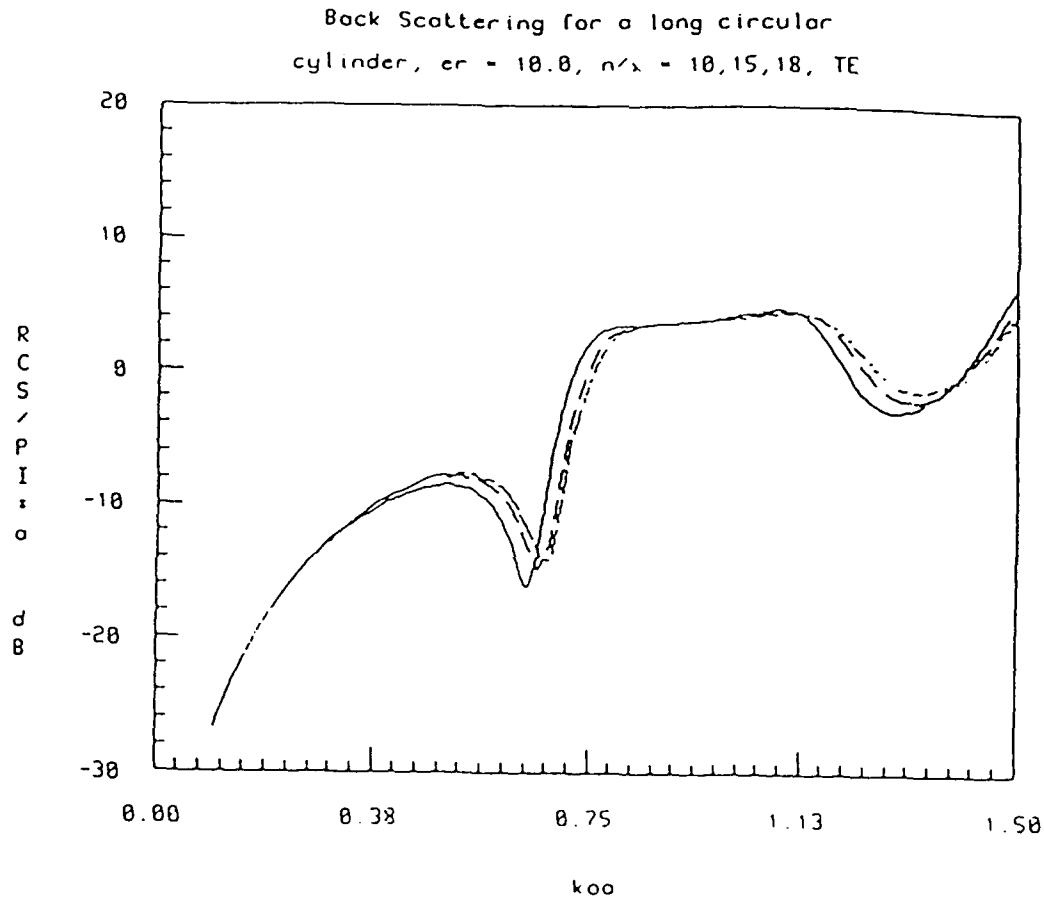
Back Scattering for a long circular
cylinder, er = 10.0, n/λ = 10,15,18, TE
RCS/PIxa dB
20
10
0
-10
-20
-30
0.00
0.38
0.75
1.13
1.50
koa

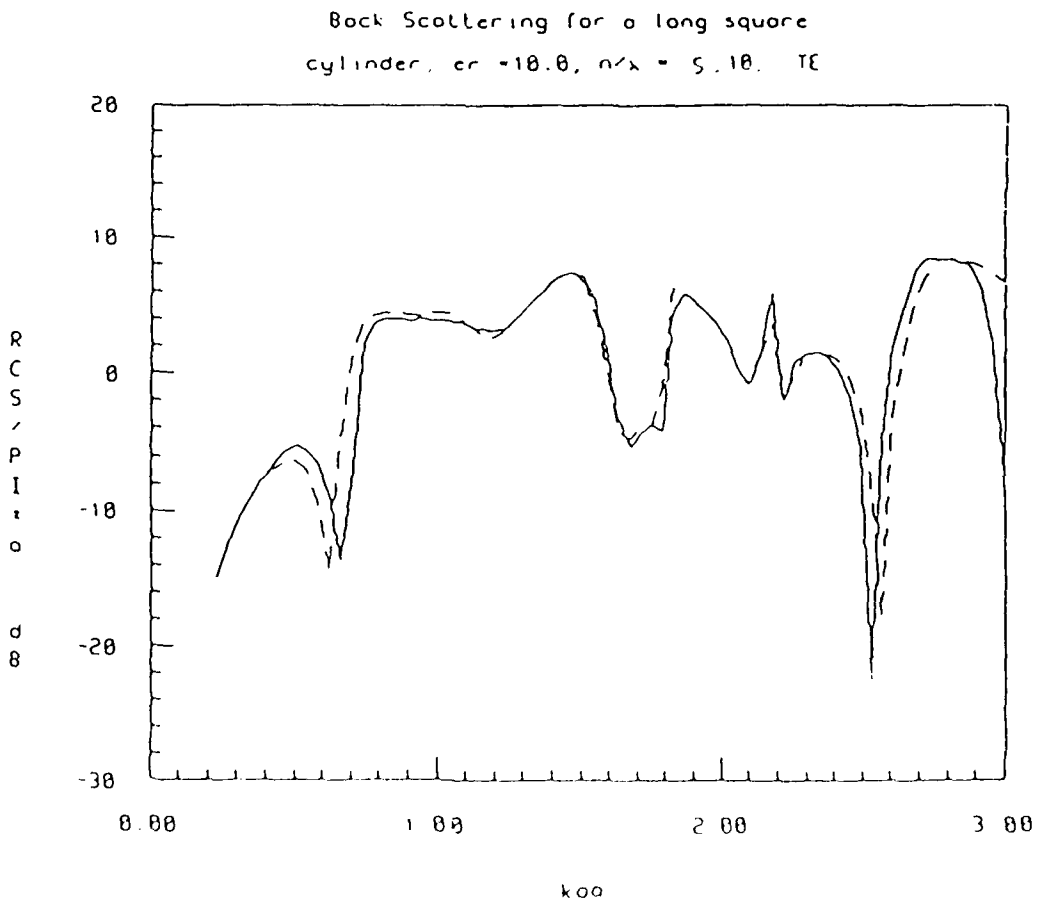
Back Scattering for a long square
cylinder, er =10.0, n/λ = 5,10, TE
RCS/PIxa dB
20
10
0
-10
-20
-30
0.00
1.00
2.00
3.00
koa

Fig. 10

area integral method with one center point. As more points are added to the area integration over the cells (e.g., 25 points in our case), the curve tends to converge to the solid curve represented by the line integral method which has 80 points.

Fig. 70 shows the back scattering from a circular cylinder and a square cylinder using three different cell sizes for TE polarization with $\epsilon r = 10$. It can be seen that decreasing the cell size tends to produce convergence to the exact solution (solid curve) for the circular cylinder. However, the curves converges very slowly. For the square cylinder, notice that at $k_o a = 3.0$ the curves for two different cell sizes seem to diverge even though the square boundary matches perfectly, and there is no jagged edges as in the case of the circular cylinder. This confirms that the jagged edges of the circular cylinder are not a large source of error.

6. CONCLUSION

The special treatment of the self cells in the volume integral equation did improve the performance of the solution for scattering from dielectric bodies. However, the improvement was slight and limited to small scattering bodies. When the relative permittivity is set equal to 10, the total number of cells needed for TE polarization is already in the range of 1800 for $k_o a=1.8$. Thus the size of the scatterer we can handle on our mainframe computer is limited. Moreover, the curves from Figs. 68-69 require at least 120 $k_o a$ points. It is very time consuming to run the simulation program 120 times to get the required curve.

One source of the inaccuracies of the solution is the square-cell approximation of the cross section of the circular cylinder. However, our computations indicated that this jagged edges problem is not a major source of error.

The most important reason for the inaccuracies, as pointed out by Peterson [1], is in the pulse-basis, point-matching formulation. Using the pulse basis functions introduces fictitious charge layers at every cell boundary with resulting

numerical error. This error tends to increase as the relative permittivity increases. However, with a new formulation of the volume integral equation which deals with the surface charge density, we hope to overcome these inaccuracies and obtain a benchmark solution for multi-wavelength dielectric scatterers using convenient pulse basis functions. Finally, making use of the symmetry of the matrices and converting to Toeplitz or tridiagonal matrices will ensure faster computing time and less storage requirements.

REFERENCES

[1] Peterson, "Analysis of heterogeneous electromagnetic scatterers: Research progress of the past decade," Proceedings of the IEEE, vol. 79, pp. 1431-1441, October 1991.

[2] Yaghjian, "Electric dyadic Green's functions in the source region," Proceedings of the IEEE, vol. 68, pp. 248-263, February 1980.

[3] Richmond, "Scattering from a dielectric cylinder of arbitrary cross section shape," IEEE Trans. AP-13, pp. 334-341, May 1965.

[4] Richmond, "TE-wave scattering from a dielectric cylinder of arbitrary cross section shape," IEEE Trans. AP-14, pp. 460-464, July 1966.

[5] Livesay and Chen, "Electromagnetic fields induced inside arbitrarily shaped biological bodies," IEEE Trans. MTT-22, pp. 1273-1280, December 1974.

[6] Joachimowicz and Pichot, "Comparison of three integral formulations for the 2-D TE scattering problem," IEEE Trans. MTT-38, pp. 178-185, February 1990.

[7] Ruck, Barrick, Stuart and Krichbaum, "Radar Cross Section Handbook," Ruck, Ed., Plenum, 1970.

[8] Barber and Hill, "Light Scattering by Particles: Computational Methods," World Scientific, 1990.

[9] Hill, Durney and Christensen, "Numerical calculations of low frequency TE fields in arbitrarily shaped inhomogeneous lossy dielectric cylinders," Radio Science vol.18, pp. 328-336, May 1983.

[10] Tsai, Massoudi, Durney and Iskander, "A procedure for calculating fields inside arbitrarily shaped inhomogeneous dielectric bodies using linear basis functions with the moment method," IEEE Trans. MTT-34, pp. 1131-1139, November 1986.

[11] Langan, "Numerical solution of transverse electric scattering by inhomogeneous two-dimensional composite dielectric and metallic bodies of arbitrary cross section," M.S. thesis, University of Houston, Houston TX, 1989.

[12] Zwamborn and van den Berg, "A weak form of the conjugate gradient FFT method for two-Dimensional TE scattering problems," IEEE Trans. MTT-39, pp. 953-960 June 1991.

[13] Schaubert, Wilton and Glisson, "A tetrahedral modeling method for electromagnetic scattering by arbitrarily shaped inhomogeneous dielectric bodies," IEEE Trans. AP-32, pp. 77-85, January 1984.

[14] Silberstein, "Electromagnetic Scattering from dielectrics - a two-dimensional integral equation solution", RL report to be published 1992.

*U.S. GOVERNMENT PRINTING OFFICE: 1993-710-093-60182

MISSION

OF

ROME LABORATORY

Rome Laboratory plans and executes an interdisciplinary program in research, development, test, and technology transition in support of Air Force Command, Control, Communications and Intelligence (C^3I) activities for all Air Force platforms. It also executes selected acquisition programs in several areas of expertise. Technical and engineering support within areas of competence is provided to ESD Program Offices (POs) and other ESD elements to perform effective acquisition of C^3I systems. In addition, Rome Laboratory's technology supports other AFSC Product Divisions, the Air Force user community, and other DOD and non-DOD agencies. Rome Laboratory maintains technical competence and research programs in areas including, but not limited to, communications, command and control, battle management, intelligence information processing, computational sciences and software producibility, wide area surveillance/sensors, signal processing, solid state sciences, photonics, electromagnetic technology, superconductivity, and electronic reliability/maintainability and testability.